Closed loop control of painful laser stimuli based on thermography and thermal modelling of the skin

Ken Steffen Frahm

4th semester master thesis - Group 1085I, June 2009

Department of Health Science and Technology,
Aalborg University

The Faculty of Engineering, Science and Medicine
Aalborg University, Denmark

AALBORG UNIVERSITY

Title:

Closed loop control of painful laser stimuli based on thermography and thermal modelling of the skin

Project period:
10th semester (4th semester Master) - Master Thesis
February 2009 - June 2009

Project group:
1085I

Group member:
Ken Steffen Frahm

Supervisors:
Carsten Dahl Mørch
Ole Kæseler Andersen

Numbers of copies: 4

Numbers of pages: 130

Enclosures: 1 CD

Synopsis:

Contact-heat evoked pain has through many years been used to conduct psychophysical studies investigating the human sensory system. During recent years contact-heat stimulations have determined an analgesic (pain relief) effect whenever the intensity of a painful stimulation is lowered slightly, still leaving the intensity above the pain threshold, this phenomenon was named offset analgesia [Grill and Coghill, 2002] [Yelle et al., 2008]. This phenomenon could prove important in the understanding and treatment of chronic pain since offset analgesia has been found to been involved with centers in the brain known to be associated with inhibitory mechanisms [Derbyshire and Osborn, 2008] [Derbyshire and Osborn, 2009].

Contact-heat stimulations, however, posses a number of limitations. Limitations which can be solved using non-contact stimulator such as lasers. Lasers have previously been used as the primary method of administering non-contact heat stimulations. However, lasers are not equipped with a build-in temperature control, like most commercial contact-heat stimulators have.

In this thesis a non-contact thermal (heat), temperature controlled, stimulator was developed, intended for psychophysical studies. To gain knowledge about the skins thermal properties during laser stimulation a detailed Finite Element Model was developed and validated through experiments. The system uses a near infrared laser to heat the skin and an infrared camera to measure the skin temperature during the stimulation. The laser power is controlled using a closed loop PI (Proportional-Integral) controller based the temperature measurement from the infrared camera. Since the developed system utilizes only passive cooling to decrease the skin temperature; the system cannot cool the skin temperature, as fast as contact-stimulator utilizing active cooling. However, experimental trials of eight subjects proved that the non-contact stimulator was able to evoke offset analgesia in all subjects tested.

Preface

The enclosed report is the product of the master thesis,
Closed loop control of painful laser stimuli based on thermography and thermal modelling of the skin. This thesis was produced by Ken Steffen Frahm, group 1085I, fourth master semester (tenth semester total), spring 2009, at the Department of Health Science and Technology, Aalborg University.
This report contains two appendices which are copies of previous projects, appendices A and E. They are meant as an elaboration and a service to the reader. A previously developed Monte Carlo simulation was used to model the heat from a diode laser, therefore a chapter desdribing the model can be found in appendix A. Should the reader be unfamilar with sensory physiology he or she could benefit from reading Appendix E.
On the enclosed CD the software developed in the thesis is found. The Labview code for the developed Non-contact thermal stimulator is found. The developed Finite Element Model can be found, (.mdl files intended for use with COMSOL multiphysics). The used Simulink models to develop and tune the temperature controller and finally the Matlab code for the Monte Carlo simulation can be found.
The author would like to dedicate a huge thank to Gunnar Svendsen, CEO, Cortex Technologies for his help in the ultrasound scan to determine the epidermal thicknesses of the subjects. A great thanks also goes to Jan Dimon Bendtsen, Associate professor at the Department of Electronic systems for his help in the controller development.
Since this thesis is the final project in the Biomedical Engineering program the author would also like to dedicate his a very special thanks to friends, and family for their patience and understanding during the stressed periods during the past five years and their help whenever it was needed. Furthermore I would like to thank fellow students, especially fellow group members, and supervisors without whom the past five years would not have been as educational as been the case.

Aalborg University, June 2009

_____

Ken Steffen Frahm

Contents

Introduction

I

Introduction 1

The human sensory system has been the research objective for many studies in the past centuries, an effort which probably will continue in the forthcoming centuries as well. In order to learn more about the sensory system, very different research techniques has been applied, such as psychophysical, electrophysical, medical imaging, and histological/anatomical.

One part of the sensory system which have received much attention is the pain system. The research have been focussed on many areas including, visceral, dental and cutaneous (skin) pain. Cutaneous tissue have often been used in pain models partly due to the easy stimulation of cutaneous tissue.

A great part of the research has been focussed on the abnormalities and disorders which can occur in the nociceptive sensory system, including lack of sensation or sensation of a stimulus when no stimulus is present. This includes painful sensation occuring either when no stimulus is present, or when only a low-intensity, innocous (not tissue damaging) stimulus is present. Such painful sensations originate from neural disorders in the sensory system (e.g. neuropathic pain [Merskey et al., 1994]). Discussing abnormal painful sensations two definitions should be know, hyperalgesia and allodynia. Hyperalgesia, is a excessive response from a stimulus which is normally painful [Merskey et al., 1994]. Allodynia is a painful sensation from a usually unpainful stimulation [Merskey et al., 1994], see figure 1.1.

In addition to hyperalgesia and allodynia which both occur in abnormal subjects, central and peripheral mechanisms exist which alter the sensation of the stimulation in both abnormal and normal subjects. Sensitization causes increased response to a prolonged or repeated stimulus, and it can occur both peripherally and centrally [Raja et al., 1999]. Sensitization is referred to as the physiological parallel to the psychophysical term hyperalgesia [IASP, 2009]. The opposite is called habituation. Meaning a decreased response to a repeated or prolonged stimulus [Dimitrijevic et al., 1972]. During habituation the sensation can be retrieved by increasing the stimulus intensity or frequency [Dimitrijevic et al., 1972].

The conducted pain research has also provided insight on how the rest of sensory system works and vice versa. One very useful of such research is Quantitative Sensory Testing (QST).

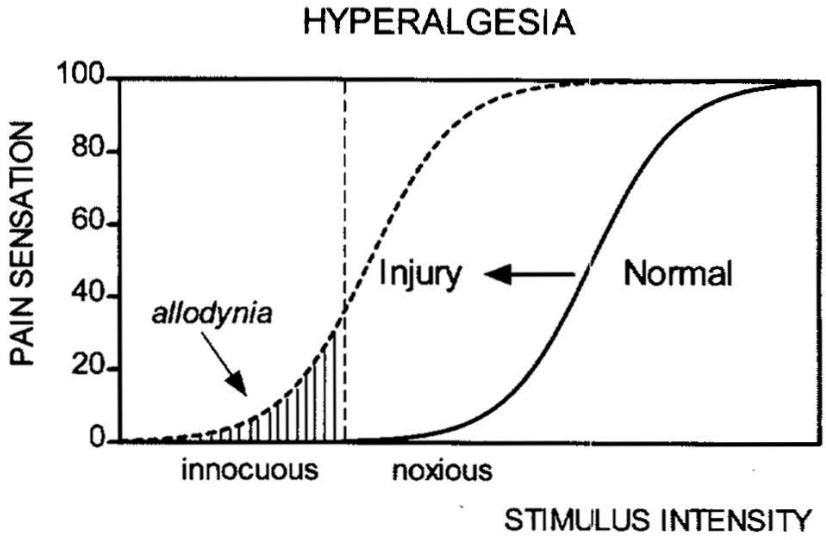

Figure 1.1: The figure illustrates the difference between allodynia and hyperalgesia. Allodynia is a painful sensation to a usually painless stimulation. Hyperalgesia is excessive response to a normally painful stimulation. Found in [Cervero and Laird, 1996].

1.1 Quantitative sensory testing

QST is a generic term ranging over techniques to determine any disorder or abnormalies in the sensory nervous system, including pain. QST studies can be used on different tissue types, however, most often it is the skin which is being stimulated. This thesis will solely focus on cutaneos stimulations.
QST incorporates a range of different stimulation modalities such as mechanical including tactile and vibration stimulation; thermal - warm and cold; and chemical - e.g. injecting capsaicin to evoke pain or hyperalgesia in the skin. See table 1.1 for an overview of modalities used in pain research and the properties of these modalities. The different stimulation modalities are, among other things, used since they correspond to different fiber population and sensory pathways, thermal and painful sensations are conducted via thinly myelinated afferent (Aδ) and unmyelinated fibers (C), via the anterior spinothalamic tract [Martini, 2004a] [Kandel et al., 1991a]. Whereas tactile sensations are conducted via medium size afferent (Aβ) via the posterier column pathway [Martini, 2004a] [Kandel et al., 1991a].
QST is a psychophysical technique since the patient or subject is required to report the intensity of the sensation evoked by the stimulation e.g. above or below sensation or pain threshold. QST is used both in clinical and research settings [Shy et al., 2003]. QST can be used as a measure of either diagnosing a neural disorder or monitoring the progress of one [Shy et al., 2003].
A review by Shy et al. from 2003 concluded that QST as clinical tool should not yet be the sole criterium on which a diagnosis is found, however, QST could often contribute to a diagnosis combined with other techniques, such as skin biopsies and medical imaging techniques. The authors also reviewed the application of QST in many scenarios both clinical and research, with varying stimuli, to review its sensitivity and specificity.
As mentioned QST can, besides being a clinical tool, be applied in research, investigating the sensory system.

	Electrical		Thermal		Pressure	Ischaemic	Cold pressure	Chemical
Requirement	Pulp	Skin	Contact	Radiation				
Fast onset	✓	✓	?	✓	?	-	-	?
Fast offset	✓	✓	✓	-	-	-	-	-
Natural	-	-	✓	✓	✓	✓	✓	✓
Repeatable	✓	✓	-	-	-	-	-	?
Objective	-	✓	✓	✓	?	?	?	?
Severe, constant	?	?	?	?	?	✓	✓	✓
Few afferents	✓	-	✓	✓	-	-	-	✓

Table 1.1: The table displays the requirements met by different stimulation modalities used in QST studies. The modalities listed, are electrical stimulation, including dental pulp and skin stimulation; Thermal stimulation, including contact and radiation (non-contact); Pressure; Ischaemic; Cold Pressure; and Chemical. The columns of highest interest in this thesis are the thermal modalities. Adapted from [Gracely, 1999]

1.1.1 QST - threshold detection

The methods applied for conducting QST differs between authors as can be seen in the discussion above. Including those used to determine thresholds, which is a central part of QST studies.
The threshold detection can be done in several ways, worth mentioning are the method of limits, the method of levels, the method of constant stimulus and the method of adjustment [Shy et al., 2003] [Gracely, 1999].
In the method of limits the subject must report whenever a stimulation reaches a threshold either detection or pain threshold. This method can incorporate both ascending or descending trials, i.e. in pain threshold detection the subject will report when a increasing stimulus becomes painful or when a decreasing stimulus no longer is painful [Shy et al., 2003] [Gracely, 1999], see figure 1.2 (left), increasing intensity.
In the methods of levels the stimulation is kept constant at increasing or decreasing levels, and the subject or patient must then report the intensity of the sensation at each level [Shy et al., 2003], see figure 1.2 (right). The method is, in a slightly different setup, referred to as the method of constant stimulus, where the order of stimulus intensities are randomised [Gracely, 1999], see figure 1.2 (right). The method of levels can also resemble that of staircase stimulation, see figure 1.2 (middle).
Finally in the methods of adjustment the subject is instructed to adjust the stimulus intensity to a certain threshold e.g. detection or pain threshold [Gracely, 1999].
Since QST is psychophysical study the sensation intensity is rated by subject. This is typically done on a Visual Analog Scale (VAS), which is numeric scale typically between 0 and 10. In most pain studies, which do not investigate subthreshold sensations, the VAS scale is anchored as 0 being "No Pain" and 10 is "Maximum imageable Pain". Since VAS is a subjective measure, some things must be considered when using it. Most subjects will try and 'fill the scale' during tests, this will cause a problem with repeated stimulations where an individual subject may rate the same sensation differently [Gracely, 1999].
Gracely (1994) also suggest treating the subjective pain as a multidimensionel sensation. This implies not only the

pain sensation itself but also how the pain alters the emotional state of the subject. However, this thesis will focus on pain as solely one dimensionel, since most psychophysical studies only uses this, as an example see the next section.

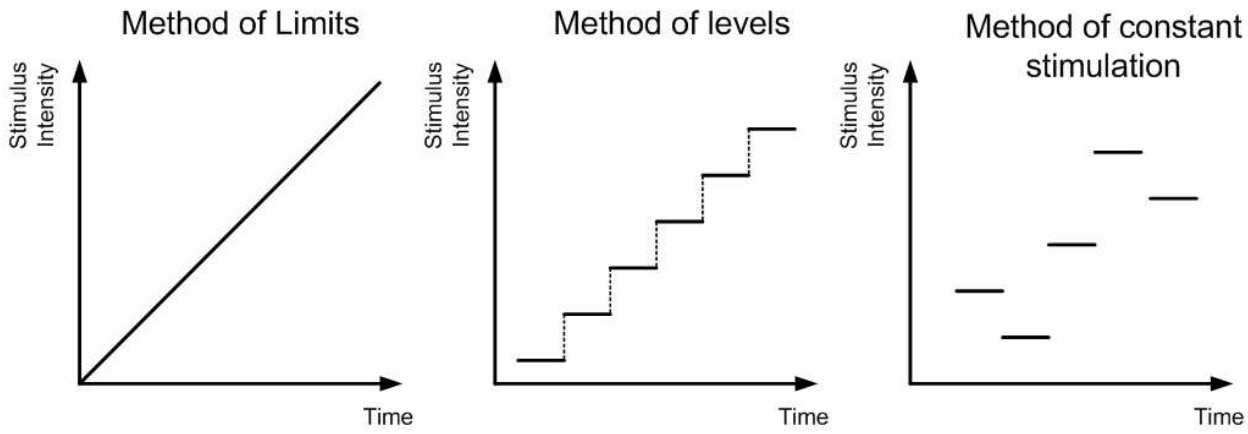

Figure 1.2: The figure illustrates different methods of threshold detection. The method of limits utilizes an increasing (or decreasing) stimulus intensity, the subject must rate whenever the intensity becomes higher or lower a certain threshold depending on the test being made. The method of levels uses increasing or decreasing levels of stimulus intenties during which the subject must rate the sensation evoked. The dotted line shows how the methods of level resemples a staircase simulation. The methods of constant stimulus uses constant stimulus levels and randomised orders to which the subject must rate the sensation evoked.

1.1.2 'Offset analgesia'

One example of a slightly different QST study is a study investigating so called offset analgesia, a phenomenon first defined and named by Grill and Coghill in 2002 [Grill and Coghill, 2002] and reproduced by other authors using the same term to define this phenomenon [Derbyshire and Osborn, 2008]. Subjects are instructed to report their pain rating on a 0-10 VAS scale (Visual Analog Score) to a thermal stimulus. Offset analgesia occur when the intensity of a noxious stimulus is slightly decreased, leaving the stimulus intensity still above pain threshold. The change of perceived sensation reported by the subject is disproportional to the actual change in stimulus intensity. The decrease in VAS score reported is up to 271 % larger than the actual decrease in stimulus intensity [Grill and Coghill, 2002].
So far no exact reason for the phenomenon has been described, however, some researchers believe that "... an active analgesic mechanism may be engaged during the termination or reduction of a noxious stimulus." [Grill and Coghill, 2002] and it is not mediated by mechanism different from both adaption or habituation [Derbyshire and Osborn, 2008]. The central inhibitory mechanism, which most likely affects and possibly causes offset analgesia may be used to investigate some of the mechanism of chronic pain [Grill and Coghill, 2002], and therefore possibly help to provide new methods to relieve and treat chronic or neuropathic pain. Evidence from fMRI studies indicate that offset analgesia is mediated by inhibitory centers found in the region of the periqueductal grey and rostral ventromedial medulla [Derbyshire and Osborn, 2009], areas known to be involved in inhibitory mechanisms [Derbyshire and Osborn, 2009]. Grill and Coghill suggested that offset analgesia might also be a mechanism to increse the temporal contrast of the painful stimulus, meaning that any change in intensity easier would be detected [Grill and Coghill, 2002].
Yelle et al. (2008) further investigated whether it was plausible that offset analgesia is a temporal mechanism to increase the contrast of stimulus intensity [Yelle et al., 2008]. Furthermore they investigated whether offset analgesia is a purely temporal mechanism or it has spatial properties as well. This was done by testing if applying two simulateneous painful stimuli, and then lowering the intensity of one or both. First both painful intensities was lowering to test whether the offset analgesia created was significantly different that the offset analgesia which can be produced with a single stimulus [Yelle et al., 2008]. Second it was tested if creating offset analgesia at only one stimulus site would

affect the pain rate at the other stimulation site. Yelle et al. (2008) found that offset analgesia includes both temporal and spatial mechanisms, since offset analgesia at one site could modulate the sensation at another [Yelle et al., 2008]. Based on their findings they concluded that offset analgesia is a central mechanism for better temporal contrast perception. Furthermore, they foreseen that further knowledge about this phenomenon may lead to better understanding and possibility treatment of pain disoders [Yelle et al., 2008].

1.2 Stimulators in psychophysical studies

To conduct thermal QST studies or offset analgesia studies similar to those seen in the litterature [Grill and Coghill, 2002] [Yelle et al., 2008] [Derbyshire and Osborn, 2008] one most utilize a thermal stimulator. In the past many different types of stimulators have been used, two main cathogories exist contact and non-contact stimulator. Contact stimulators is typically of the Peltier type, where a transducer is either cooled or heated based on the current sent through it. One such device is the CHEPS Medoc system which has been used in several studies [Grill and Coghill, 2002] [Yelle et al., 2008] [Derbyshire and Osborn, 2008] [Granovsky et al., 2008], this system utilizes the Peltier principle and has a built-in temperature control, which heats the skin to a desired temperature and maintains it at that level. During the stimulation the temperature can be increased or decreased as desired.
Non-contact stimulators are typically radiant heat from an infrared lamp. This principle has been modernised and is used in lasers, which also are used for non-contact stimulations [Gracely, 1999]. Contact probes posses a number of disadvantages most importantly the fact they not only elicit painful thermal, but also slight tactile sensations. Besides this the rise time of such often contact probes are typically quite low (in the magnitude 10's $^{\circ}$C per second) [Granovsky et al., 2008], whereas lasers are able to heat with a much higher rise time, e.g. CO_2 lasers can give rise time in the magnitude of 1000 $^{\circ}$C per second. The SMI (Center for Sense-Motor Interaction) pain lab has for several years applied lasers as a thermal stimulator for pain and tactile research [Arendt-Nielsen and Chen, 2003].

1.3 Lasers as a thermal stimulator

The use of lasers in both medicine and biomedical research has increased during the past three decades [Welch and van Gemert, 1995a]. Several types of lasers have been used with different optical properties. Especially infrared laser have been used due to their ability to deliver large amounts of energy in very short time. Such properties are useful as a surgical tool and in research as a method of delivering a high intensity noxious stimulation. The infrared laser used range from near-infrared ($\sim 1\mu$m) to far-infrared lasers ($\sim 10\mu$m). The optical properties of such laser depend on their wavelength, near-infrared laser such as the diode laser typically have longer penetrations depth, than far-infrared lasers such as the CO_2 laser.
When using lasers as a method of delivering a noxious stimulus most researchers simply deliver a short high powered burst of energy to the skin increasing the temperature above a certain threshold (43 ^{o}C [Treede et al., 1995]) so nociceptors are activated. The CO_2 laser has the advantage of delivering extremely high amounts of energy, furthermore the CO_2 laser has very short penetration into the skin, causing the energy from the laser to be absorbed very superficial in the skin, not damaging any deeper structures. However, such lasers does not have a temperature control system, which controls the target temperature. Instead you only control the intensity of the laser output (Power (W) of the emitted light). This means that without such control the lasers can easily create skin injuries and stimulate either more or less intense than intended. In fact skin injuries has not been a rare scenario in the early pain research using lasers [Granovsky et al., 2008].
Using lasers as a thermal stimulator instead of contact probes have another advantage. The size of the stimulation site can be varied using lasers, and the stimulation site can rapidly be moved to different sites of the skin using a scanner head. This opens the possibility for conducted psychophysical studies which are impossible to do with contact devices, such as graphesthesia [Mørch et al., 2008]. Furthermore, this will give an opportunity to conduct further examination of the mechanism behind psychophysical conditions as distal inhibition [Quevedo and Coghill, 2007]. One place where lasers might have a disadvantages compared to CHEPS devices is the lack of non-contact cooling. Meaning all cooling after laser stimulation will be passive, caused by heat transport into the surrounding tissue.
To sum up, lasers as thermal stimulators offer both advantages and disadvantages. The advantages include higher

temperature rise rates, and the possibility to vary the of the simulated skin area. The disadvantages include that lasers offer no means of active cooling, meaning only heat studies can be performed and the temperature fall rates will be lower than that of contact probes; and commercially available laser systems does not offer temperature control during the stimulation.

1.4 Laser control system

A control system which can control the laser to heat the skin to a desired temperature but also control the skin temperature within narrow ranges will provide the possibility to conduct new both electrophysical and psychophysical studies. Especially quantitative sensory tests require very accurate stimulus paradigms and so does does offset analgesia, since the analgesic effect occur when the temperature is lowered 1 °C. The laser can be controlled by measuring the skin temperature and subtracting this from the desired temperature, thus determining the error. Based on the error the laser is controlled, so called close-loop control [Haugen, 1994] [Franklin et al., 1994], see more in appendix B.
So far offset analgesia has only been reproduced using contact stimulators [Grill and Coghill, 2002] [Yelle et al., 2008] [Derbyshire and Osborn, 2008] [Derbyshire and Osborn, 2009], if offset analgesia can be evoked by using temperature controlled laser stimulators, this will increase the flexibilities and possibilities in similar psychophysical studies. E.g. due to possibilities of rapidly varying the size of the stimulation area and location. This could increase the possibilites of expanding by the existing work on the spatial components of offset analgesia, such as [Yelle et al., 2008], investigating how different spatial stimulation paradigms can modulate the analgesic effect.
For the reasons listed above, it is proposed to develop a non-contact system to thermally stimulate the skin. This system is intended for use in psychophysical studies and a method of using a non-contact stimulator in studies, which previously only were possible using a contact stimulator. The developed system should be able to elicit purely thermal sensations without touching the skin and control the skin temperature to exact levels.

1.5 Aim

The sections above lead to the following aim for this thesis.
The development of a temperature controlled non-contact thermal stimulator to conduct psychophysical studies.
This includes the development of a system to monitor and maintain skin temperature during infrared radiation. The developed system is intended as a different way of conducting studies which previously only was possible using a contact heat evoked potenial stimulator (CHEPS), such as offset analgesia studies. It will be investigated whether lasers with their advantages and disadvantages, is able to do this. For the developed system to be a succesful, it must be able to evoke similar results seen as with contact stimulators. As a measure of this, the possibility of evoking offset analgesia [Grill and Coghill, 2002] will be used as reference. The system must be able to make repeatable stimulations in different subjects.
Since the system will be used to evoke offset analgesia, the accuracy of the system be higher than 1 °C. The accuracy is defined by two parameters; first the mean temperature error at steady state and the fluctuations during steady state. Steady state meaning when the controller output has reached a steady level, in response to a certain set point, and the mean controller output does not increase or decrease. The difference between mean temperature during steady state and the desired temperature should not be greater than 0.1 °C, meaning less than 10 % of the step size used to evoke offset analgesia. The second parameter is the size of any temperature fluctuations during steady state. Since some error sources are expected, such as movement of the stimulation area, and varying levels of blood flow, some fluctuation must be accepted. The fluctuations is allowed to be twice the size of the steady state error (0.2 °C) so the skin temperature will oscillate around the desired temperature.
In previous offset analgesia studies different rise rate have been used ranging from 5 °C per second [Yelle et al., 2008] to 30 °C per second [Derbyshire and Osborn, 2008] [Derbyshire and Osborn, 2009]. In this thesis the goal for the rise time is set to 5 °C per second. In some QST studies using the determination of heat pain threshold is done by contionously increasing the temperature at a fixed rate [Shy et al., 2003], therefore the system should allow the user to change the heating rate.
Since the system will be used for psychophysical studies a pain rating technique must be used, and to ease data analysis

the pain rating should be recorded simultaneously along with stimulation parameters, such as desired skin temperature, actual skin temperature, and so on. For this reason a custom made VAS scale is used, which gives a voltage output in the range 0-10 volts corresponding to ratings of 0-10.
In order to prevent skin damage, the control system should prevent the temperature becomes too high, if the this occur the system should shut down the laser. In fact if the skin temperature becomes unrealistic cold, the laser should be shut down as well, since this could indicate that the body part being stimulated has been moved, or that the skin temperature measurement is corrupted.
The development should aim for highest possible temporal resolution, which the used hardware allows.
When controlling a process, such as temperature, there is the change of overshoot. During heating overshoot will cause the temperature to exceed the steady state value before settling. High overshoot could e.g. produce slight offset analgesia, due to the decreasing temperature until steady state is reached. The overshoot should be limited to the same magnitude as the steady state oscillations, (0.2 ^{o}C). The settling time after any overshoot be short (< 1 second), meaning the overshoot should only persist for that period before the controller settles at a steady level.
The developed system must be implemented on a Laptop and have a easy-to-use graphical user interface (GUI). On the GUI all relevant settings must be editable, including stimulation parameters. The stimulation is solely controlled via the GUI, except the stimulation site which is done by moving the bodypart being stimulated.

1.5.1 Specification of requirements

Below is found a list of requirements which the developed system must fulfill

- Measure the skin temperature
- Maintain the mean skin temperature within 0.1 °C of the desired temperature
- Steady state fluctuations less than 0.2 °C
- Ability to evoke offset analgesia
- Record intensity rating from subject
- The highest possible temporal resolution (less than 1 second)
- Limited overshoot (< 0.2 °C), in the same order as any steady state fluctuations
- Short settling time (<1 second)
- Temperature rise time of 5 °C per second
- Controllable heating rate (set 0-5 °C per second)
- Prevent tissue damage, shut down laser if skin temperature is too high or too low
- Implement a GUI for easy use

1.6 Rationale

When developing a controller it is very useful to have a detailed knowledge of the process being controlled [Haugen, 1994] [Franklin et al., 1994], in this case laser heating of the skin. This knowledge can be expressed as a mathematical model which describes how e.g. changing the laser power will change the skin temperature. Depending on the controller principle (open- vs. closed-loop) such a model can be a neccesity. A mathematical model also gives the developer the possibility to test a controller before it is implemented.
The thermal stimulation principle of contact stimulator is fairly simple, the probe is touching the skin, and according to the zeroth law of thermodynamics the thermal energy will be conducted from the probe into the skin (if the probe is warmer than the skin) and via conduction transported to locations of the heat sensitive nociceptors. However, when

using lasers, the energy from the stimulator is not absorped at the surface and conducted from there. Instead the photons from the lasers will penetrate into the skin where the photons either are scattered or absorped. The number of scatterings before the photon is absorped depends on the wavelength of photons.
Depending on the number of scatters before the photon is absorped, modelling the heat source can be done using a simple analytical expression, if the photon is more likely to be absorped before any scattering occurs; otherwise a more complex model, such as the Monte Carlo random walk method, must be used.
Besides developing a mathetical model for the controlled process, it also important to know some physiological and anatomical parameters, such as receptors depth. Therefore, the model must also provide the means the investigate this. If the developed model is sophisticated enough this can be investigated based on the model.
Some studies have investigated the laser skin interaction using 1D models [Bromm and Treede, 1983] [Treede et al., 1995] [Al-Saadi et al., 2006]. But in the long run the developed system will be used for different studies including some investigated spatial properties and sizes of receptive fields, therefore, the developed model must be applicable to support this further development of the system.
The developed model must be validated through experimental trials. Through such trials it must be investigated how the temperature at the skin surface is related with the sensations reported by the subjects in different skin type.
Based on existing litterature which have used the CO_2 laser in pain research as a method of noxious stimulation of the skin [Bromm and Treede, 1983] [Treede et al., 1995] [Treede et al., 1998] [Granovsky et al., 2008] [Arendt-Nielsen and Chen, 2003] and the fact the heat source can be modelled using a simple analytical expression this laser type will be used to develop the model.

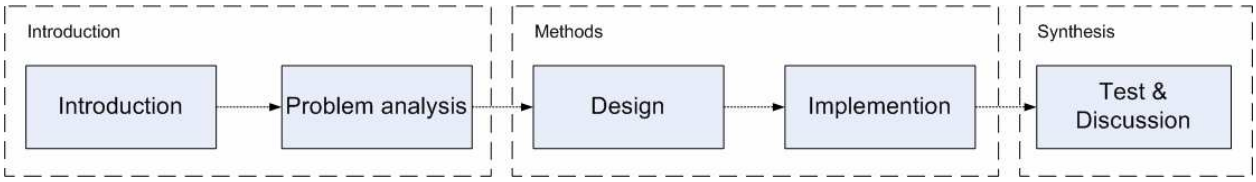

Figure 1.3: The figure illustrates the structure of the rest of this thesis. After this introduction an analysis will be made to invesigate the thermal properties of the skin during laser stimulation, developing a mathematical model. Based on this analysis the system will be design and implemented. The developed system will be tested, including investigating whether offset analgesia can be evoked. Finally the thesis will be summarised and the results discussed.

In the next chapter a detailed model of the laser skin interaction will be developed. Based on the model it will be investigated how the skin temperature changes during laser stimulation, how the heat is transported into the skin, and how deep the heat sensitive nociceptors are found in the skin.

Problem analysis 2

As stated in the previous chapter a study must be conducted before the development of the system can begin, (section 1.6). This study will focus on the development of heat transfer model for two main reasons; first to investigate how skin temperature increases during laser stimulation. Second to investigate the physical and anatomical aspects behind laser stimulation of the human skin, including the sensation reported by subjects exposed to laser stimulation.
First a brief discussion of exiting models is made and the reasons why such models are inadequate. Then a new model is developed, validated and based on the model the investigations listed above are performed. Finally a conclusion sums up this chapter, and the result to be used in the further system development.

2.1 Existing heat transfer models

As mentioned the penetration depth of the emitted laser light depends on the wavelength of the photons. Infrared light form CO_2 lasers has a very short penetration depth (20 μm), causing most of the energy to be absorbed in the upper layer of the epidermis [Bromm and Treede, 1983] [Brugmans et al., 1991]. Since the nerve endings of heat sensitive nociceptors are located deeper than the light from a CO_2 laser penetrates, the thermal energy must be conducted into the skin to activate these nociceptors. Tillman et al. (1995) investigated the nociceptor depth of C fibers in monkeys and found the average to be 201 μm in hairy skin. Therefore part of the delay in the transduction process leading to action potentials in nociceptors, must be due to conductance of the thermal energy through the most superficial skin layers.
In order to predict the temperature at different depths evoked by a laser stimulus, mathematical modeling is an option. Previously simple 1D heat transfer models have been used for this [Bromm and Treede, 1983] [Brugmans et al., 1991] [Treede et al., 1995] [Al-Saadi et al., 2006]. However, those models did not incorporate different thermal properties of the different skin layers e.g. epidermis and dermis [Bromm and Treede, 1983] [Brugmans et al., 1991]. Furthermore, the 1D models only predicted the heating directly below the center of the laser beam. Theoretically, a small beam width ($\sim$ 1 mm) might not even activate any nociceptors. Since the activation threshold is not reached if the temperature at the location of the nociceptor is too low because the energy is absorbed in between nociceptors. Instead a model should incorporate the spatial profile of the beam. Furthermore, the model must allow investigation of the spatial dispersion of the heat both perpendicular and parallel to the skin surface, as mentioned in section 1.6; for these reasons 1D models are obsolete.
Some 2D axial and 3D models exist [Verhey et al., 2003] [Gowrishankar et al., 2004], but these models were developed for other purposes than pain stimulation, for instance prevention of tissue damage or ablation of malignant tumors [Verhey et al., 2003]. The model developed by Verhey et al. (2003) incorporates an interstitial heat source and this is modelled very different compared to a radiant heat sources such as lasers. Furthermore, this and other models treat the skin as one bulky tissue with similar thermal and optical properties in the entire skin. Assuming this similarity is not correct [Wilson and Spence, 1988] [Jiang et al., 2002] [Gowrishankar et al., 2004] [Seteikin and Krasnikov, 2006]. However, some techniques proposed by Verhey et al. (2003) can be used as inspiration in the model development, such as the method of solving the model and applied software tools (COMSOL Multiphysics and Matlab).
The objectives of this preliminary study were to develop a model of the temperature distribution in the skin and subsequently to investigate the temperature distribution at different depths. Secondly to investigate the correlation between the predicted temperature and the pain intensity reported. To simplify the controller design based on the model the developed model it would be appropriate to use software which allows the developed model to be combined with controller developing software, such as Simulink.

2.2 Finite element model development

The bioheat equation first proposed by Pennes in 1948 (Eq. 2.1) is intended as a way of describing heat transport in biologic tissue. Therefore, it is a very suitable to base the laser-skin model on.

$$\rho c \frac{\partial T(\mathbf{r},t)}{\partial t} = \nabla(k\nabla T(\mathbf{r},t)) + \rho_b c_b w_b (T_{art}(\mathbf{r},t)) - T(\mathbf{r},t) + Q(\mathbf{r},t) \tag{2.1}$$

[Pennes, 1948]
T is the tissue temperature, t is time, ρ is the tissue density, c is the specific heat capacity of the tissue, k is thermal conductivity, w_b is the density of the blood, c_b is the specific heat capacity of blood, w_b is the tissue average volumetric blood perfusion, T_{art} is the temperature of the arterial blood, and Q is the heat source. Ignoring any temperature changes due to perfusion this reduces to Eq. 2.2

$$\rho c \frac{\partial T(\mathbf{r},t)}{\partial t} - \nabla(k\nabla T(\mathbf{r},t)) = Q(\mathbf{r},t) \tag{2.2}$$

The simplified model (Eq. 2.2) is easiest to solve numerically. This was done by finite element modeling (FEM; COMSOL multiphysics, Stockholm, Sweden). COMSOL multiphysics was used for several reasons. First, other authors have used the software in similar problems [Verhey et al., 2003]. Second, due to COMSOLs ability to be combined with Matlab including the fact that a numerical model can be exported to Simulink and used in the controller design.
The numerical model was created using a 2D axial symmetrical geometry. The model is comprised of two vertical rectangles placed on top of each other each representing epidermis and dermis respectively, see figure 2.1. The temperature change (ΔT) was normalized setting the initial temperature change to 0 °C, ignoring any phase changes. The temperature of the lower boundary is kept constant at the initial temperature (ΔT = 0 °C). The upper boundary (the skin surface) is set as thermally insulated, ignoring any heat transfer into the adjacent air.
Due to different thermal properties of the epidermis and dermis, see table 2.1, the thickness of epidermis was measured in order to create a model with accurate geometry. The epidermal thickness of each subject was measured at two skin sites on the left volar forearm and two sites on the left palm using a Derma scan, high resolution (25x60 μm) ultrasound scanner (50 MHz) [Cortex technology, 2007]. The sites were shaved prior to the assessment.
To validate the model experimental trials will carried out using a CO_2 laser, thus the characteristics of this laser was entered in the model. The spatial beam profile of the laser was modeled as Gaussian. The light absorption in the tissue is modeled using Beers law, which is a good approximation when using a high absorption source like the CO_2 laser. Combining these conditions, the heat source, Q is modeled as outlined in Eq. 2.3. P_{in} is the laser power setting, μ_a is the absorption coefficient of the tissue (50000 m^{-1}), z is the depth from the tissue surface, σ is standard deviation of the Gaussian beam profile equal to 2.85 mm for the used laser. The thermal constant and geometry used in the model is found in table 2.1 and figure 2.1.

Constant	**Epidermis**	**Dermis**	**Unit**
ρ (density)	1200	1200	kg/m^3
c (specific heat capacity)	3600	3800	J/(kg*K)
k (thermal conductivity)	0.21	0.58	W/(m*K)
Thickness	Hairy: 49.6 Glabrous: 133	1000	μm

Table 2.1: The table displays the constant used in the Finite Element Model. The density, specific heat capacity and thermal conductivity were found in Wilson and Spence (1988). The thickness are based on high resolution ultrasound scans.

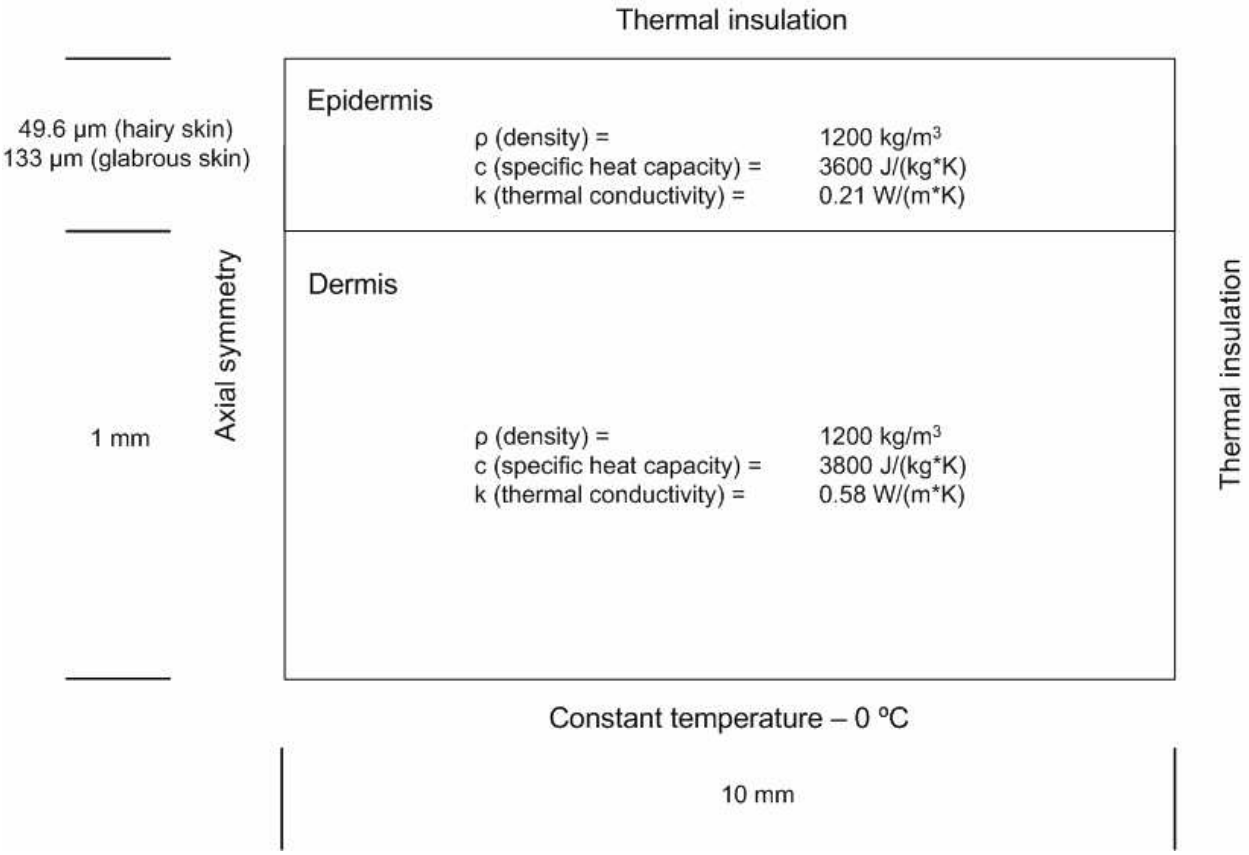

Figure 2.1: The figure illustrates the geometry and general model settings in Finite Element Model. The geometry is comprised of two rectangles (subdomains) the upper corresponding to the epidermis, and the lower to the dermis. The thermal properties of each subdomain can be seen in the figure. The boundary conditions of the four boundaries is also seen. The thermal constants were found in Wilson and Spence (1988).

$$Q(\mathbf{r},t) = P_{in}\mu_a exp(-\mu_a z)\frac{1}{\sigma\sqrt{2\pi}}exp(\frac{-r^2}{2\sigma^2}) \tag{2.3}$$

In order to validate the model a number of subjects was tested, this was carried out as a scientific experiment.

2.3 Model validation

2.3.1 Subjects

Sixteen healthy subjects (age range 23-34 years, 9 females, 7 males) participated in this study. Informed written consent was obtained from all subjects in accordance with the Helsinki declaration and approval for the study was obtained from the local ethics committee (N20080026).

During the experiments the subjects were seated on a chair with their left hand and forearm placed flat on a table with the volar forearm perpendicular to the laser beam. The subject and investigator wore protective goggles for the duration of the experiment. An inter-stimulus interval of one minute was used to ensure sufficient cooling of the skin between stimuli.

2.3.2 Laser stimulation, infrared recording and subjective pain rating

Heat stimuli were produced by a Synrad Firestar 100 W CO_2 (wavelength 10.6 μm) laser controlled by a Synrad UC-1000 control box, and a custom made Labview (National Instruments, Austin, Texas, USA) application. The laser power was calibrated before each experiment. Two output power levels were used, 1W and 5W. Five stimulation energies were applied by varying stimulation duration and intensity; 0.2J (1W, 0.2s), 0.4J (1W, 0.4s), 0.6J (1W, 0.6s), 0.8J (1W, 0.8s), and 0.6 J (5W, 0.12s).
An infrared camera (Thermovision 900, Agema Infrared system, Sweden) continously monitored the skin temperature (30 Hz frame rate). A 1x1 cm aluminum square was placed on the skin adjacent (approx. 5 cm from the stimulation site) to the stimulation site for spatial calibration in the infrared recordings.
The volunteers were instructed to press a button as soon as any sensation was felt, to give an indication of the latency of the transduction process. Furthermore, the subjects were instructed to rate the pain intensity from the laser stimulation on a Visual Analog Scale (VAS) anchored by '0' as No sensation, '5' as Pain threshold, and '10' as Maximum pain.

2.3.3 Experimental protocol

A total of four stimulation sites was used; two in hairy skin, in the volar left forearm; and two in the glabrous skin of the left palm. The order of stimulation sites was randomized in a balanced way so no site was ever stimulated at two consecutive stimulations. A single stimulation paradigm including all four stimulation sites. In each paradigms the energies of the 1 W stimulations were randomised. In the 5 W paradigm no randomisation was made. Each of the 1 W paradigms were tested 8 times, meaning a total of 32 stimulations. Each of the 5 W paradigms was tested 4 times, meaning a total of 16 stimulations. For overview see table 2.2.

Repititions at each site	**Hairy**	**Glabrous**
Site number	1 & 2	3 & 4
0.2 J (1W, 0.2s)	2	2
0.4 J (1W, 0.4s)	2	2
0.6 J (1W, 0.6s)	2	2
0.8 J (1W, 0.8s)	2	2
0.6 J (5W, 0.12s)	4	4

Table 2.2: The table displays the experimental protocol used. Each stimulation at 1 W was delivered twice at each site. Meaning a total of 4 stimulations in hairy skin and 4 stimulations in glabrous skin, and a total of 64 stimulations. Each stimulation at 5 W was delivered 4 times at each site, meaning 8 times in hairy skin and 8 in the glabrous skin, and a total of 32 stimulations.

2.3.4 Data analysis and statistics

Spatial surface temperature profiles at the center of the stimulation sites were obtained from the thermographic images starting 1 s before laser onset and lasting for 11 s. The temperature profiles were normalized to the surface skin temperature at the stimulation site 1 s before laser onset. Mean surface temperature profiles, including a 95 % confidence interval, were calculated for each stimulation paradigm and for each skin type (glabrous or hairy) and compared to results from the FEM model.
To compare the model and the mean experimental data; the maximum temperature profiles were tested for correlation. The correlation coefficients between the reported VAS score and modeled temperature at all depths (5 μm step) were calculated to estimate the depth of the heat sensitive nociceptors in different skin types.
Differences between pain intensities and response latencies between skin types were assessed using a non-paired t-test, since not all stimulations could be rated by the subjects, resulting in unequal sample sizes.
All results are presented as mean $\pm$ one standard deviation (SD).

2.4 Experimental and modelling results

2.4.1 Sensations and latencies reported

The reported sensations in the glabrous skin were generally lower than in the hairy skin (Tables 2.3 and 2.4). A non-paired t-test comparing equal stimulation energies, showed that the differences were significant for stimulation energies above 0.2 J ($p < 0.05$). At the 0.2 J energy, p was 0.81.

Skin type	**Glabrous skin** (site 1 & 2)			
Duration (sec)	0.2	0.4	0.6	0.8
1W VAS	0.4±0.48	0.43±0.67	0.66±0.92	1.15±1.31
1W Latency (sec)	1.98±0.88	1.61±0.5	1.56±0.92	1.51±0.47
Duration (sec)	0.12			
5W VAS	1.29±1.73			
5W Latency (sec)	1.34±0.48			

Table 2.3: The table displays the reported sensations and latencies in glabrous skin, the results are presented as mean ± SD. Five different stimulation energies were tested in both glabrous and hairy skin. Five energies were tested based on a 1W power setting and four different duration (0.2s, 0.4s, 0.6s, and 0.8s) and one 5W power setting (0.12s)

The reported latencies in the glabrous skin were generally higher than those in the hairy skin (Tables 2.3 and 2.4). A non-paired t-test of equal stimulations energies, showed that the differences were significant for stimulation energies above 0.2 J ($p < 0.05$). At the 0.2 J energy, p was 0.60.

Skin type	**Hairy skin** (site 3 & 4)			
Duration (sec)	0.2	0.4	0.6	0.8
1W VAS	0.48±0.68	1.23±1.34	2.01±1.58	2.97±1.86
1W Latency (sec)	1.69±1.13	1.3±0.37	1.21±0.2	1.15±0.32
Duration (sec)	0.12			
5W VAS	4.82 ±1.89			
5W Latency (sec)	0.55±0.26			

Table 2.4: The table displays the reported sensations and latencies in hairy skin, the results are presented as mean ± SD. Five different stimulation energies were tested in both glabrous and hairy skin. Five energies were tested based on a 1W power setting and four different duration (0.2s, 0.4s, 0.6s, and 0.8s) and one 5W power setting (0.12s)

	Glabrous skin (site 1 & 2)		**Hairy skin** (site 3 & 4)	
Site	- 1 - Root of thumb	- 2 - Root of lateral palm	- 3 - Volar forearm (5 cm from elbow)	- 4 - Volar forearm (10 cm from elbow)
Average epidermal thickness (mm)	0.101±0.038	0.164±0.071	0.049±0.012	0.050±0.017
Average pr. skin type (mm)	0.133±0.064		0.0496±0.014	

Table 2.5: The table displays the mean measured epidermal thicknes for all four site stimulated. All results are displayed as mean ± SD. The epidermal thicknesses were measured using a high resolution ultra sound scanner.

2.4.2 Maximum surface temperature

The temporal profiles of the maximum skin surface temperature are depicted in figures 2.2 and 2.3 (1W stimulations for glabrous and hairy skin respectively) and figure 2.4 (5W stimulations in both glabrous and hairy skin). It is evident that the majority of the modeled temperature profiles were found inside the 95 % confidence interval. Towards the end of the stimulus all profiles were within the calculated confidence interval. There was a strong correlation between the modeled temporal profiles and the experimental data $r > 0.95$ (except for the lowest energy tested (0.2J) where r was 0.9043.), for all cases the correlation was significant ($p < 0.0001$).

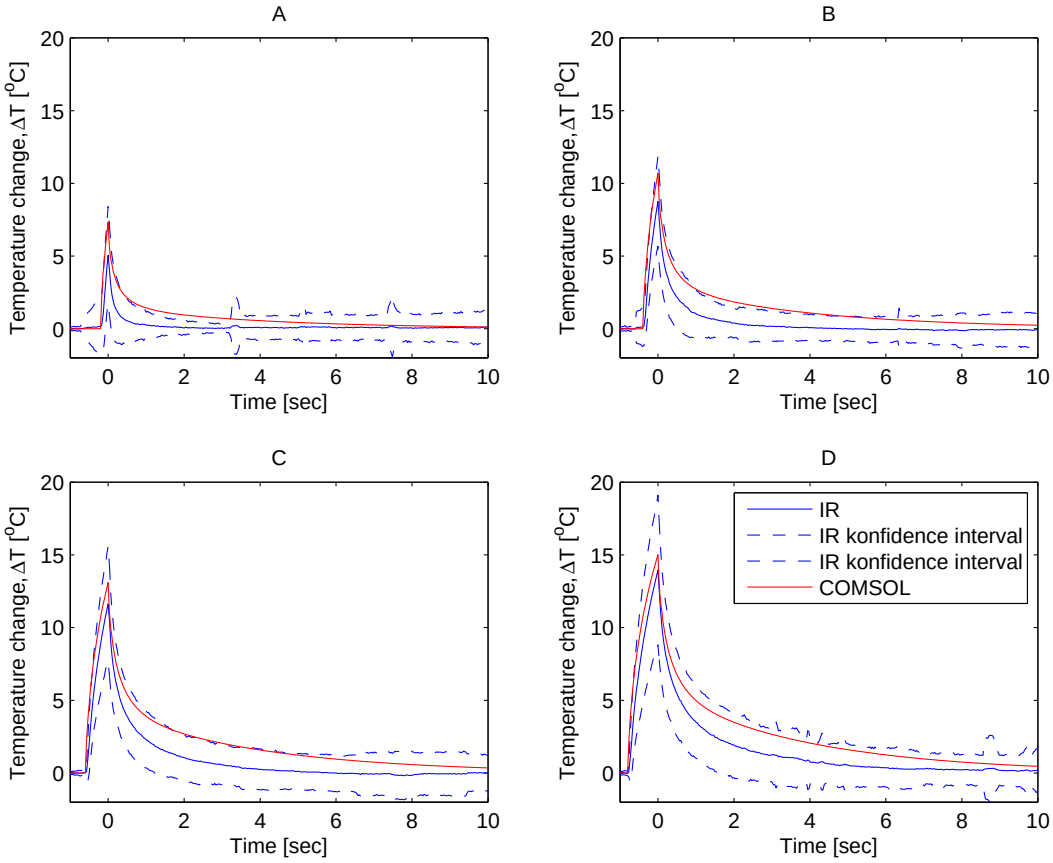

Figure 2.2: The figure illustrates the maximum surface temperature during laser heating and cooling in the glabrous skin. Time, t=0 is set at stimulus end (maximum surface temperature). The red plot is the prediction of temperature profile based on a finite element model. The blue is experimental data; the dashed lines are 95% confidence interval. The fluctuations seen in the cooling phase is due to arm movement artifacts. A) glabrous skin, 1W, 0.2sec, 0.2J B) glabrous skin, 1W, 0.4sec, 0.4J C) glabrous skin, 1W, 0.6sec, 0.6J D) glabrous skin, 1W, 0.8sec, 0.8J.

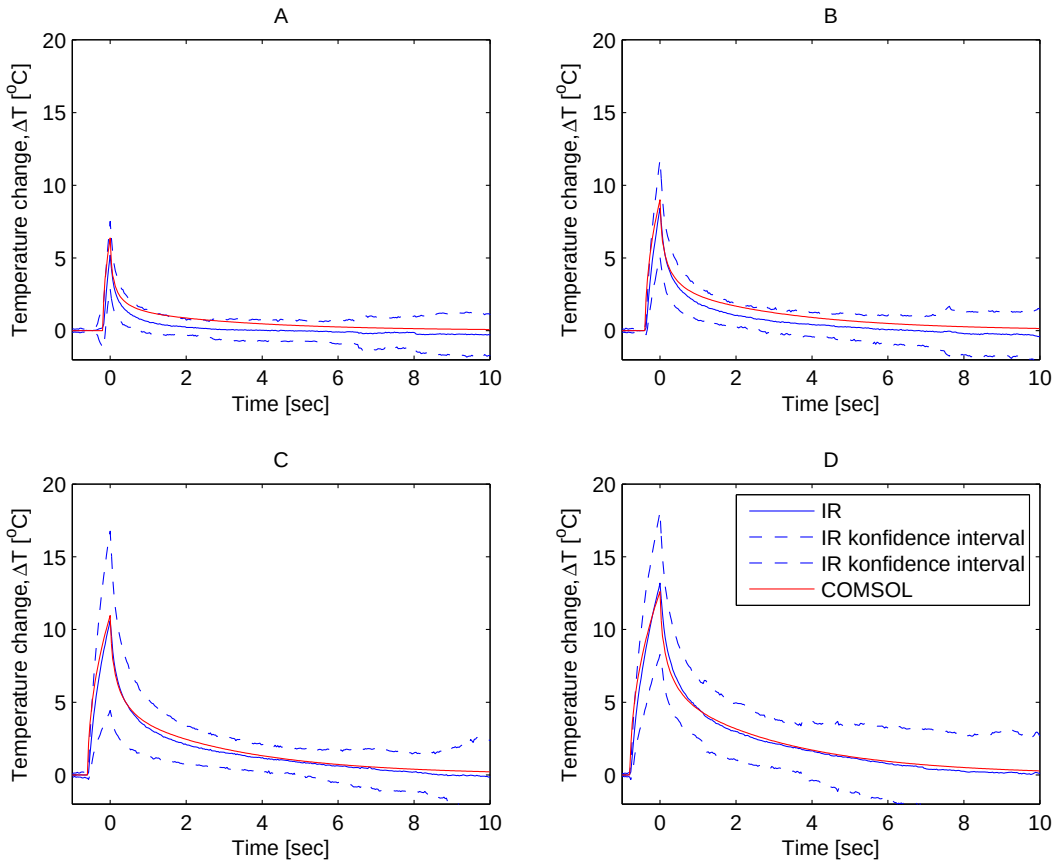

Figure 2.3: The figure illustrates the maximum surface temperature during laser heating and cooling in the hairy skin. Time, t=0 is set at stimulus end (maximum surface temperature). The red plot is the prediction of temperature profile based on a finite element model. The blue is experimental data; the dashed lines are 95% confidence interval. The fluctuations seen in the cooling phase is due to arm movement artifacts. A) hairy skin, 1W, 0.2sec, 0.2J B) hairy skin, 1W, 0.4sec, 0.4J C) hairy skin, 1W, 0.6sec, 0.6J D) hairy skin, 1W, 0.8sec, 0.8J.

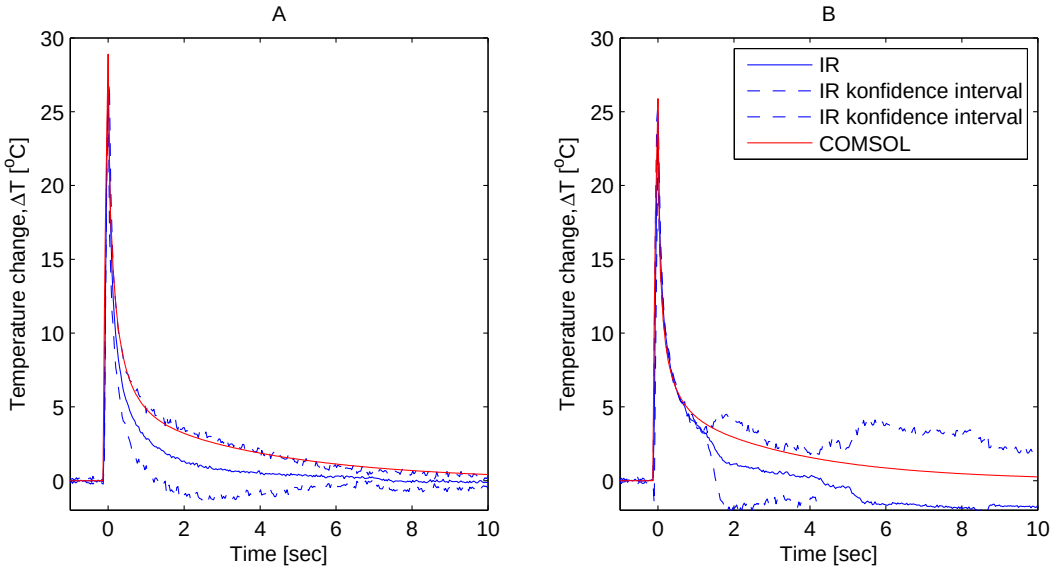

Figure 2.4: The figure illustrates the maximum surface temperature during laser heating and cooling. Time, t=0 is set at stimulus end (maximum surface temperature). The red plot is the prediction of temperature profile based on a finite element model. The blue is experimental data; the dashed lines are 95% confidence interval. The fluctuations seen in the cooling phase is due to arm movement artifacts. A) glabrous skin, 5W, 0.12sec, 0.6J B) hairy skin, 5W, 0.12sec, 0.6J.

2.4.3 Spatial temperature profiles

The spatial surface temperature profiles are depicted in figures 2.5 and 2.6, for the 1W stimulation in glabrous and hairy skin respectively, and figure 2.7 for the 5W stimulations in both glabrous and hairy skin. All spatial temperature profiles of the model were within the 95 % confidence interval of the infrared recordings.

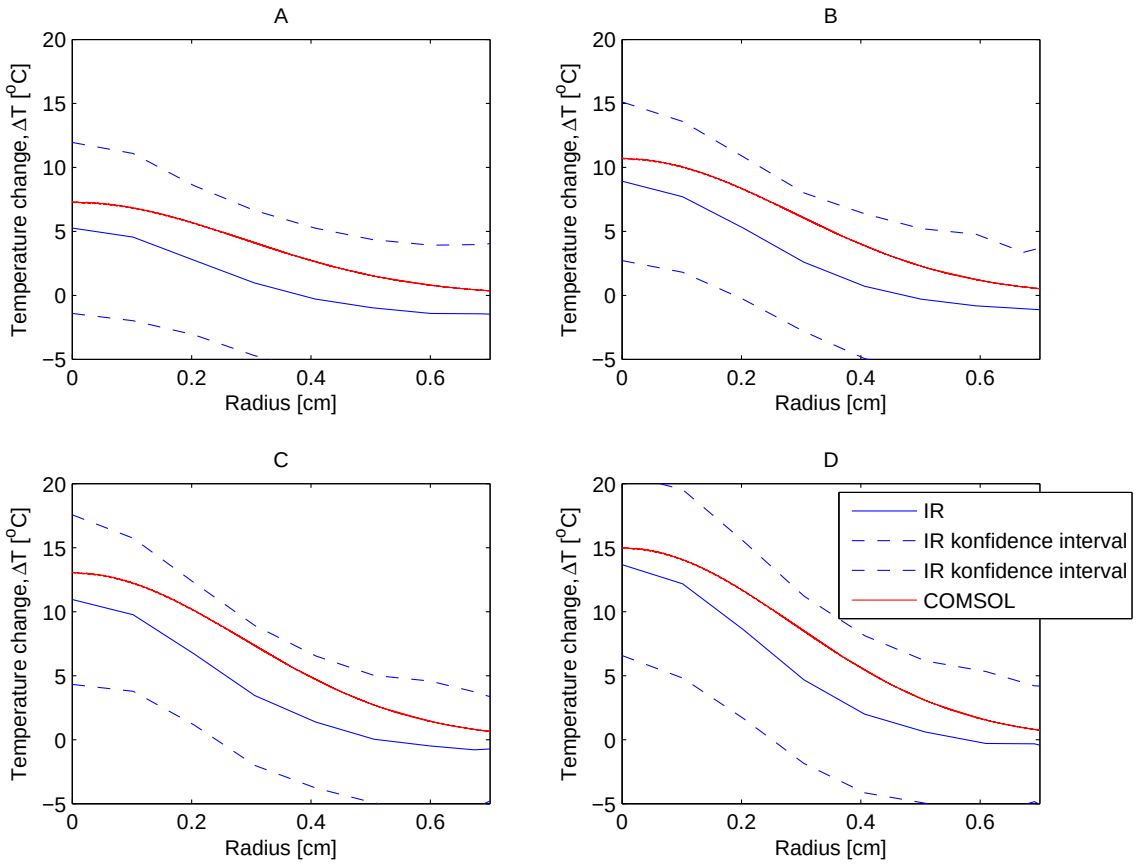

Figure 2.5: The figure illustrates the spatial surface temperature profile at stimulus end (maximum surface temperature) in the glabrous skin. The red plot is the prediction of temperature profile based on a finite element model. The blue is experimental data; the dashed lines are 95 % confidence interval. A) glabrous skin, 1W, 0.2sec, 0.2J B) glabrous skin, 1W, 0.4sec, 0.4J C) glabrous skin, 1W, 0.6sec, 0.6J D) glabrous skin, 1W, 0.8sec, 0.8J.

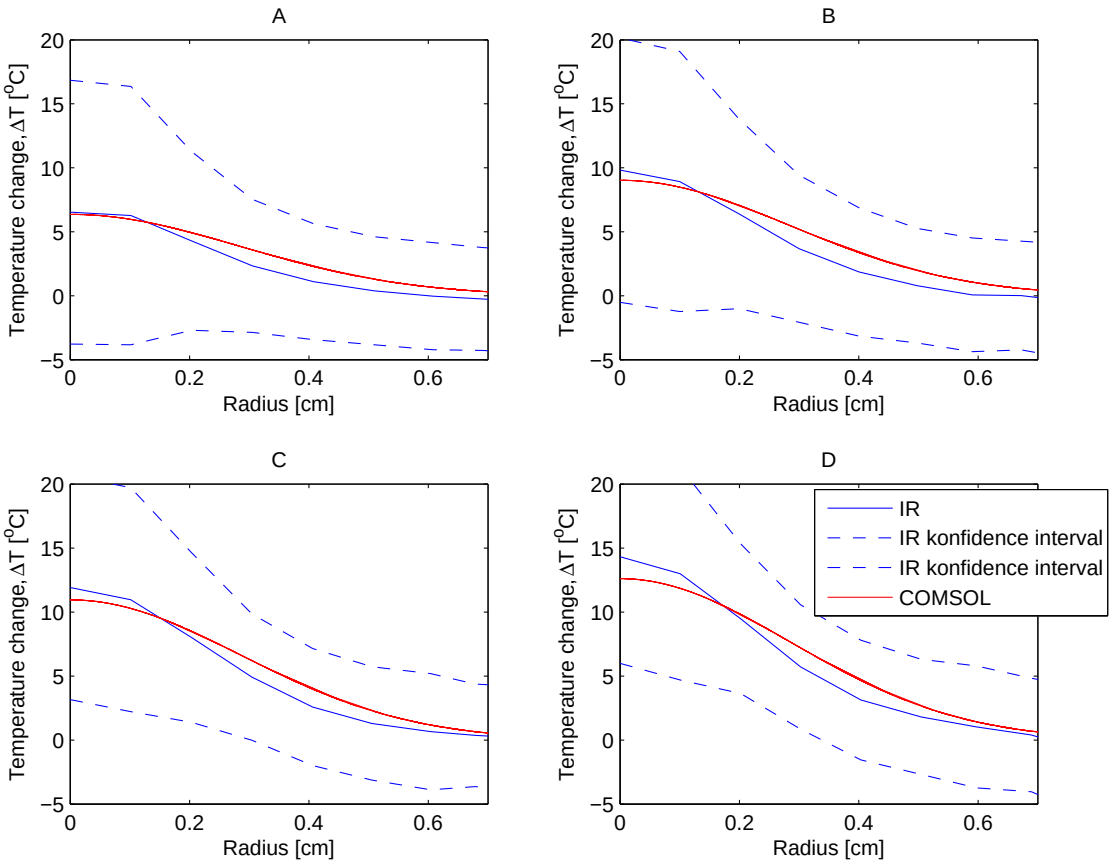

Figure 2.6: The figure illustrates the spatial surface temperature profile at stimulus end (maximum surface temperature) in the hairy skin. The red plot is the prediction of temperature profile based on a finite element model. The blue is experimental data; the dashed lines are 95 % confidence interval. A) hairy skin, 1W, 0.2sec, 0.2J B) hairy skin, 1W, 0.4sec, 0.4J C) hairy skin, 1W, 0.6sec, 0.6J D) hairy skin, 1W, 0.8sec, 0.8J.

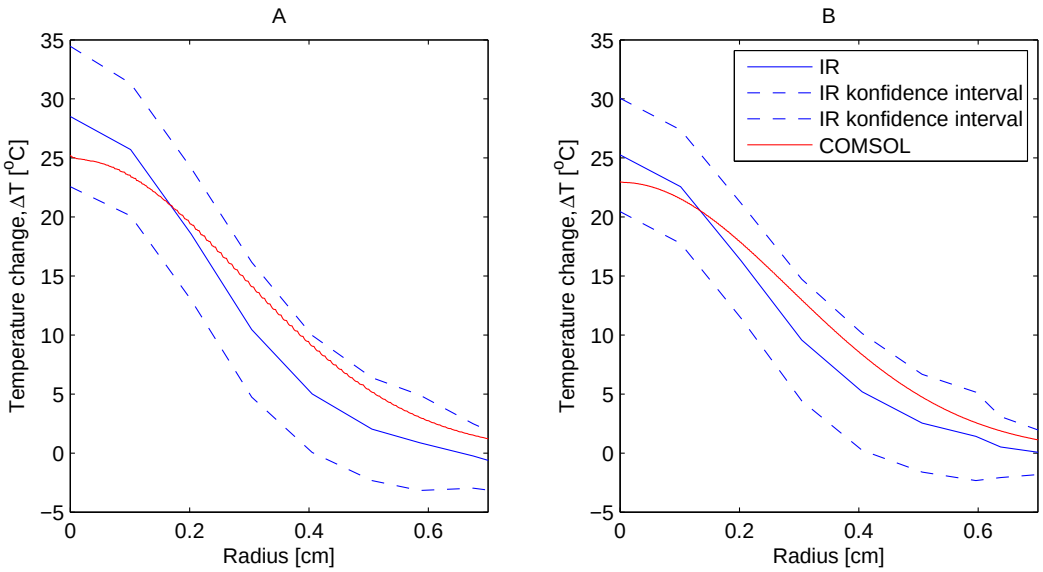

Figure 2.7: The figure illustrates the spatial surface temperature profile at stimulus end (maximum surface temperature) in the hairy skin. The red plot is the prediction of temperature profile based on a finite element model. The blue is experimental data; the dashed lines are 95% confidence interval. A) glabrous skin, 5W, 0.12sec, 0.6J B) hairy skin, 5W, 0.12sec, 0.6J.

2.4.4 Estimation of nociceptor depth

In hairy skin the strongest correlation was found for the temperature profile at ~ 50 μm and with only on distinct peak. For glabrous skin, two peaks in the correlation coefficients were found; one at ~ 50 μm but the strongest correlation was found at a depth of ~ 130 μm, see figure 2.8.

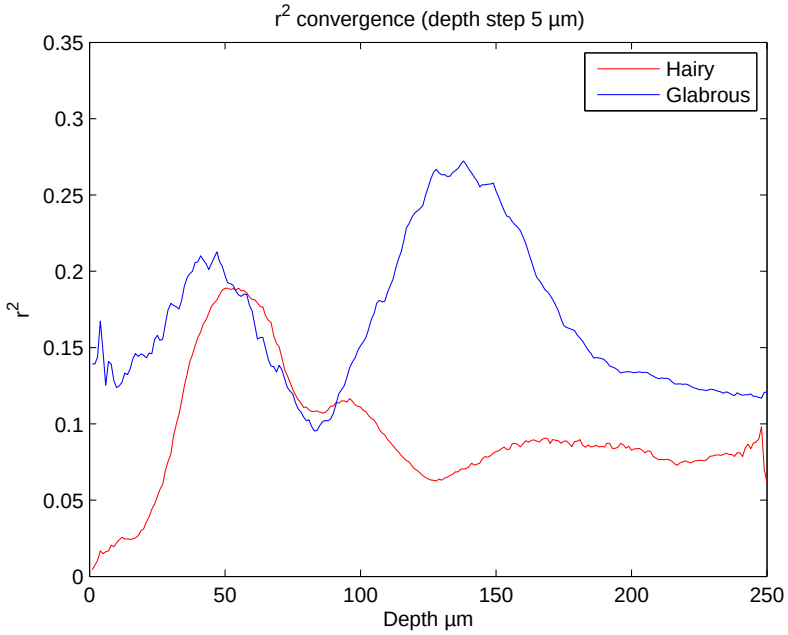

Figure 2.8: The figure illustrates how correlation (r^2) between the reported sensations depends on the depth. Due to high fluctuations of raw psychophysical data (VAS) a lowpass filter was applied to the plots to remove measuring artifacts. For hairy skin the highest correlation is found at ~ 50 μm and for the glabrous skin the highest correlation is found at ~ 130 μm.

2.4.5 Sub-surface temperature profiles

The temporal development in temperature of the surface and five different depths were computed from the FEM model, see figure 2.9. In the figure only the 0.6 J stimulation energies are displayed, this was done to compare the 1W and 5W power settings. It is evident, that sub-surface temperatures were shifted both in time and intensity. Increasing the power setting will further increase this shift. Lower maximum temperatures for increasing skin depth were observed

and the delay of the peak temperature also increased with depth. The surface temperature (0 μm) is identical to the red plots seen in figures 2.2-C and 2.6-C.

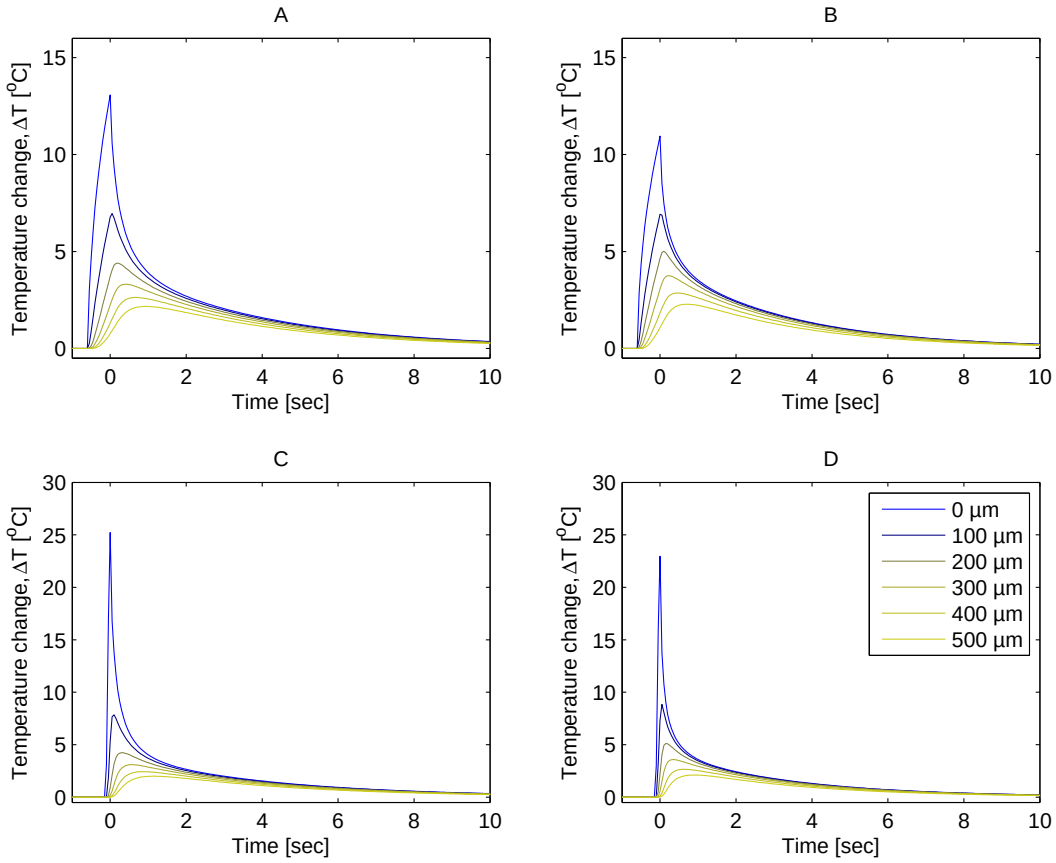

Figure 2.9: The figure illustrates how the sub-surface temperature for the 0.6 J stimulation energy in glabrous and hairy skin. A) glabrous skin 1W 0.6s, 0.6 J, B) hairy skin 1W 0.6s, 0.6 J, C) glabrous skin 5W 0.12s, 0.6J D) hairy skin 5W 0.12s, 0.6J. It is seen that a higher power setting (5W) will further increase the shift in the subsurfaces temperatures.

2.5 Conclusion

Based on the findings above it is concluded that the developed finite element model is valid. The maximum temperature found during the experiments correlated with the those of the FEM. The experimental spatial temperature profiles also correlated with the those of the FEM.

Based on the model the most likely depths of nociceptors were evaluated. It was found that the depth in glabrous skin is almost three times greater than the depth in hairy skin (130 μm in glabrous vs. 50 μm in hairy). This finding compared to figure 2.9 could also serve as indication as one of the factors why the reported sensation is lower in the glabrous skin compared to the hairy skin, since the maximum temperature reached decreases with depth.

Similar could this indicate why the latency in the glabrous skin, is higher than that found in the hairy skin, as the latency to the maximum temperature decreases with depth, however this is most likely not the sole reason for the

increased latencies in glabrous skin [Treede et al., 1995] [Treede et al., 1998].
The used software tool, COMSOL multiphysics, allows the further development to incorporate the FEM to develop a control system to maintain the skin temperature over time. Including control modelling in simulink.
The CO_2 laser was used, among other reasons, due to it is simple to model the laser as a heat source, simplifying model validation. Having validated the model, the heat source can be exchanged with another expression or model describing the heat source, such as contact probes or high penetration lasers. One method of modelling high penetration lasers is to use a Monte Carlo simulation to model the distribution of the photon absorption. In fact such a Monte Carlo simulation has earlier been developed by the author (8th semester project - 2nd semester Master), which could be combined with the FEM to model the heat distribution from a high penetration laser.

Methods

II

Design 3

This chapter will in detail provide the overview over the design of a system which fulfills the requirements listed in section 1.5.1. The reason and rationale for each design feature will be analysed in depth, to ensure the most beneficial system is developed.
Each element will be evaluated and the most practical and applicable solution will be used.
In order to control the temperature which is sensed by the heat sensitive receptors in the skin, a study was conducted to determine the skins temperature reaction to laser stimulation, see chapter 2. The study was conducted using a CO_2 laser, because the heat absorption from this laser can easily be modeled by an analytical expression. During the study evidence was found for depth at which the heat sensitive nociceptors are located in both glabrous and hairy skin, see chapter 2.

3.1 Developing environments

This section will brief discuss the software developing environments which will be applied in this project. This system requires software interface to a sensor measurering the skin temperature, furthermore, hardware interface to control the laser is needed, this should be combined with some kind of GUI (Graphical User Interface) to which the user can control the system, including the requirements in section 1.5.1.
To conduct precalculations and modeling describing the control system, a program providing mathematical and engineering aid is applied. The previously developed model, was based on the COMSOL Multiphysics software, therefore, it would be advantageous if the used software could take advantage of this model.

3.1.1 Labview

To create the necessary hardware interfaces and GUI, National Instruments', Labview 8.6 was chosen. Labview provides easy GUI creating, and provides several predefined hardware interface such as RS-232 protocols, and serial communications such as USB and Firewire. Furthermore the applied temperature sensor, is equipped with a Labview driver for easy implementation, see more below.
Other low level languages such as C or Java could also have been applied but based on the advantages for Labview listed above, Labview was seen as more preferable.

3.1.2 Matlab & Simulink

Mathworks Matlab & Simulink will be used to aid the development. Matlab provides an excellent enviroment for mathematical calculations and script programmering, including the Simulink simulation environment which provides easy modelling for several engineering modalities, such as control. Furthermore, the FEM developed in chapter 2 can be exported and combined with a Simulink model, see more below.

3.1.3 SPSS

For the statistical tests of the various experiments, the data will be imported into SPSS where the appropriate test will be performed.

3.2 Temperature sensor

Temperature sensing can be made in many ways, using a wide range of techniques, the most simple include thermometers where a liquid expands depending on the temperature. Electrical thermistors change their electrical properties

based on ambient temperature, detecable by sending a small electric current through them. However, all such temperature sensors have the problem of having to touch the element to measure its temperature, meaning that their own thermal properties will effect the element, by either cooling or heating it slightly. Instead non-contact heat sensing is possible, this technique is often a bit more advanced and expensive, but provides very accurate temperature sensing and the advantages of not effecting the element being monitored.
Non-contact temperature sensors exploit the blackbody radiation emitted by the element. Blackbody radiation is electromagnetic radiation emitted over the entire spectrum [Welch and van Gemert, 1995a]. The entire energy which a perfect blackbody emits (unity emissity, ε) over all wavelengths expressed as

$$E_b = \int_0^\infty W_b(\lambda, T)d\lambda = \sigma T^4 \quad [W/m^2] \tag{3.1}$$

[Welch and van Gemert, 1995a]
W_b is the monochromatic emission by a perfect blackbody expressed as

$$W_b(\lambda, T) = \frac{2\pi hc^2}{\lambda^5(e^{h\cdot c/\lambda k_B \cdot T}) - 1} \quad [W/m^3] \tag{3.2}$$

T is absolute temperature, σ is the Stefan-Boltzmann constant σ = $5.67 \cdot 10^{-8}$ $[W/m^2 \cdot K^4]$, h is Planck's constant = $6.626 \cdot 10^{-34}$ [J·s], c is the speed of light = $3 \cdot 10^8$ [m/s] and k_B is Boltzmanns' constant = $1.380 \cdot 10^{-23}$ [J/K] [Welch and van Gemert, 1995a]. For a less than perfect blackbody (less than unity emissivity), the entire power of the blackbody radiation is expressed as

$$E(T) = \varepsilon\sigma T^4 \quad [W/m^2] \tag{3.3}$$

[Welch and van Gemert, 1995a]
Noncontact temperatur sensor utilized these formulas in which a sensor, often of the Indium antimonide (InSb) type, sence the radiation in a certain part of the electro-magnetic spectrum. The Indium antimonide requires cooling due to an operating temperature of approx. 80 K. InSb detector typically work in the 1-5 μm range. Newer types of detectors exist such as the microbolometer. The microbolometer work by the incident blackbody radiation heats the detector and alters the electrical resistance of the detector, the microbolometer does not require cooling. The range of microbolometer is typically 8-13 μm. The detector chip can have one or more single detectors, a chip with a single detector is often referred to as a pyrometer or IR sensor. If multiple detectors are arranged in an array similar to the CCD chip in a digital camera, the result is a socalled infrared camera. At SMI two infrared cameras are available available. An Agema 900 utilizing the InSb detector and a FLiR A40 utilizing the microbolometer technique.

3.2.1 Infrared camera

The advantages of using an infrared camera as temperature sensor are multiple. One can extract the temperature of an entire area and select the either the maximum or minimum temperature depending on the application. Therefore, alligning laser and temperature sensor is not a critical issue. Allmost all infrared cameras have internal calibration mechanisms (both the Agema and FLiR system have such) ensuring accurate temperature sensing. And last a more practical reason, there is already an infrared camera available to use, no additional equipment needs to be purchased. And the cameras have previously being used during research to monitor skin temperature so their application have been thouroughly tested.
One disadvantage of using infrared cameras is that the sample rate of an infrared camera, is usually low compared to that of pyrometers, and infrared detectors.
The two cameras have different advantages and disadvantages to be discussed. First the framerate of the cameras. The Agema 900 is capable of linescanning, but this technique has the same disadvantage as a pyrometer regarding aligning, furthermore, we do not currently have the software to utilize this option. In normal mode, the Agema 900 is capable of sampling at a rate of 30 frames per second [Thermotec, 2009]. The FLiR A40 has a framerate of 50 frames per second [Infrared Systems, 2009]. Both cameras provide high accuracy, the Agema provide an accuracy of 1 °C [Thermotec, 2009], and the FLiR of 2 °C [Infrared Systems, 2009]. The Agema camera has a image resolution 204 x 128 pixels [Thermotec, 2009], where the FLiR camera have a resolution of 320x240 pixels [Infrared Systems,

2009]. The spectral range of the cameras is distinctly different and will effect the choice of laser source and vice versa, see next section. The measuring range of the Agema system is 2-5.4 μm [Thermotec, 2009], and for the FLiR system it is 8-13 μm [Infrared Systems, 2009]. However, the most determining factor is the software available for the cameras. The software available for the Agema system only provide the possibility of using the cameras with third party software (ThermaCam Research PRO) for measuring and recording of the infrared image, no drivers or developers kit are provided, furthermore, the camera is connected to a pc using third party hardware of which the documentation is very sparse. Instead we have a Labview developers kit (National instruments, Thermovision) for the FLiR system, which provides several VIs for camera control, data extraction and so on. As described above Labview was chosen as developing environment for the system, and thus it is very advantegous that the FLiR camera has additional Labview drivers and software which provides the user with good possibilties of interfacing the camera from Labview.
To sum up the FLiR camera provides higher frame rate; the FLiR camera has higher spatial resolution; and last and most importantly we have a Labview developing kit for controlling the camera and extracting thermographic data. The measurement accuracy is almost identical in both cameras.
For the reason listed above the FLiR A40 camera was chosen as temperature sensor.

3.3 Laser source

In the SMI lab at Aalborg University there are two lasers used for cutaneous stimulation in research. One is a Synrad Firestar t100 100 W CO_2 laser (10.6 μm), the second is a 20 W DL20 diode laser (970 nm). Both lasers have previously been used to stimulate the skin to elicit warm and heat pain sensations.

3.3.1 CO_2 laser

The CO_2 is by far the most powerful of the two lasers available. The high absorption of the emitted infrared light ensures that almost all of emitted energy is absorped in the skin, less than 1 % is reflected. The CO_2 laser system in the lab is equipped with a socalled scanner-head, consisting of two small, moveable mirrors which can alter the direction of the emitted light, by the turning the mirrors. Therefore, the lasers can stimulation larger area (>5 cm^2) or be used to perform graphesthesia studies [Mørch et al., 2008].
However, one major problem involving the use of the CO_2 laser is the wavelength of the emitted light, 10.6 μm, which is in the middle of recording spectrum of the FLiR A40 camera, meaning that any reflection, whatever small it might be, will give rise to higher power of radiation from the skin, causing the skin temperature to be sensed higher than the actual case. The power of such reflection will be in the order of, or greater than that of the blackbody radiation. Even more so, experience have shown that the reflection of laser light will saturate the camera completely, and thus it is impossible to combine this laser and the FLiR infrared camera for this system.
Finally the study we conducted using the CO_2 laser showed further undesirable features of the CO_2 laser as stimulator in a control loop, see section 2.5. The study showed that the temperature at the receptor level (50 or 130 μm deep) was several degrees lower than that at the skin surface, which means that the temperature seen by the infrared camera is different to that affecting the receptors, including both thermal receptors and nociceptors. Furthermore, the study indicated that the maximum temperature at the receptor level had a time lack compared to that at the skin surface. Therefore the skin temperature does not correspond to the actual temperature at the receptor level, which is what we want to control, and the measurement from the infrared give a incorrect temperature reading.

3.3.2 Diode laser

The diode laser emits only a fifth of the power of the CO_2 laser. The shorter wavelength of the near infrared light gives the photons higher penetration in the skin, almost 100 times greater than that of the CO_2 laser (penetration depths: 20 μm vs. 1.4 mm). The lower absorption of the light causes photons to be scattered in the tissue, the means some propertion of the photons entering will leave the tissue before they are absorped. Besides this, reflection will cause around 4-7 % of the incoming light to be reflected at the surface, never entering the tissue [Anderson and Parrish,

1981]. All of these optic phenomena are very rare using the CO_2 laser and can be neglicted. The wavelength of the diodelaser is different to the spectral range of the FLiR A40 camera, meaning that there are nothing to hinder using the laser and camera simultaneously. The diode laser is not equipped with a scannerhead, instead it has two hand pieces which the control the beam size of the emitted light. But those handpieces could most likely be fitted to the scanner head of the CO_2 laser. In fact the light entrance of the scanner head is a cylindrical metal tube and so are the handpieces, simply with a smaller diameter - using some sort of middle tube, it is possibly to decrease the diameter of the light entrance making the hand pieces fit snugly inside it.
In addition Iannetti et al. [Iannetti et al., 2006] showed that using a laser with high penetration it is possible to elicit first pain in both glabrous and hairy skin, something CO_2 lasers are incapcable of [Treede et al., 1995]. Since it has not been determined whether the system will be applied to either glabrous or hairy skin, it would be advantageous to use a laser which could elicit similar sensations in both skin types, making the system as flexible as possible.

3.3.3 Diode laser as thermal stimulator

An optical filter in front of the camera, eliminating the 10.6 μm radiation, could give the possibility to use the CO_2 laser in conjunction with the FLiR infrared camera. Furthermore, to determine exactly how large the different the temperature profile between the surface and receptor level a Monte Carlo simulation, was combined with the FEM to model the heat distribution when using a high penetration laser like the diode laser.
Two 0.5 seconds burst of 1W energy from the diode laser were modelled and the surface and receptor level temperatures were extracted and plotted over time. The results of the combined simulation are seen in figures 3.1 and 3.3. In hairy skin the temperature profile at the surface and receptor level are extremely similar, see figure 3.1. Comparing this to a simulation of a CO_2 laser which is seen in figures 3.2 and 3.4, it is seen how the CO_2 laser creates very different temperature profiles at the skin surfaces and at the receptor depth.

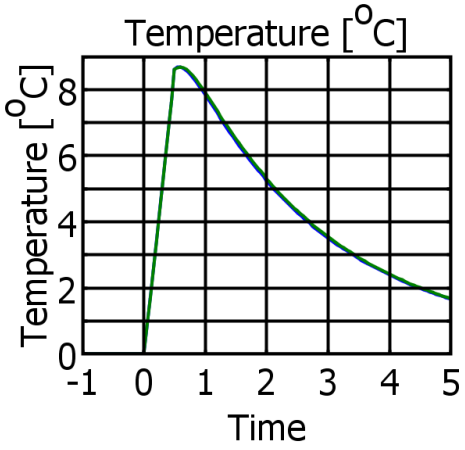

Figure 3.1: The figure illustrates the temperature profile at the skin surface (green) and receptor level in the hairy skin (blue) over time (seconds). The simulation is based on 0.5 seconds 5 W stimulation from a diode laser (970 nm), starting at t = 0. It is clear to see that the temperature at these two levels are very similar, both during the heating phase (0-0.5 sec.) and cooling (0.5-5 sec.).

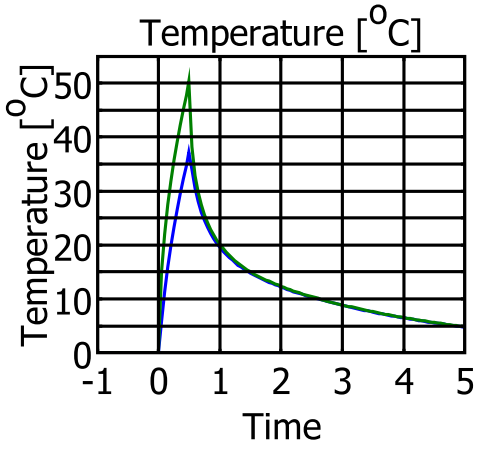

Figure 3.2: The figure illustrates the temperature profile at the skin surface (green) and receptor level in the hairy skin (blue) over time (seconds). The simulation is based on 0.5 seconds 5 W stimulation from a CO_2 laser (10.6 μm , starting at t = 0. It is clear to see that the temperature at these two levels are quite different, the maximum temperature difference is almost 15 °C.

In glabrous skin the temperature was also similar, with a small deviation at the maximum temperature. But as it can be seen in figure 3.3, the difference is than 0.5 °C and 0.5 seconds, and in fact the surface temperature is lower than the one at the receptor level, which is not correct, therefore, the difference is most likely due to a small inaccuracy in the Monte Carlo simulation. Probably due to the spatial resolution in the Monte Carlo simulation. For the CO_2

laser - figure 3.4 - the difference is even more pronounced in glabrous skin than in hairy skin. This difference is of a magnitude which undoubtly will effect the sensation of the stimulus.

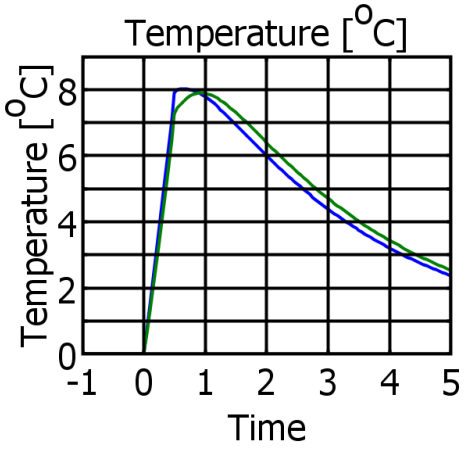

Figure 3.3: The figure illustrates the temperature profile at the skin surface (green) and receptor level in the glabrous skin (blue) over time (seconds). The simulation is based on 0.5 seconds 5W stimulation from a diode laser (970 nm), starting at t = 0. It is seen that the two temperature profiles are almost identical, except, around the end stimulus end at 0.5 seconds. However, the difference is very small (less than 0.5 °C), the predicted surface temperature is slightly lower than at the receptor level, which is inaccurate. This difference is due to a small inaccuracy of the Monte Carlo simulation.

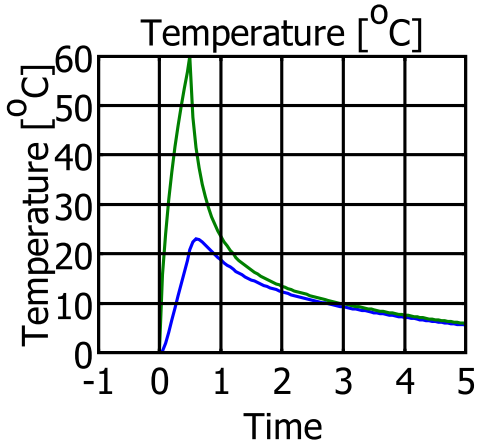

Figure 3.4: The figure illustrates the temperature profile at the skin surface (green) and receptor level in the glabrous skin (blue) over time (seconds). The simulation is based on 0.5 seconds 5 W stimulation from a CO_2 laser (10.6 μm , starting at t = 0. It is clear to see that the temperature at these two levels are quite different, the maximum temperature difference is almost 40 °C.

Comparing figures 3.1 and 3.3 to figures 3.2 and 3.4 it is also clear to see how much higher surface temperatures the CO_2 laser is able to create, using similar stimulation paradigms.
Based on the discussion and the results based on the combined Monte Carlo simulation and FEM above, the diode

laser was chosen as laser source to ensure that the laser would not sature the camera, furthermore, it would ensure that the surface temperature is similar to that found at the receptor level.

3.4 Temperature control

In appendix B the basics for controller development is elaborated. In that chapter the two basic control principles are defined, open and closed loop control. Eventhough a model for the heat distribution in the skin have been developed, it was choosen not to use open loop to control the laser. Instead closed loop control will be applied. This was done for several reasons, most importantly due to the fact that the blood flow in the tissue will change during prolonged heating causing a sligth change of the thermal properties of the skin, (more heat is transported due to convection, which alters the relationsship between convection and conduction), this would results in error when using a open loop system. Furthermore, the heat transport due to convection was ignored in the developed FEM. The disturbance, change of blood flow, could be measured, but this would be very cumbersome to implement. Closed loop control will also give the possibilty of adding several safety features in the system, e.g. shut down system if skin temperature is too high.
A very simple closed technique is a so called on/off control, in our case it would work by increasing the laser power, whenever the process output is lower than the reference and vice versa [Haugen, 1994]. The technique is very simple but the output of the process will oscillate around the reference, and is thus not preferable. Instead another technique will be applied. The most widely used closed loop technique is the so called three-term controller or PID (Proportional-Integral-Derivative) controller [Haugen, 1994] [Franklin et al., 1994]. It consists of three different terms which alters the control input to the actuator based on the error measurements. The PID controller can be applied to number of very different processes, due to relative simplicity of the current problem, the PID controller will be a provide sufficient response to control the current problem. PID controllers are very useful for simple systems such as single input, single ouput types of systems, such as the one in this project. Due to its simplicity, relative easy implementation and good controller performance the PID controller will be implemented in this project.
A mathematical model of the system (process and regulator) can be very benificial in the further development of the controller [Haugen, 1994]. However, in most physical systems the model will only provide an approximation of the system, and a certain error must be incorporated in the model. Eventhough not entirely correct, the model can still be helpful to describe the basic properties of the system. Depending on the validity of the system model, the model should only be trusted as far it agree with reality, e.g. in the case of stability, a theoretical stable system might not be the case if the system model is inaccurate [Haugen, 1994]. To test how the controller works, developers often use software tools to model and predict how the process behaves and thus which controller would be appropriate. One such tool, Simulink will be used in this project to aid the controller development. The mathematical model is simply obtained from the flow diagram seen in appendix B, figure B.2-A and Eqs. B.1, B.2, B.3, and B.4. The model of the process must react similar to input from the controller that it would in real life, the better the model, the better value of the simulation.

3.4.1 Process model

To develope a process model, the study conducted in chapter 2 will be used. In this study a heat distribution model was developed and validated using a simple analytical expression as the heat source. However, this is not valid when using a high penetration laser, such as the diode laser. Instead the results from a Monte Carlo simulation is used as the heat source in the heat distribution model.
This heat distribution model was developed in COMSOL Multiphysics. This program has several advantages, including a Matlab interface. Via this Matlab interface it is possible to export a COMSOL model into Simulink. The model being exported must be solved before it it exported. In order to reduce the simulation time a coerce mesh in the finite element model is used. When exporting the model the inputs and outputs must be selected. The model have one input, the laser power, and one output, temperature in the center of the laser beam (selected as point 3 when implementing the model in COMSOL). In Simulink, the model is added using the block named COMSOL Multiphysics Subsystem, this block will only be available when using the "COMSOL with Matlab" option.

3.4.2 Complete simulink model

When combining the process model and PID model in simulink with a signal builder to generate a reference signal similar to that applied in research, the results can be seen in figure 3.5. In the figure 3.5 one scope, named Temp, can be seen, this scope illustrates the desired signal (from the Signal Builder), the Laser power (u) and the temperature (Temp), this gives the developer an idea of how the power and temperature responses are when changing, either the reference signal or the gains in the PID controller. The signals tested should obviously correspond to and cover the range of the actual signals which would be used in the implemented system.

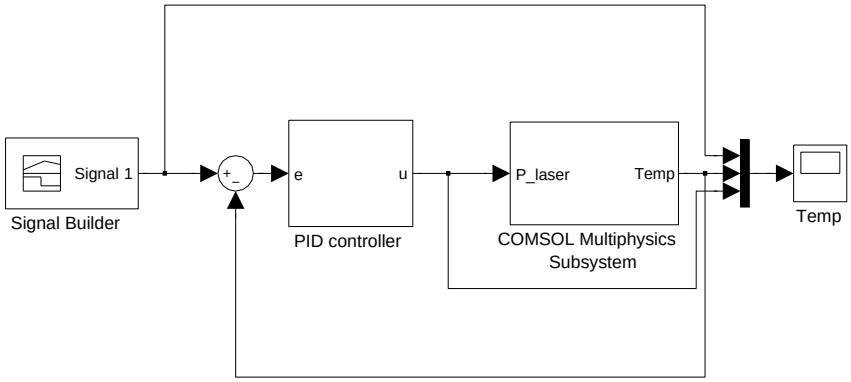

Figure 3.5: The figure illustrates the complete Simulink model used for analysed the control scheme. The PID and process models are both seen as two subsystems, see figure B.8 and section 3.4.1 for more insight.

3.5 System overview

To summarize this chapter, this section will give a brief overview of the main principles and elements of the system to be implemented. The system will be comprised of the following main elements

- Diode laser
- Infrared camera
- Laptop computer including

  Graphical user interface (GUI)

  PID control algorithm

  Laser control interface

  Infrared camera interface

In figure 3.6 a flow diagram between the main elements of the system is seen. The user determines the desired temperature on the GUI, and then the controller increases the laser power which heats the skin, the controller maintains the skin temperature at the desired level using the feedback from the infrared camera.

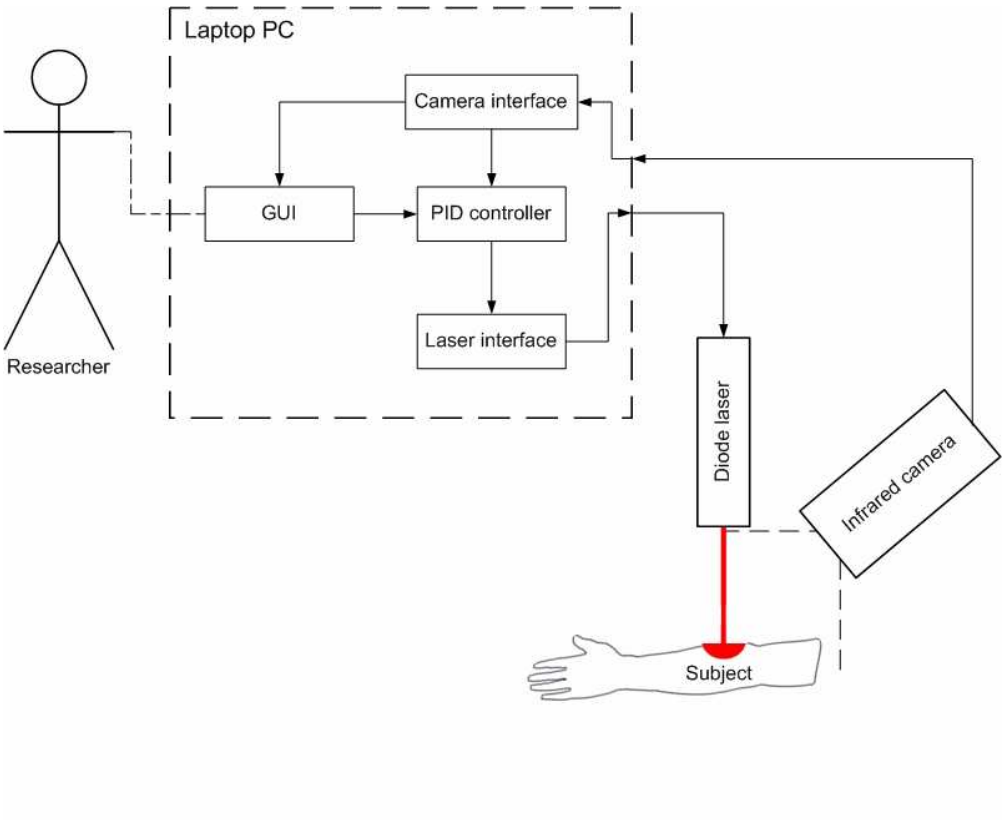

Figure 3.6: The figure illustrates the complete system to be implemented. The user decides what temperature the subjects skin should be - then the controller increases the laser power, the effect on the skin temperature is measured by the infrared camera, which is fed back to both the user on the GUI, but also the PID controller, which adjust the laser power accordingly.

Furthermore the implemented system should satisfy the features listed in section 1.5.1.

Implementation 4

In this chapter the system designed and sketched in the Design chapter will be implemented. Each major part of the system will be described in a section. Very technical labview describtions will be left out, since it is assumed that the reader is familar with Labview basics, and that the attached VI's are somewhat self-explanatory having read this chapter. The detailed implementation of the infrared camera control and laser control are found in appendices C and D.

4.1 System functionality

The user will interact with the system through a graphical user interface (GUI) on this GUI the system settings, stimulation type and settings are selected. Since this system is intended for psychophysical studies the subjects being stimulated will rate the intensity of stimulation on a electronic VAS scale (0-10), this rating is measured and sampled. During the stimulation the GUI displays the skin temperature can be monitored along with the laser power and intensity rating. During the stimulation, the time, desired skin temperature, actual skin temperature, laser power and subject intensity rating is logged. At startup the system will prompt the user to specify the file (.txt) to save the logged data into. The logged data is saved when the stimulation finishes.

4.1.1 Graphical User Interface - GUI

The GUI is divided into three main sections or panes, corresponding to three different states of the system. The first pane is the Initial system setup, the next is Stimulation setup and control and the final pane is Stimulation Monitoring. The three main panes are arranged similar to the reading direction, meaning the pane which requires attention first is placed to the left, and the pane being used last is placed on the right. In figure 4.1 the implemented GUI is seen.
After prompting the user to specify which file to save the logged data into, the filename and path will be displayed on the top of the GUI.
The stimulation starts when the user presses the *Start heating* button and stops when the duration is complete or when the user presses the *Stop heating* button. When the stimulation is complete the logged data is saved into the specified

file. Below the functions in each pane are described and the functionalities are elaborated.

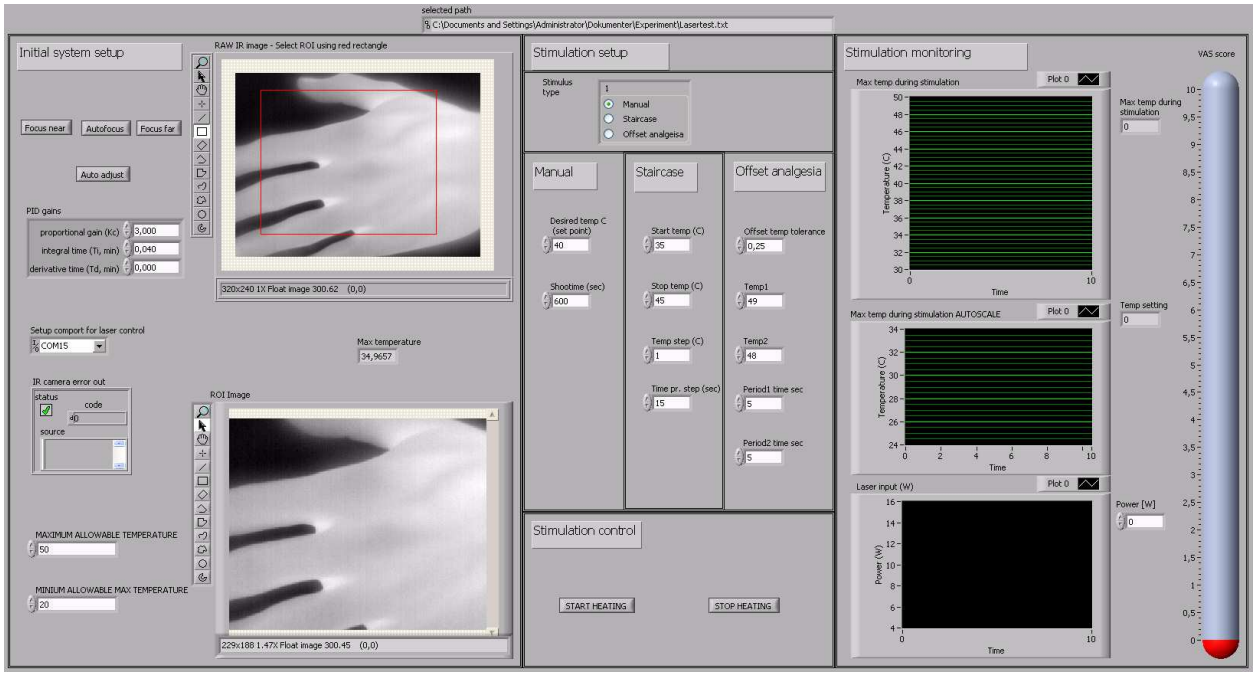

Figure 4.1: The figure illustrates the Graphical User Interface (GUI) in the system. The GUI have three main panes, on the left the Initial System setup, in the middle the Stimulation setup and Stimulation control, and to the right the Stimulation monitoring.

4.1.2 Initial system settings

The user will be able to select a number of settings before the stimulation is started. First the user can choose to auto calibrate the camera using the internal calibration mechanism, the user can change the focus of the camera, by choosing either auto focus or manually change the focus (moving focus point nearer or farer). Second the user can the set the minimum and maximum skin temperature allowed during stimulation (to prevent skin damage). The maximum temperature is by default 50 °C and the minimum is by default 20 °C. The user can change the setting of the PID controller by changing the Proportional, Integral and Derivative gains. Finally the user selects which comport to use for communication with laser.
On the Initial system settings pane the user can select a region of interest (ROI) on the raw infrared image. The ROI has multiple purposes, first it is used the select the skin area being stimulated, ensuring an more exact temperature measurement; then it helps to prevent measuring the minimum temperature as the background in the image (not skin); finally the ROI selected is enlarged and displayed on the GUI, meaning the user will have a better idea of whether the focus and the selected area are correct. The ROI is selected by drawing a rectangle in the raw infrared image. The maximum temperature of the ROI is set as the process output. If no ROI is selected the skin temperature is defined as the maximum temperature in the raw image, and no ROI image is displayed on the GUI.
All of the settings are placed in the left most part of the GUI, indicating that these should be selected before starting the stimulation. When the stimulation starts (after the *Start heating* button is pressed) most of the Initial system setup pane is disabled to improve system performance, this include the two infrared images, which are no longer active. During stimulation only the PID gains can be altered.

4.1.3 Stimulation settings and control

The developed system will be able to deliver three different kind of stimulation paradigms. The first paradigm is a manual setting where the user selects the stimulation time in seconds and desired skin temprature in °C. During the stimulation the user can alter the desired temperature. The second stimulation paradigm is a threshold detection using equal steps between two temperatures. The user selects the starting temperature, the stop temperature, the duration of each step and the size of each step. This paradigm is a type of QST trial and in the system it is named Staircases. The stimulation duration is calculated based on the number of steps and the duration of each step, see figure 4.2 A) for an example of such a paradigm, stimulating the skin from 35 to 45 °C in steps of 1 °C and a step length of 15 seconds. This paradigm was selected because it resembles the methods of levels, often used in QST studies, see chapter 1.
The third paradigm is an offset analgesia test which heats the skin to two defined temperatures, maintains the exact temperature plateau for a defined time and then change the temperature to another plateau and maintains this for another specified time. In this paradigm the time spend at each plateau can be exactly controlled by the user. The user can also specify the offset tolerance (in °C) indicating when the system treats the temperature as having reached the desired plateau, meaning when the counter starts. The two temperatures can be the same, in this case the two stimulation times will be summed. The temperature can both be increased or decreased between the first and second plateau, see figure 4.2 B) for an example of this paradigm, in the figure a 49-48 °C stimulation is seen, both temperatures is maintain for 5 seconds. The stimulation duration is calculated based the duration of the two plateaus, and added a period of 30 seconds to give the system time to both heating and possible cooling of the skin. However, the stimulation stops when the final step has been held at the desired time.

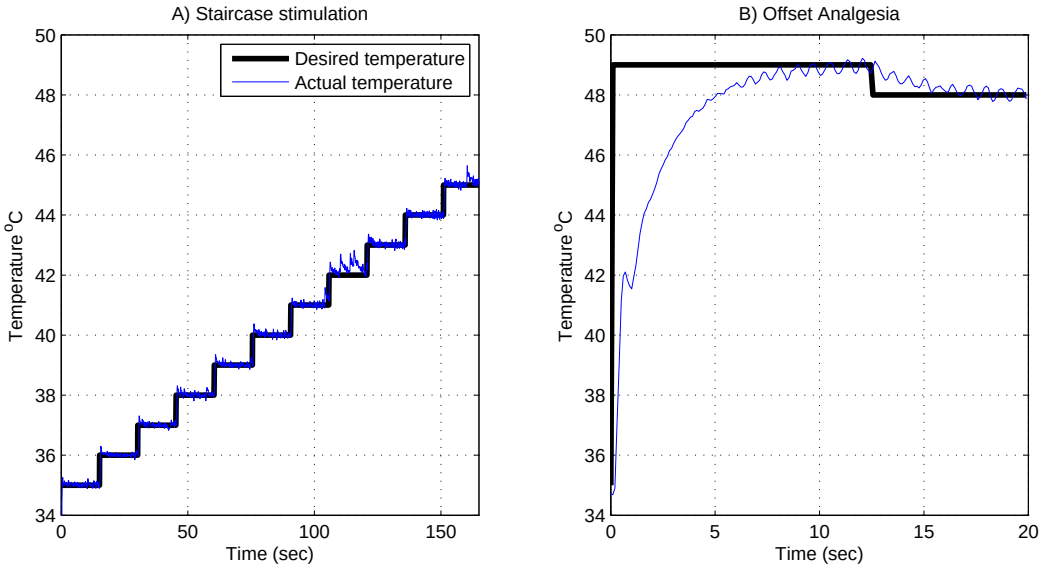

Figure 4.2: The figure illustrates the two automated stimulation paradigms implemented. In A) is seen a staircase stimulation, where the user can select a stepwise increase or decrease in temperature between two temperatures. Here the start temperature is 35 °C and the stop temperature is 45 °C, this stimulation uses a step of 1 °C, and each step has a length of 15 seconds. In B) is seen a stimulation paradigm for an Offset Analgesia test. The first desired temperature is 49 °C, which is helt for 5 seconds, then the temperature is lower a single degree to 48 °C, which is held for another 5 seocnds. A tolerance of 0.25 °C was used. The entire stimulation is longer than 10 (5+5) seconds since it takes the system some time to both heat the skin to 49 °C and let it cool from 48 to 49 °C.

All stimulation must be kept within the min-max range specified in the system settings, if not the system will stop the stimulation as a safety measure.

When the stimulation starts the controls on this pane is disabled except the *Stop heating* button - and when using manual stimulation, the desired temperature control is still active.
To help the user, not select the wrong stimulation type by mistake, only the parameter for the chosen stimulation type are displayed, e.g. if a manual stimulation is selected the parameters for Staircase and Offset analgesia are invisible and cannot be changed. When the stimulation starts the stimulation settings are grayed and disabled. This is done to indicate that the parameter no longer can be changed but still remind the user what kind of stimulation is taking place. The arrangement of this pane is seen figure in 4.1.

4.1.4 Stimulation monitoring

During the stimulation the skin temperature, laser power and intensity rating is monitored. The skin temperature is monitored in three different ways to give the user the best idea of any changes, along with an overview of its progress. Using two graphs with different graphs the temperature is monitored (x-axis: time and y-axis: temperature). The first graph has a fixed 30-50 $^{\circ}$C temperature scale, while the other is autoscaling the y-axis, both graphs have a 10 seconds time base (running). The fixed graph gives the user an overview of the temperature progress, while the other gives detailed view of the actual temperature, including any steady state error, fluctuations and so on. On both graph there are horisontal grid lines for easier temperature reading. Finally the skin temperature is displayed in a numeric indicator.
The laser power is displayed using a similar graph with a running time base of 10 seconds and auto scaling y-axis. This graph has no grid lines. The laser power is also displayed in a numeric indicator next to the laser graph.
During stimulation the desired skin temperature is displayed in a numeric indicator, next to these three graphs.
The stimulation intensity rated by the subject is displayed in a vertical bar with fixed range of 0 to 10.
This right-most pane of the GUI is disabled before the stimulation and when pressing the *Start heating* button the system halts for 5 seconds to allow the infrared camera to be internally calibrated and then the stimulation starts and the pane is activated. The arrangement of this pane is seen figure in 4.1.

4.1.5 Hardware used for implementation

To interact with the different hardware used the computer used must have a comport, a Firewire port and USB port. The operating of the computer must be Windows XP since the driver for the infrared camera only supports this. The control system wille be implemented using a Zepto laptop with 2GB ram and a 1.83 GHz Intel Dual Core CPU, Firewire, USB 2.0, and Windows XP. The used laptop does not have a comport, instead a USB-to-Comport converter is used.
The infrared camera, is controlled via a Firewire interface. The laser used is a 20 W DL20 diode laser (970 nm), and is controlled using a comport. The VAS meter used (AAU VAS meter) to rate the stimulation intensity has an analog output. The range is 0 to 10 volts corresponding to ratings between 0 and 10. This voltage is sampled using a National instruments USB 6009 AD converter.

4.2 Implementation principles

The implementation of the system roughly follows the three states described above. As soon as the system is started, the interfaces to the infrared camera and the laser is initiated, see more in the next sections 4.3 and 4.4. On startup the system prompts the user for the path and filename to save the logged data into.
After having finished these initial commands, a while loop controls the system. This while loop corresponds to the Initial system setup, see the details in section 4.3. The system stays within this while loop until the *Start heating* button is pressed (see figure 4.1).
Then the system enters a single iteration while loop with a 5 second pause. During which the system is prepared for the stimulation, included both changing the GUI, see above, and setting up the camera, see below.
Then the system enters a final while loop corresponding to the stimulation process. This while loop contains the controller which regulate the skin temperature. The while loop takes a number of inputs including the desired temperature,

stimulation duration and the stimulation type.
The hardware which limits the system clock cycle was expected to be the infrared camera which can sample a frame every 20 ms (50 Hz), however, the implementation showed that it was not possible to acquire a frame and process the data faster than approx. 15 Hz. To ensure good timing and not running the system at its limits, a clock cycle of 10 Hz was chosen and tested. This was done so that further expansion of the system would not demand the system to operate beyond its limits. In order to control this, a wait of 100 ms was placed inside the while loop. If the system is unable to run at this rate, the laser will receive a power command rarer than each 100 ms. This means that the output of the laser will fluctuate and so will the temperature, therefore this performance of the system should be tested after implementation.
In each iteration of this while loop the following happens

- The temperature is measured - meaning a frame from the infrared camera is acquired and the maximum value is found
- Based on the desired temperature and measure temperature the PID controller calculates the appropriate laser power for the next 100 ms
- The power setting is sent to the laser
- The voltage generated by the VAS meter is sampled
- The system check if the temperature is either too high or low - if so the while loop stops
- The system check if the selected stimulation is completed (if so the desired temperature will be set to -1) or the shoot duration is finished - if so the while loop stops
- The system checks if the *Stop heating* button has been pressed - if so the while loop stops
- The time, desired temperature, actual temperature, laser power, and intensity rating is logged

When the while stops, the interfaces to the infrared camera and AD converter are closed and the logged data is saved into the specified file.
Next will the implementation of the camera control, laser control and PID controller be described.

4.3 Infrared camera control

The infrared camera is connected to the computer via a Firewire interface. Control of the infrared camera is done using the FLiR Thermovision Toolkit for Labview. Using this toolkit will give a number of opportunities to both acquire data from the data but also control different settings on the camera such as focus, calibration, sample rate and so on. Before frames can be acquired from the infrared camera, the communication between Labview must be established, when this is done the frame acquisition can start. In order to ensure a continous flow of frames, the image acquisistion is placed within a while loop. When there is no longer any need to sample frames from the infrared camera, then the connection between the computer and camera, is terminated.
For more details, including the Labview implementation, on the setup of the infrared camera and the acquisition of image frames, see appendix C.

4.4 Laser control

The DL-20 diode laser is controlled using an RS-232 interface (Com-port). The laser is controlled by sending a package of five bytes via the RS-232 interface to the laser. The first byte lets the laser know, which kind of signal it is receiving. The next two bytes is used to set the power (0-20 W), the final two bytes determines the shoot duration (0-1635 ms).
Since the actual output power of the laser does not correspond the desired power, the laser was calibrated and the

transfer function between the actual and desired power was implemented in the software. This ensures that the actual power output from the laser matches the desired power set by the controller (actual output range i 0-16W see appendix D).
For details on the laser control, including the Labview implementation, see appendix D

4.5 PID controller implementation

The details of the PID control theory is found in appendix B. To implement the PID controller the NI PID control toolbox was used. Obviously it is possible to implement a PID controller from scratch, if one have very special requirements for the controller. Since this was not the case in this thesis the toolbox was used. The PID controller from the toolbox is equipped with anti integral windup, and takes a number of inputs. First the Process output (or process variable in Labview), next the reference (or Set point in the Labview toolbox), the range of the actuator (meaning the range of the laser 0 to 16 W), and finally the three constants corresponding to each of the three terms, proportional, integral and derivative. Instead of integral and derivative gains this PID controller used the socalled integral time, (T_I), and deritative time, (T_D), - both in minutes. These constants are defined as

$$T_I = \frac{K_P}{K_I} \tag{4.1}$$

$$T_d = \frac{K_D}{K_P} \tag{4.2}$$

using this configuration of the PID controller the flow chart will look like the one seen in figure 4.3. The PID setup in the GUIs Initial system setup pane will therefore be proportional gain, and the integral and derivative time corresponding to the PID control toolbox.

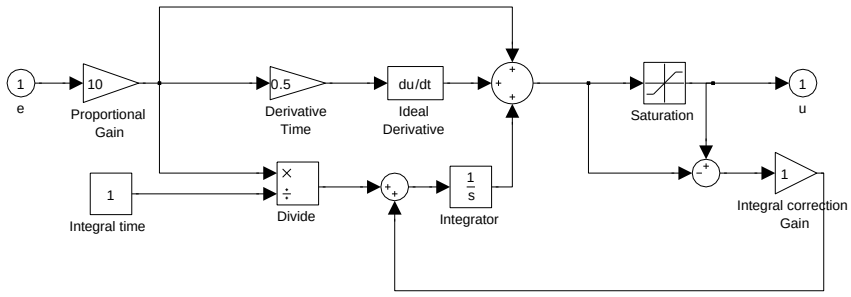

Figure 4.3: The figure illustrates the Simulink implementation of the PID controller using integral and derivative times instead of integral and derivative gains, complete with anti integral windup. The conversion between time and gain can be seen in Eqs. 4.1 and 4.2.

4.5.1 Theoretical controller tuning

Based on the controller seen in figure 4.3 and the model described in section 3.4.2, the theoretical controller was tuned. When tuning the laser the developer must decide on the characteristic of the controller. An ideal controller would obviously control the temperature very fast and give no error, including both steady state error or over/undershoot. The developed system will mainly be used for psychophysical studies, including offset analgesia tests. In offset analgesia a small decrease in temperature gives rise to decreased pain sensation, therefore if the system has extensive overshoot before settling at the desired temperature this might give rise to an offset analgesic effect which is undesirable. Therefore, overshoot should be limited. However, this require the integral time to be reduced, which would increase the time it the takes controller to let the skin cool meaning the cooling phase will be extended. This is not desirable either,

since offset analgesia has been proposed to be a contrast enhancing mechanism [Grill and Coghill, 2002] [Yelle et al., 2008]. Therefore slow cooling would decrease the temporal contrast during the stimulation, and thus its ability to evoke offset analgesia. If the system is unable to evoke offset analgesia, it is not capable of reproducing the results previously found using contact stimulators, which was set as the aim to ensure proof of concept. Therefore, this should be tested when the implementation is complete. Furthermore, any steady state error should be eliminated so the user can be certain that the desired stimulation temperature is also the actual skin temperature.
To sum up the controller should posses the following properties

- Limit overshoot to the same magnitude of the steady state error or oscillations
- Cooling should be as fast as possible, causing better possibilities for offset analgesia and similar psychophysical tests, which needs high temporal contrast.
- Small steady state error

It is impossible to satisfy all three requirements completely, therefore, a trade off must be made. Using the equations by Ziegler Nicols (see Appendix B for detailes) to tune the controller will give a controller which have some overshoot, but reasonable fast response, therefore the Ziegler Nicols can be used to give a good starting point for the tuning and then customizing the controller to meet the requirements. Ziegler Nicols method was tested in Simulink, however, it was found that it was not possible to determine neither the critical gain or the critical period, because no constant oscillations could be evoked. Only extreme oscillations could be evoked when using very high gains.
Therefore a trial and error approach was used. The different theoretical tunings methods, such as Ziegler Nicols is solely applied to save time during the tuning phase, tuning by trial and error is an equally approved and used method. In table 4.1 the ranges tested is seen. As a good starting point a PI controller with a gain of 1 and an integral time of 1 was chosen.
During the tuning the target was find to a tuning which satifies the requirements listed in section 1.5.1.

Ranges tested		
$\mathbf{K}_P$	$\mathbf{T}_I$ (seconds)	$\mathbf{T}_D$ (seconds)
1,3,5	1,3,4,5	0,0.01,0.1

Table 4.1: The table displays the ranges which were tested of K_P, T_I, and T_D in the theoretical PID model. A good rule of thumb is to use a T_I which is at least a factor 10 larger than T_D.

At first all the proportional gain and integral time was set to 1 and the derivative term was for the start left out, meaning setting the derivative time to 0. The antiwindup gain was kept constant at 1. In figure 4.4 the result of the first

simulation is seen. It is clear that the overshoot is much too large to accept. Furthermore, the cooling phase is slow. This means that the proportional gain and integral time are too low.

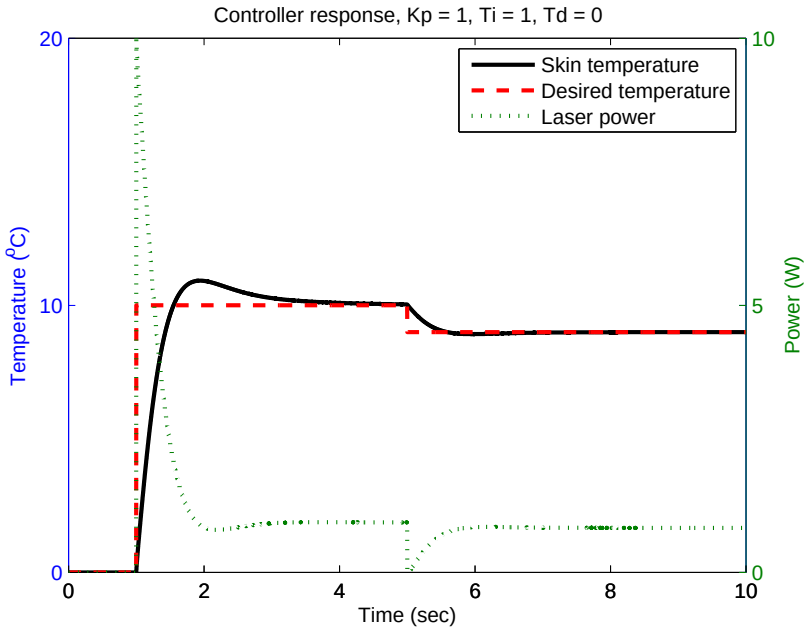

Figure 4.4: The figure illustrates the K_P = 1, T_I = 1, T_D = 0. This controller tuning gives a very high overshoot and thus it is not preferable.

In response to the results seen in figure 4.4 the proportional gain was increased to 3. The result of this in figure 4.5. This change decreased the overshoot, but this is still too large, and there is a small steady state error.

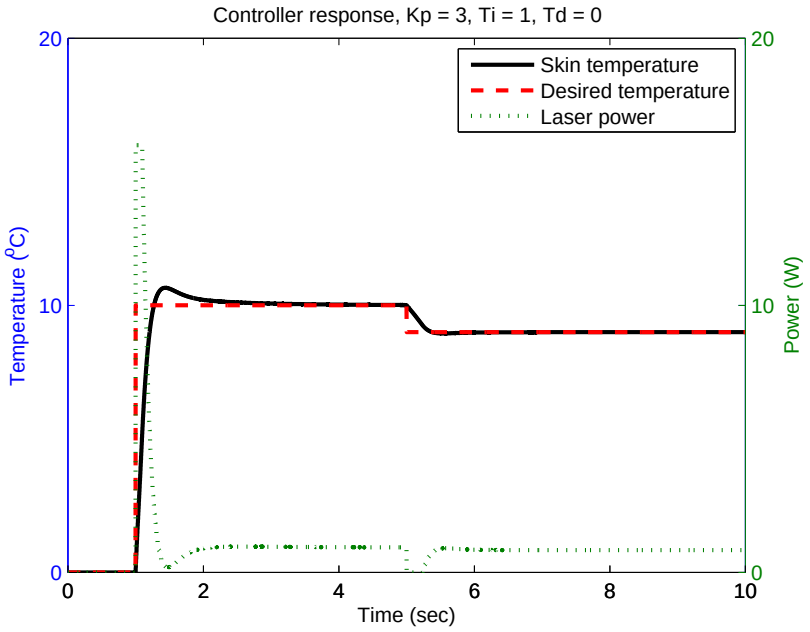

Figure 4.5: The figure illustrates the $K_P = 3$, $T_I = 1$, $T_D = 0$. This controller tuning gives a overshoot which is much higher than the steady state error.

Then the integral time was increased to 3, to increase the control effort slightly, which was hoped to decrease both overshoot and steady state error. The result of this is seen in figure 4.6. It is seen that the overshoot has been reduced; there is very little steady error, and the cooling phase is quite fast.

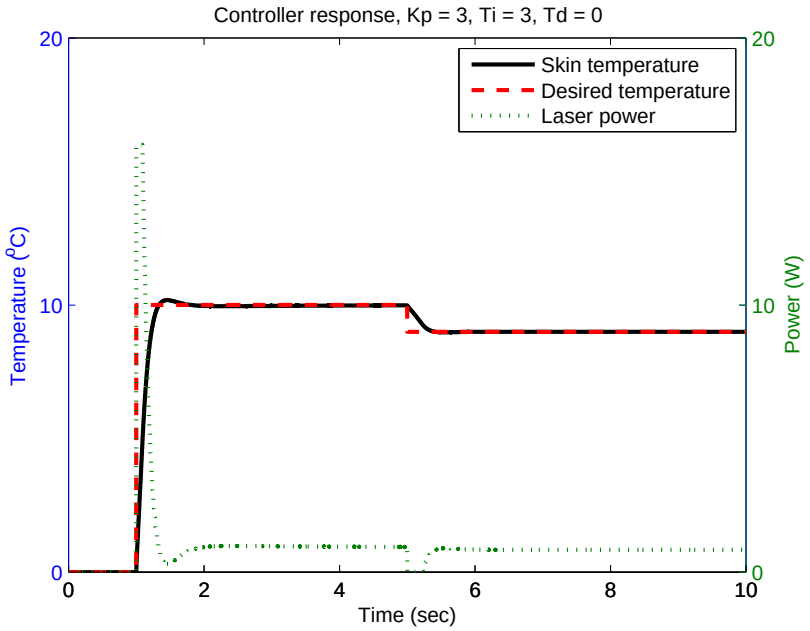

Figure 4.6: The figure illustrates the K_P = 3, T_I = 3, T_D = 0. This controller tuning gives only small overshoot which is approximately equal to the steady state error. Furthermore, the cooling phase is fast, approximately 1 °C per second.

It was investigated whether further increasing the proportional gain and integral time would give better controller performance. The result of increasing the proportional gain to 5 and integral time to 5 is seen in figure 4.7. The overshoot is still low, but the steady error has increased.

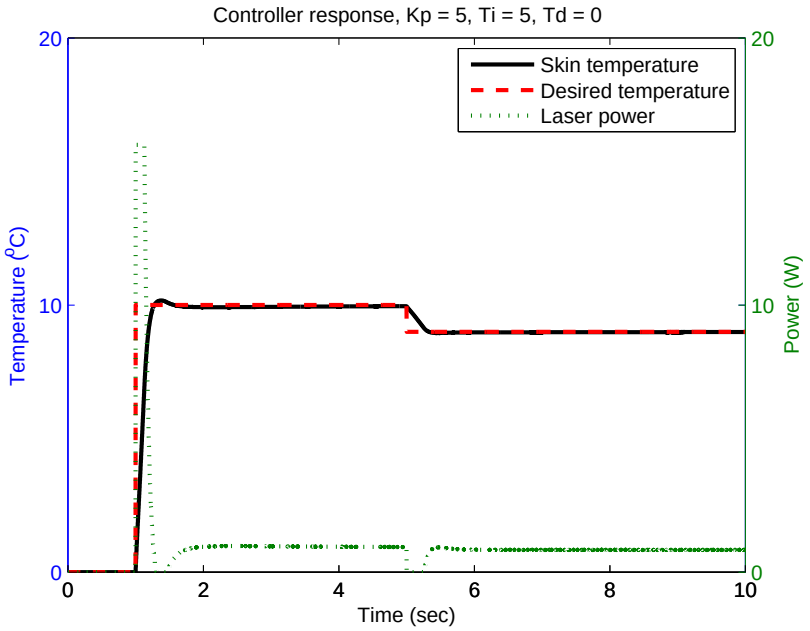

Figure 4.7: The figure illustrates the $K_P = 5$, $T_I = 5$, $T_D = 0.1$. Adding the derivative term gives some overshoot which is not desirable in the controller. It is seen that the steady state error is larger (the dotted line from the desired temperature is more visible) than in figure 4.6

Reducing the proportional gain to 3 does not help, see figure 4.8

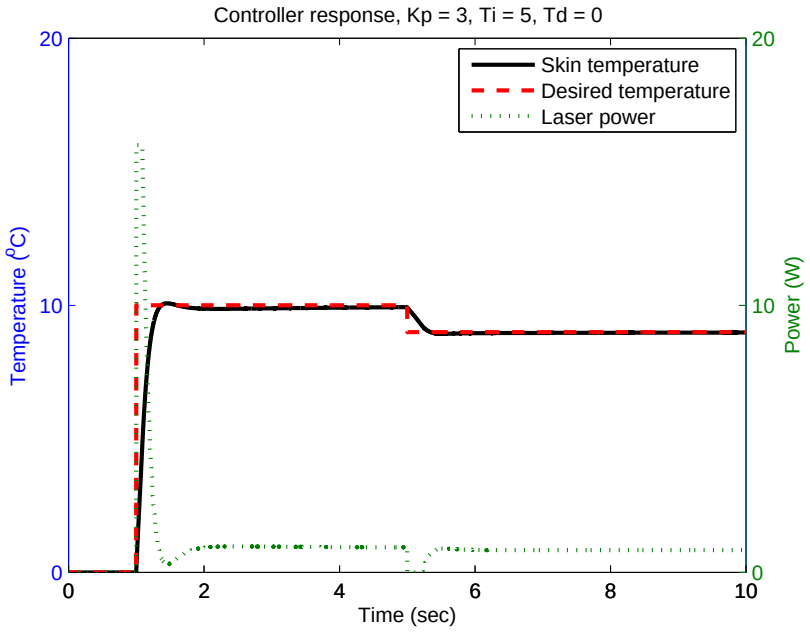

Figure 4.8: The figure illustrates the $K_P = 3$, $T_I = 5$, $T_D = 0.01$. This small derivative time reduced the overshot, but gave a steady error. Compared to the settings used in figure 4.6 it is still less preferable.

Finally the integral time was reduced to 4, to test whether this could keep the overshoot low, and reduce the steady state error. This was not the case, som steady state error still remained, see figure 4.9.

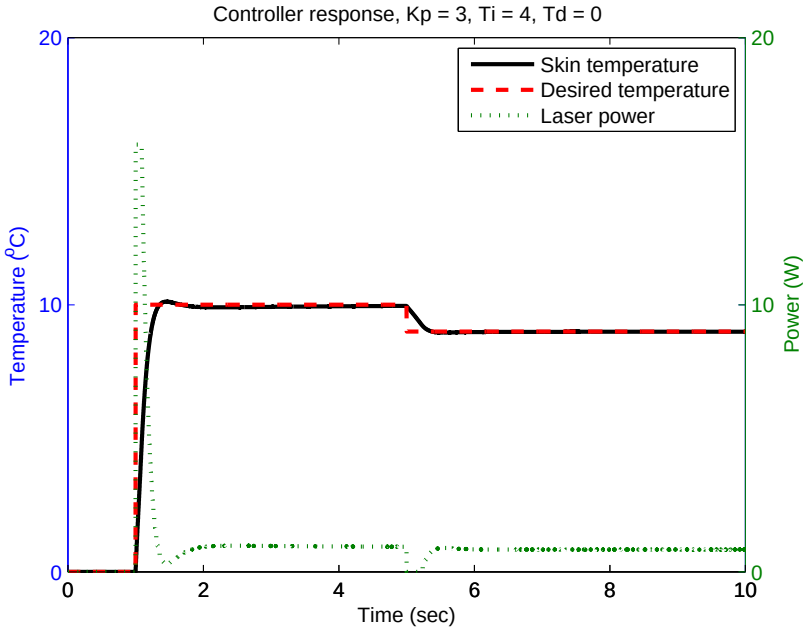

Figure 4.9: The figure illustrates the K_P = 3, T_I = 4, T_D = 0.

Based on the above it was agreed that the best tuning for the PI controller would be a proportional gain of 3 and an integral time of 3.
In all of the tuning process above, the derivative term have been left out. This is partly done because some high frequent measurement noice is expected and furthermore, the useful effect of the derivative term was hard to find in

this process. In figure 4.10 the result of a derivative time of 0.1 is seen, it seen how the overshoot is increased compared to figure 4.6, and so is the settling time.

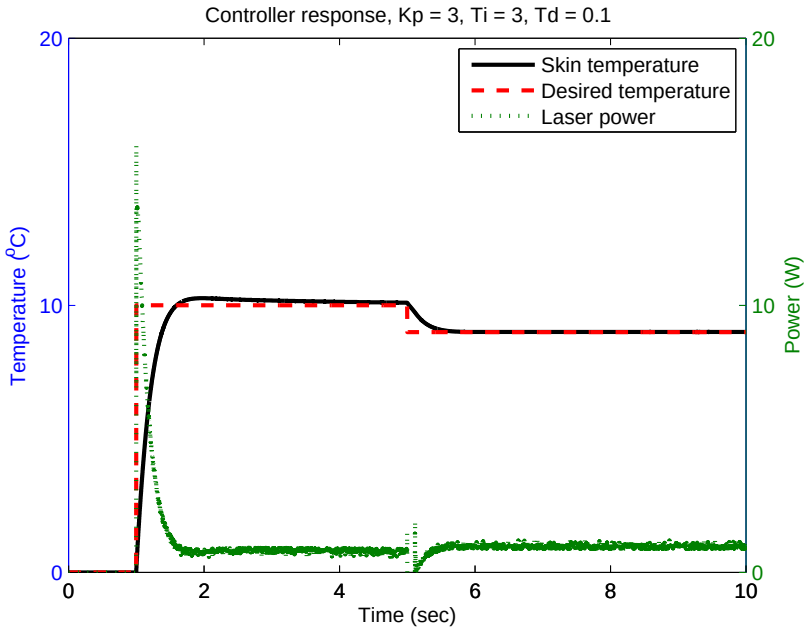

Figure 4.10: The figure illustrates the K_P = 3, T_I = 3, T_D = 0.1. It is seen that the steady state error has increased compare to figure 4.6.

Decreasing the derivative time to 0.01, will reduce the overshoot but increase the steady state error. But compared to figure 4.6 the PID controllers are not as preferable.

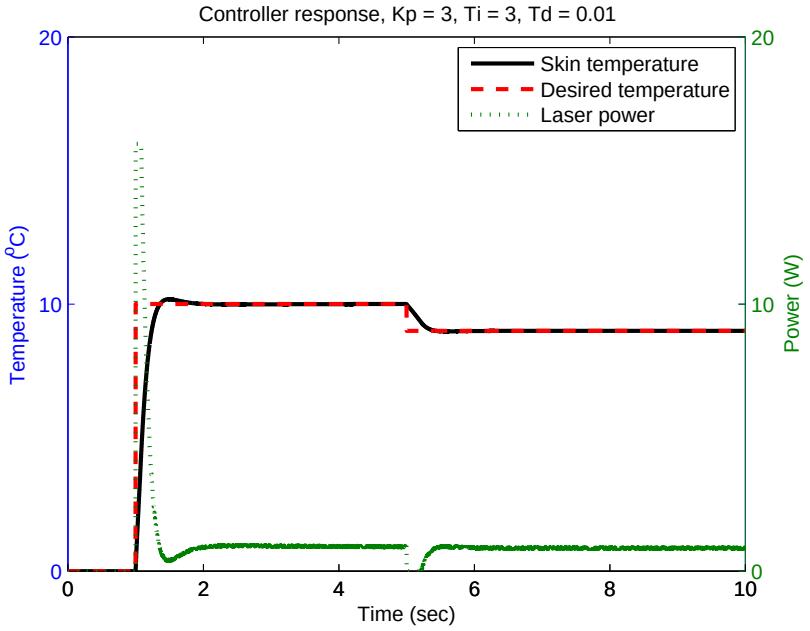

Figure 4.11: The figure illustrates the K_P = 3, T_I = 3, T_D = 0.01. It is seen that the overshoot and settling time has increased causing a significant steady state error.

In figures 4.10 and 4.11 it is also seen how the power input to the laser starts to fluctuate when the derivative term is added.
To sum up, the simulation indicates that a PI controller will be most preferable to implement.
In the above it was mentioned that the overshoot should be of the same magnitude as the steady error, which in reality would be due to measurement error in the infrared camera, therefore, this should be tested when the system is implemented.

4.6 Tuning theoretical model into the real world

After having theoretically simulated the laser skin interaction and having implemented the PI controller interacting with the infrared camera and the laser. The controller was first tested using the modelled settings for the controller. This was first done on pig skin, the controller was tuned until satisfactory results was obtained. Then the system was tested using in vivo human skin, again was the controller tuned until satisfactory results was obtained.
Due to high frequent noise on the temperature measurement, and the simulation results above, the derivative term was left out. Including it would cause the error to increase, and then the skin temperature would simply rise until the maximum allowable temperature was reached, causing the system to shut down.
Since the Labview PID toolkit used to implement the controller uses minutes as the unit for T_I and T_D the values from Simulink must be converted from seconds to minutes, however, the tuning process revealed that the integral time should be tuned further after the vivo test. Using LabViews implementation of the PID controller, the control tuning which had the best propertioes was a proportional gain of 3, an integral time (in minutes) of 0.04 (converting the simulated integral this should have been 0.05, but 0.04 showed better controller perfomance), and a derivative time of 0. Meaning only a PI controller was implemented and tuned. In the next chapter this controller is tested and used in a few psychophysiological experiments.

Synthesis

III

Test 5

In this chapter the developed system will be tested. First the accuracy of the system will be tested. Following the behaviour of the implemented controller will be tested. Then the developed system will be compared with the list of requirements found in section 1.5.1. Finally, the systems ability to be used in psychophysical studies will be tested. This was among other things accomplished by trying to reproduce the results found by Grill and Coghill (2002).

5.1 System accuracy

The accuracy of the system will depend on several factors such as the implemented controller and the temperature sensor used. Since the developed system utilizes a closed loop controller the accuracy of the used sensor, limits the accuracy of the system. Therefore, the first thing to test, is the used temperature sensor, the FLiR A40 infrared camera.

5.1.1 Infrared camera accuracy

The accuracy of the infrared camera was found by comparing the used FLiR camera to the Agema camera. The two cameras are set to measured the temperature in same reference. For reference the Medoc CHEPS system (ATS thermode) is used. This system has a repeatability of ± 0.1 °C and an absolute accuracy of 0.3 °C. The surface of the thermode of the Medoc system was placed perpendicular to the cameras line of sight. The Medoc system was also chosen as reference in order to test the systems controller properties, other references could have been used as well, but since the Medoc system was available during the test phase, this system was chosen.
The ThermaCAM researcher pro software was used for this test, for each camera the mean temperature of the stimulation area and the temperature at the center of the stimulation area were extracted. In figures 5.1 and 5.2 this is seen as Mean temperature (left) and Point temperature (right).
In order to obtain precise results from both cameras, the emissivity was calibrated in both cameras at two reference temperatures, 35 and 45 °C. The emissivity was taken as the mean of these two temperatures.
Two temperature paradigms were tested, using the same staircase stimulation technique which is used for the psychophysical studies, see below. The first paradigm was between 35 and 45 °C, the staircase had steps of 1 °C, and

each step was held for 15 seconds. The second paradigm was similar, but ran from 45 to 35 °C, and used the same steps as the first. The rise time between each step was set to 8 °C/s.

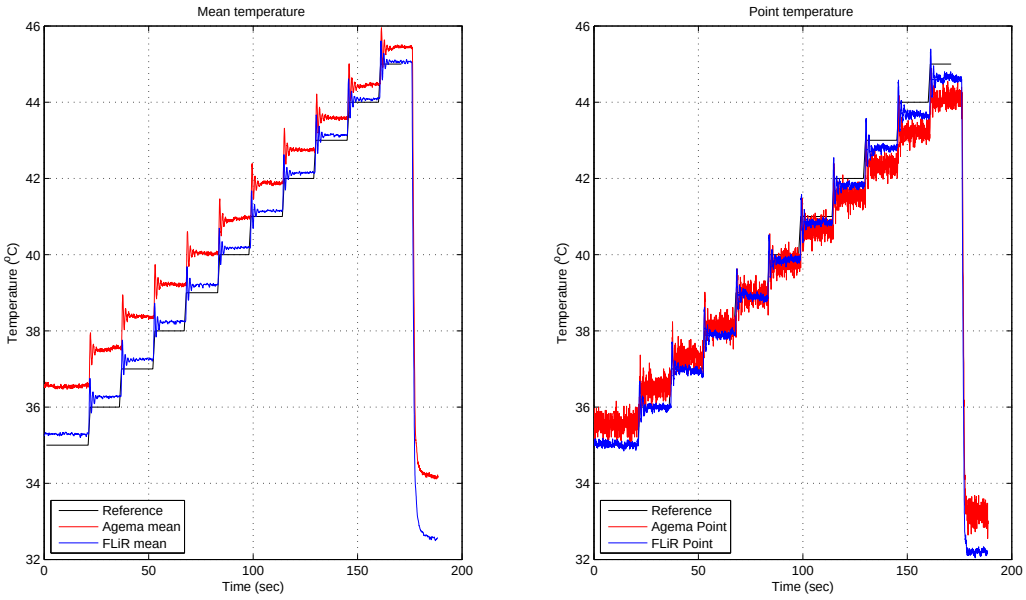

Figure 5.1: The figure illustrates the test of the infrared cameras in the 35 to 45 °C paradigm. Of the two cameras tested, it can be seen that the FLiR (blue) is closer to reference temperature set by the thermode. The deviation between the FLiR camera and the thermode is approximately 0.3 °C for the mean temperature, and 0.2 °C for the point temperature. For the Agema camera the deviation is at some points more than 1 °C for the mean temperature, and 0.5 °C for the point temperature. It can be seen that the controller in Medoc system causes some overshoot when the refence is changed.

In figures 5.1 and 5.2 the result of the camera tests at the 35-45 °C and 45-35 °C paradigms are seen. It is seen that even though both cameras were calibrated for the correct emissivity the FLiR camera is more accurate than the Agema,

compared to the reference value. The deviation of the FLiR camera is approximately 0.3 °C which is the same as the absolute accuracy of the Medoc system.

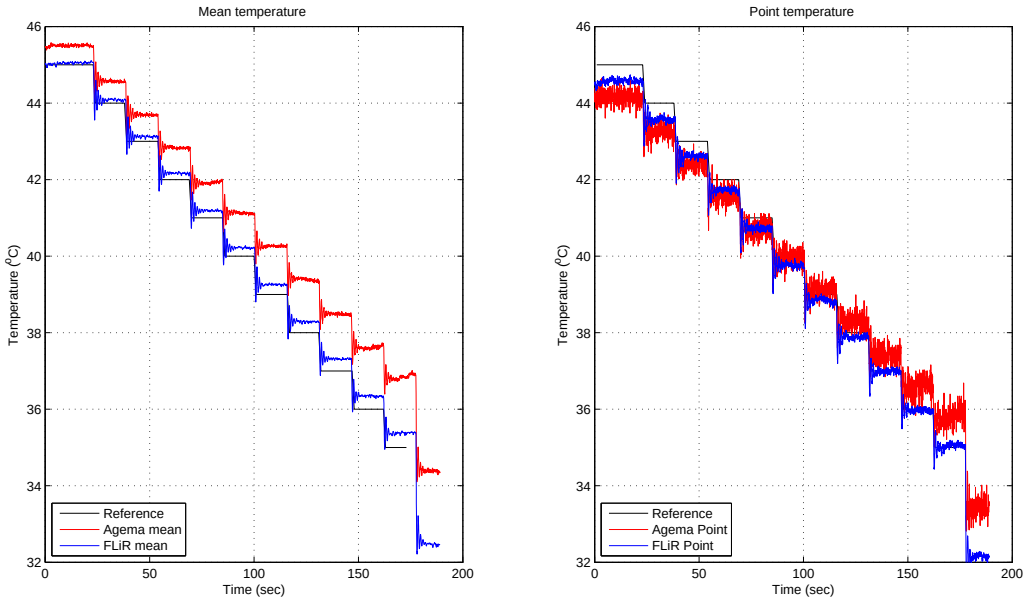

Figure 5.2: The figure illustrates the test of the infrared cameras in the 45 to 35 °C paradigm. Of the two cameras tested, it can be seen that the FLiR (blue) is closer to reference temperature set by the thermode. The deviation between the FLiR camera and the thermode is approximately 0.3 °C for the mean temperature, and 0.2 °C for the point temperature. For the Agema camera the deviation is at some point more than 1 °C for the mean temperature, and 0.5 °C for the point temperature. It can be seen that the controller in Medoc system causes some overshoot when the refence is changed.

In figures 5.1 and 5.2 is it seen that the medoc system have an overshoot of approximately 0.5 °C, when the reference is changed. Eventhough the infrared cameras are not 100 % accurate, the size overshoot seen is the camera is a good representative of the magnitude of the overshoot. Furthermore, the internal temperature monitor in the Medoc system also indicated an overshoot of 0.5 °C. As seen in figures 5.1 and 5.2 the controller in the controller in the Medoc system has ringing in approx. 5 seconds after the overshoot.
To test the camera only one staircase is necessary but this test will further be used as an evaluation to compare the controller response of the developed system with the Medoc system, therefore two staircases were used.
For most of the semester the Medoc CHEPS system was unavailable, thus it was not tested if the similar protocols in both the developed system and the Medoc system would produce similar sensations in the subjects.

5.1.2 Accuracy of the developed system

Having established the accuracy of the used temperature sensor, the steady state accuracy of the system can be tested. To evaluate the accuracy of the system a number of experiments were performed. A total of eight subjects were tested. During the experiments the subjects were stimulated using two paradigms; a staircase stimulation and a test for offset analgesia, see figure 4.2. The subjects were instructed to rate the sensation evoked on a VAS meter anchored such that ’0’ was no sensation, ’5’, was pain threshold and ’10’ was maximum pain. Based on these experiments the system accuracy was determined.
In the list of requirements in section 1.5.1 the steady state requirements are listed. The error between the desired

temperature and actual temperature must be less than 0.1 °C and the oscillations during the steady state must have an amplitude of less than 0.2 °C.
As seen in chapter 2 and appendix A the thermal and optical properties of the skin depends on the epidermal thicknes, which further depends on the skin type (glabrous vs. hairy). Therefore, the controller most likely will have different properties in the different skin types.
An example of the temperature profiles from one subject, during four staircase experiments including both paradigms and both skin types, are seen in figure 5.3 and 5.4. In the figures it is seen that the steady state error is acceptable for most temperature both in the glabrous and hairy skin. However, in both paradigms, there are some steady state errors at 35 and 36 °C (figure 5.4). These steady state errors are, during the 35-45 °C paradigm, caused by an inital skin temperature above 35 °C, and since the system utilizes no active cooling, this temperature cannot be decreased. In the 45-35 °C paradigm the errors are caused by the slow passive cooling, due to a low temperature gradient in the tissue, see Eq. 2.2, caused by an initial skin temperature close to or possibly above 35 °C.
In the left column of figure 5.4 (35-45 °C) it is seen that the steady state fluctuations in the glabrous are lower than those in the hairy skin, except at the lower temperatures (35-36 °C). However, both are within the 0.2 °C requirement.

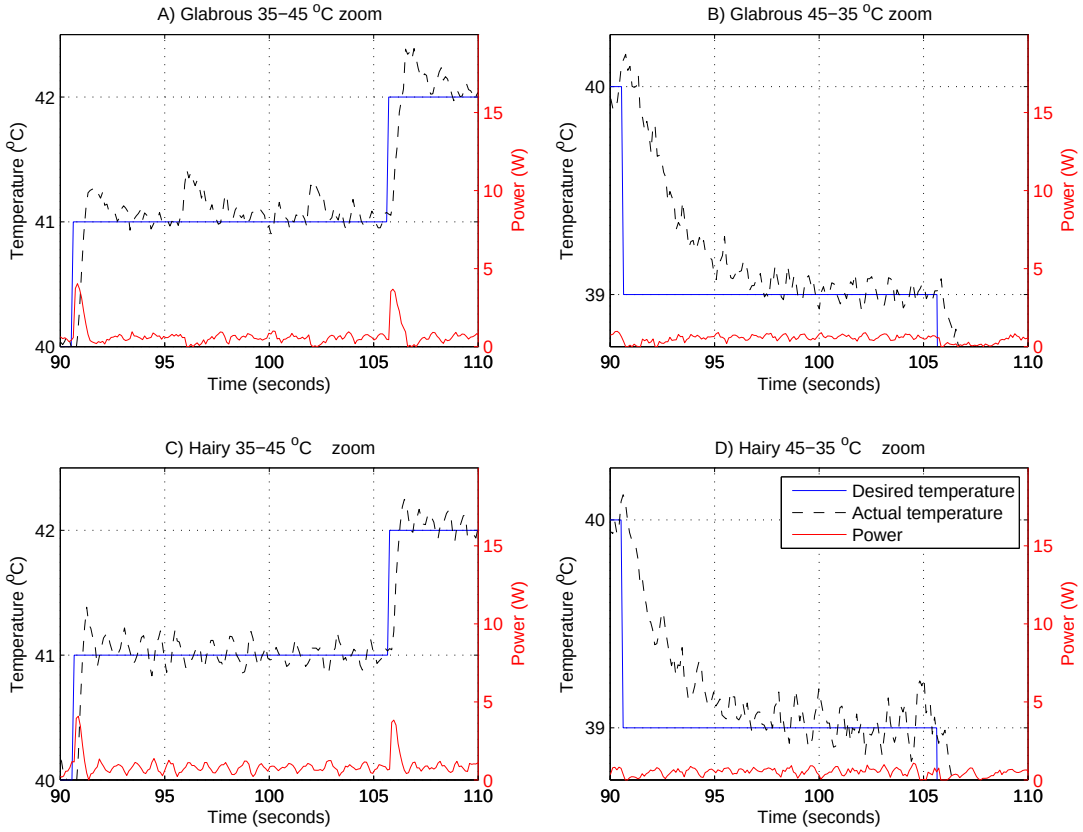

Figure 5.3: The figure illustrates a zoom-in of the temperature response during four staircase experiments. In the left column (A and C, 35-45 °C) it is seen that there are more rapid fluctuations in the hairy skin. In the right column (B and D, 45-35 °C) it is seen how the lack of active cooling prolongs the cooling rate compared to figure 5.2. In general the steady state errors are less than 0.1 °C, however, in A) there is a single peak in the error at approx. 96 seconds, this peak is most likely to a small movement of the stimulated area.

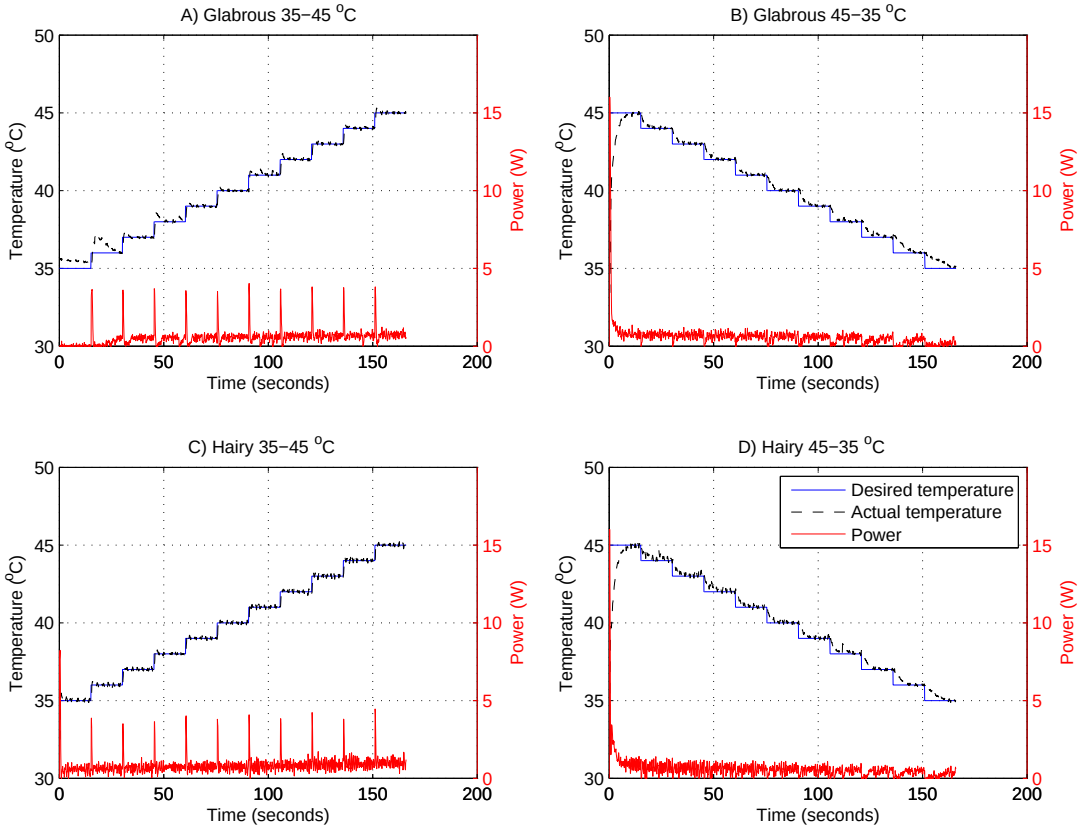

Figure 5.4: The figure illustrates the temperature response during four staircase experiments. In the figurs left column (A and C, 35-45 °C) it is seen that there are more steady state fluctuations in the hairy skin. In the right column (B and D, 45-35 °C) it is seen how the lack of active cooling prolongs the cooling rate compared to figure 5.2. The cooling rate is obviously higher when the temperature is higher, due to a higher temperature gradient in the tissue. The errors seen in A) around 35-36 °C is due an initial skin temperature of approx. 35 °C, this causes large overshoot when the desired temeprature is increased to 36 °C, however, these errors are eliminated when the desired temperature increases to 37 °C.

In figure 5.3 it is seen that the *mean* steady state error is much less than 0.1 °C, (meaning the mean of the fluctuating temperatures, is close to the desired temperature), except in A) there is a single peak in the error at approx. 96 seconds, this peak is most likely to a small movement of the stimulated area. Thus the requirement is fulfilled.

5.2 Temperature controller response

In the section above, it was determined that the system fulfills the accuracy requirements listed in section 1.5.1. In this section it will be evaluated whether the temperature control fulfills the requirements. In figures 5.3 and 5.4 the magnitude of the overshoot in the heating and cooling phase can be seen. In the cooling phase there is no overshoot, as expected, due to the relative slow passive cooling. In the heating phase the overshoot is approx. 0.2-0.3 °C, this is slightly above the requirement of 0.2 °C, however, the settling time of the system is fast enough to ensure that the

overshoot persists for less than 0.5 sec. Tests also showed that a larger step (> 5 °C) in the reference would cause the system to have less overshoot, than if the step was small $\sim$ 1 °C, this is due to unlinearity of the controlled process (skin heating and cooling).
When the controller was implemented a trade off was made, between rise time, overshoot, and cooling time in order to fulfill the requirements, see chapter 4. The overshoot in the heating phase could be reduced, however, this would cause the cooling phase to be prolonged, which is not desirable.
There were a number of requirements for the system rise time during heating. One requirement was an adjustable rise time in the range 0-5 °C per second. However, a variable rise time has not been implemented in the system and thus this requirement is not fulfilled. Another requirement was that system should be able to have a maximum risetime of 5 °C per second. In figure 5.3 it is seen that the rise time is at most 2 °C per second. This is below the requirement set, however, in figures 5.3 and 5.4 it can be seen that controller does not use the entire spectrum of the laser power (0-16 W). By re-tuning the controller to give a higher control effort the risetime could be increased. However, this would cause more overshoot, which contradicts another very important requirement. In the psychophysical studies which the system is intended for, a low rise time (< 5 °C per second) would be more preferable than a high overshoot ($\sim$ 0.5 °C). Based on the above it is evaluated that the controller tuning applied is appropriate for this system.

5.3 Psychophysical experiments - staircase stimulation and offset analgesia

As mentioned above, eight subjects were tested in order to evaluate whether the developed system was able to be used in psychophysical experiments. As a measure for this, it was tested if the system was able to evoke offset analgesia. Furthermore, each subject was tested with a staircase stimulation, mainly to test the implemented controller, but also since the staircase stimulation resembles the method of levels a stimulation often used in psychophysical studies.

Furthermore, the results in different skin types could be compared with the FEM developed in the previous study. The results of the staircase stimulation is seen in figure 5.5

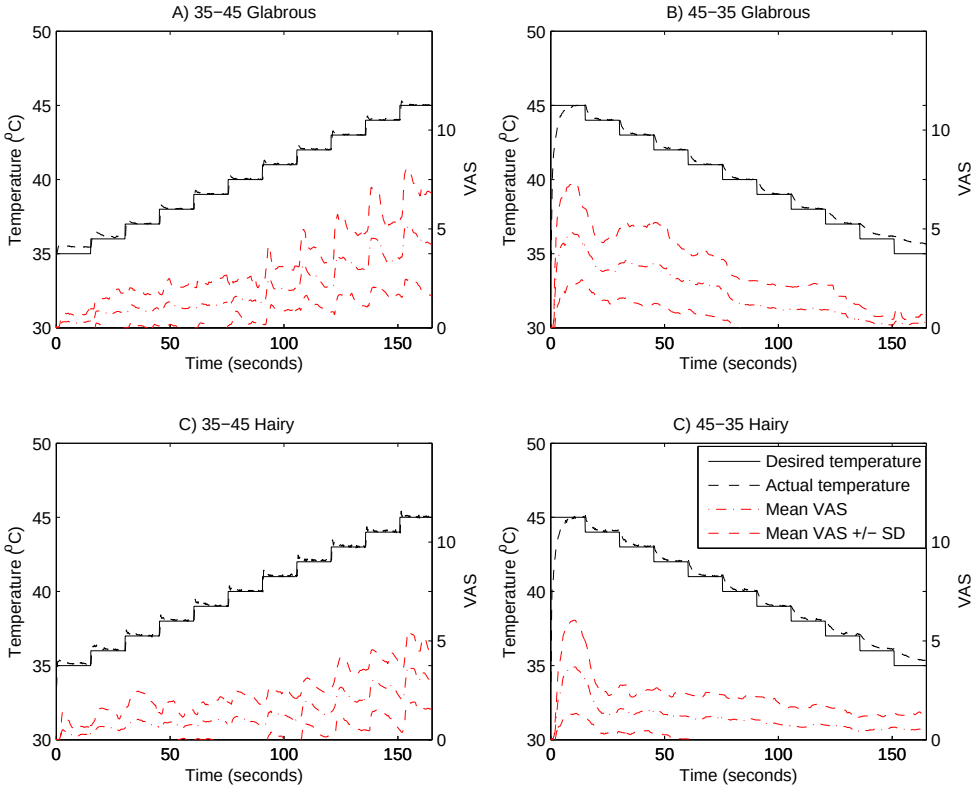

Figure 5.5: The figure illustrates the test of the staircase stimulation meaned over eight subjects. The VAS is anchored such that '0' was no sensation, '5', was pain threshold and '10' was maximum pain A) and C) is the 35-45 °C paradigm (1 °C step and 15 seconds at each step) tested in glabrous (A) and hairy skin (C). B) and D) are the reversed paradigm (45-35 °C) tested in glabrous (B) and hairy skin (C). In A) and somewhat also in C) it can be seen how the VAS score increases everytime the skin temperature is increased, and then during the plateau the VAS score decreases.

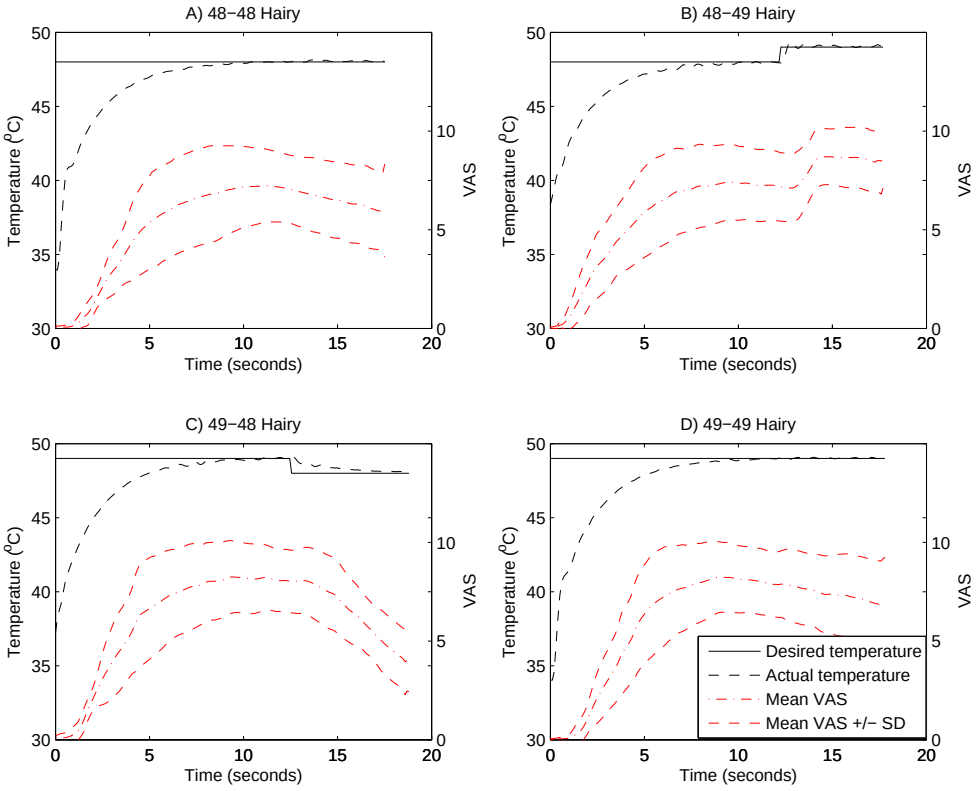

Figure 5.6: The figure illustrates the test of offset analgesia test meaned over eight subjects. The VAS is anchored such that '0' was no sensation, '5', was pain threshold and '10' was maximum pain. A) is a control of 48 °C in 10 seconds. B) is a test of increase of 1 °C from 48 °C in 5 seconds to 49 °C in 5 seconds. C) is the actual test for offset analgesia, the initial skin temperature is set to 49 °C in 5 seconds, this is then lowered to 48 °C and maintaind for 5 seconds. D) is a control of 49 °C in 10 seconds. In the test a temperature tolerence of 0.25 °C was used, see chapter 4. Comparing B) and C) it can be seen that there is a tendency that the temperature decrease causes a higher change of the pain rating, than an equivalent increase does.

In figure 5.6 it seems that the decrease in temperature will give an reduction in the VAS which is unproportionally large, compared the VAS increase following a similar temperature increase. If this proves statistically significant then the requirement, of the system being able to evoke offset analgesia, is fulfilled.

5.3.1 Statistical tests

To test the data (VAS ratings) from the staircase stimulations a repeated 1-way ANOVA was applied. The subjects were the random factor; the fixed factors were each combination of temperature and stimulation paradigm (increasing or decreasing staircase) (a total of four 35-45 °C in glabrous and hairy skin; and 45-35 °C in glabrous and hairy skin). The four combinations *a*, *b*, *c*, and *d* is seen below.

a - 35-45 °C in glabrous skin

b - 45-35 °C in glabrous skin

c - 35-45 °C in hairy skin

d - 45-35 °C in hairy skin

Differences between a, b and c, d would indicate differences between skin type. Differences between (*a*, *c*) and (*b*, *d*) would indicates differences related to stimulation paradigm, either increasing or decreasing staircase.
The dependent variable was the mean VAS rating at each stimulation temperature extracted for each temperature and each stimulation paradigm. If there was significant difference between the fixed factors a posthoc test was made to determined which groups were different.

The statistical tests used to test the data from the offset analgesia stimulation will mainly be inspired by those used by Grill and Coghill (2002). First a repeated measures 1-way ANOVA will be conducted to test whether the change in VAS is different in the 48-49 °C step compared to the 49-48 °C step.
Then two repeated measures 1-way ANOVA was used to test whether the difference between similar temperatures, either 48 or 49 °C. For each temperature four groups were tested. These groups were named *a*, *b*, *c*, and *d* is seen in Table 5.1. It is seen that for each temperature two groups were extracted from the constant stimulations, and one group was extracted from each of the step stimulations.
If any factors showed a significant difference a posthoc test was performed to determine which groups were different from each other.

Temperatures	48 °C		49 °C	
Group name	**Stimulation type**	Time	**Stimulation type**	Time
a	Constant (48-48)	6 sec before end	Step-up (48-49)	1 sec before end
b	Constant (48-48)	1 sec before end	Step-down (49-48)	1 sec before step
c	Step-up (48-49)	1 sec before step	Constant (49-49)	6 sec before end
d	Step-down (49-48)	1 sec before end	Constant (49-49)	1 sec before end

Table 5.1: The table displays the four groups tested in the ANOVA for the offset analgesia data. One ANOVA was conducted for two temperatures (48 & 49). The term *end* refers to stimulus, after 5 seconds at the second plateau (if step stimulation was used) or 10 seconds after the plateau has been reached (if constant stimulation was used). *Step* refers to the step between 48 and 49 °C.

Statistical findings

The repeated ANOVA on the staircase data showed data that there were difference between different stimulation types ($p < 0.001$) and between different stimulation temperature ($p < 0.001$). Differences between the stimulation types are seen in Table 5.2. It is seen that for similar stimulation paradigms there is no difference in similar skin type *a* vs. *b* and *c* vs. *d*. Meaning that the direction of staircase, increasing or decreasing has no effect on the VAS rating. Comparing the skin types in table 5.2, meaning *a* and *b* vs. *c* and *d*, it is seen that there is significant difference between skin type for identical stimulations paradigms (*a* vs. *c* and *b* vs. *d*). From the confidence intervals it is seen that VAS in the glabrous skin is higher than in the hairy skin. Comparing all stimulation paradigms it is seen that there is significant difference between the skin types, disregarding the stimulation paradigm, except between *b* and *c* ($p = 0.117$). Comparing the confidence interval of these two groups it is seen that they are only slightly overlapping, increase the repitions would most likely decrease the variation and the difference between these two groups would also be significant. Meaning a significant difference between skin type would be seen for all stimulations.

Results		*p*-value	Confidence interval
a	*b*	0.936	1.689 : 2.206
	c	0.008*	
	d	<0.001*	
b	*a*	0.936	1.521 : 2.038
	c	0.117	
	d	0.003*	
c	*a*	0.008*	1.087 : 1.605
	b	0.117	
	d	0.824	
d	*a*	<0.001*	0.873 : 1.391
	b	0.003*	
	c	0.824	

Table 5.2: The table displays the *p*-values and confidence intervals from the posthoc test following the ANOVA test on the staircase stimulation. It is seen that there is no difference between different stimulation types in the same skin type (*a* vs *b* and *c* vs. *d*). This indicates that the direction of the staircase, increasing or decreasing, has no effect on the VAS reported by the subjects. Comparing stimulations between different skin type it is seen that there is a differencee between *a* between *c* and *d*, however, *b* is not significantly from *c* ($p = 0.117$), however, comparing the confidence interval of *b* and *c* it is clear that they are only just overlapping, increasing the number of repitions could decrease the variance and create a significant difference. The confidence intervals indicate that identical stimulation paradigms are rated significantly higher in the glabrous skin than in the hairy skin - except between *b* and *d*. * indicate significant difference between groups at significance level 0.05.

For the posthoc test between the temperatures (Table 5.3) it was found that the difference between the VAS score corresponding to the temperatures increased with temperature. Meaning that the subjects ability to discriminate between the different temperatures increases with temperature. There was found no differences between temperatures below 40 °C but the highest temperature 45 °C was significantly different from all other temperatures, except 44 °C.

Temperature		*p*-value	Temperature		*p*-value	Temperature		*p*-value
35	36	1.000	36	35	1.000	37	35	1.000
	37	1.000		37	1.000		36	1.000
	38	0.989		38	1.000		38	1.000
	39	0.864		39	1.000		39	1.000
	40	0.281		40	0.834		40	1.000
	41	0.002*		41	0.025*		41	0.344
	42	<0.001*		42	<0.001*		42	0.005*
	43	<0.001*		43	<0.001*		43	<0.001*
	44	<0.001*		44	<0.001*		44	<0.001*
	45	<0.001*		45	<0.001*		45	<0.001*
38	35	0.989	39	35	0.864	40	35	0.281
	36	1.000		36	1.000		36	0.834
	37	1.000		37	1.000		37	1.000
	39	1.000		38	1.000		38	1.000
	40	1.000		40	1.000		39	1.000
	41	0.616		41	0.904		41	1.000
	42	0.014*		42	0.049*		42	0.341
	43	<0.001*		43	<0.001*		43	0.002
	44	<0.001*		44	<0.001*		44	<0.001*
	45	<0.001*		45	<0.001*		45	<0.001*
41	35	0.002*	42	35	<0.001*	43	35	<0.001*
	36	0.025*		36	<0.001*		36	<0.001*
	37	0.344		37	0.005*		37	<0.001*
	38	0.616		38	0.014*		38	<0.001*
	39	0.904		39	0.049*		39	<0.001*
	40	1.000		40	0.341		40	0.002*
	42	1.000		41	1.000		41	0.253
	43	0.253		43	1.000		42	1.000
	44	0.007*		44	0.423		44	1.000
	45	<0.001*		45	<0.001*		45	.037*
44	35	<0.001*	45	35	<0.001*			
	36	<0.001*		36	<0.001*			
	37	<0.001*		37	<0.001*			
	38	<0.001*		38	<0.001*			
	39	<0.001*		39	<0.001*			
	40	<0.001*		40	<0.001*			
	41	0.007*		41	<0.001*			
	42	0.423		42	<0.001*			
	43	1.000		43	0.037*			
	45	0.669		44	0.669			

Table 5.3: The table displays the *p*-values from the posthoc test comparing differences between different stimulation temperatures. In the table is seen how the subjects ability to discriminate between temperature increases with temperature. Whereas there is no significant difference between temperatures below 40 °C, the highest temperature 45 °C is significant different from all other temperatures except 44 °C. * indicate significant difference between groups at significance level 0.05.

On the offset analgesia data the repeated measures ANOVA testing a 1 °C temperature increase or decrease, showed that the decrease evoked a change in sensation intensity which was significantly larger than a corresponding increase ($p < 0.001$).
The repeated measures ANOVAs for the two temperatures (48 and 49 °C) both showed a significant difference between the groups (48 °C - $p < 0.001$ and 49 °C - $p = 0.002$). After the ANOVA a posthoc test was performed for each temperature to determine which groups was different. The results for both temperatures are seen in Table 5.4.
In the table it is that for the group *d* in 48 °C all other groups are clearly significantly different ($p < 0.001$), this means that offset analgesia could be evoked with the developed system.
For the 49 °C stimulation group *d* was significantly different from groups *a* and *b*, however, not group *c* though a tendency was seen, $p = 0.165$.

Temperatures		48 °C	49 °C
Group 1	**Group 2**	*p*-value	*p*-value
a	*b*	0.113	0.840
	c	0.998	0.375
	d	<0.001*	0.001*
b	*a*	0.113	0.840
	c	0.036*	0.984
	d	<0.001*	0.030*
c	*a*	0.998	0.375
	b	0.0.36*	0.984
	d	<0.001*	0.165
d	*a*	<0.001*	0.001*
	b	<0.001*	0.030*
	c	<0.001*	0.165

Table 5.4: The table displays the *p*-values from the posthoc followed the ANOVA test. It is seen that for the group *d* in the 48 °C column, all other groups are different. Group *d* for 48 °C is the test to evoke where offset analgesia, since all other groups are significantly different, the test shows that offset analgesia in fact was evoked. In contrast the step-up of the 49 °C stimulation, group *a* was not significant from all other groups, indicating (as expected) that the contrast is increased during stimulus decrease, not increase. * indicate significant difference between groups at significance level 0.05.

5.4 Fulfilment of requirements

From the sections above it can be conclude that all but two requirement has been fulfilled. The two requirements considering the magnitude and adjusting of the risetime are not fulfilled. The magnitude of the risetime was less than half ($\sim$ 2 °C per second) of the requirement (5 °C per second). The requirement considering overshoot is on the limit of the requirement but it is accepted as fulfilled.
Statistical tests showed that the system was able to evoke offset analgesia.
These results will now be discussed in the next chapter.

Discussion

6

In this thesis a non-contact heat stimulator for psychophysical studies has been developed. Before the development started a number of requirements was listed for the system (section 1.5.1). In order to gain detailed knowledge of the thermal properties of the skin being heated, a thorough study was conducted. In the study a CO_2 laser was used as heat source. The study focussed on developing a model which simulates the heat distribution in the skin during thermal laser stimulation. The developed model was validated through experimental trials testing 16 subjects. Based on the study, evidence for the depth of heat sensitive receptors increasing with the epidermal thickness was found. In hairy skin the receptors were found approx. 50 μm deep, where in glabrous skin they were found as deep as 130 μm, almost three times deeper. This distance will increase the thermal insulation of the receptors, and thus affect how the thermal energy from contact stimulators or low penetration lasers reach the receptors.
The energy from a CO_2 laser is absorped so superficially that the thermal energy, when absorped, does not affect the majority of the receptors, if any at all. The heat must be conducted into the depth where the receptors are found, the deeper location of the receptor, the longer it takes to conduct the heat, causing longer latencies in skin with thicker epidermis (glabrous). This corresponds well with the fact that first pain only can be elicit in glabrous skin if using a laser with high penetration depth [Iannetti et al., 2006]. Something which is not feasibible using a CO_2 laser [Treede et al., 1995].
In chapter 5 a series of tests were performed to evaluate the perfomance of the system. The tests mainly held the systems perfomance against the list of requirements. The most important of the tests was to verify the systems ability to be used in psychophysical studies. Two stimulation paradigms were tested, first a staircase stimulation and second a test to see if it was possible to evoke offset analgesia.
Before the psychoohysical tests the system accuracy was determined. The closed loop controller used, rely on a temperature measurement to adjust the laser power. If the temperature measurement, from the infrared camera, is inaccurate then the system accuracy will be impaired. Therefore, the accuracy of the infrared camera was determined. It was found that the temperature measurement corresponded with the reference used (Medoc CHEPS system). Since the reference has a absolute accuracy of 0.3 °C and the deviation between the infrared camera and the reference was also 0.3 °C, thus, it was concluded that the infrared camera is no more inaccurate than the reference. Still this accuracy was found to be satisfying. The steady state accuracy was following evaluated. Both requirements were fulfilled; it was found that the mean steady state error was less than 0.1 °C and the steady state oscillations had an amplitude of less than 0.2 °C.
The response of the implemented controller was evaluated, and based on the requirements it was found that the cooling rate and magnitude of overshoot was on the limits of the requirements, but still acceptable. However, the two requirements regarding the rise time were not fulfilled. During the controller tuning a tradeoff was made between the requirements, a limited overshoot was more important than the magnitude of the rise times.
During the developed and implementation a varity of different controller tunings were tested, of the tested parameters it is concluded that the temperature controller implemented is the best tradeoff to reach the requirements.

When the initial system test was completed the system was tested as a stimulator in psychophysical studies. First each subject was stimulated using an increasing and decreasing staircase paradigm, the results of this is seen in figure 5.5. It is seen how the sensations reported by the subjects have a peak following each temperature increase from 40 °C and up, after this peak the VAS score settles at a steady level.
A repeated measures 1-way ANOVA was used to test if there were significant difference between different stimulation types (four groups: increasing or decreasing staircase in two skin types). The test showed significant differences between the groups, therefore a posthoc test was performed to seperate which skin types and temperatures were different. In tables 5.2 and 5.3 the results of the posthoc test is seen. In table 5.2 it is seen that the administration of different temperatures does not affect how the sensation is rated on the VAS scale. However, there was significant differences in the sensations following similar stimulation paradigms in different skin types. In fact a clear tendency was seen for all stimulation paradigms indicating a significant difference between skin types; all but one combination showed

evidence for this, this combination showed a tendency towards a significant difference ($p = 0.117$).
The confidence intervals showed that the VAS scores for the glabrous skin was higher than the VAS scores in the hairy skin. This finding is quite interesting when comparing it to the study made with the CO_2 laser. In that case the VAS scores are higher in the hairy skin, see chapter 2. Comparing this to the FEM provides further indications that the model gives good understanding of the heat distribution in the skin, when using different heat sources. The model proves that the temperature at receptor level is much lower in glabrous skin than in hairy skin following a CO_2 laser stimulation. Whereas a stimulation from a diode laser would cause the temperature to be similar at receptor levels disregarding the skin type, see figures 3.1, 3.2, 3.3, and 3.4. However, the FEM model does not explain why the stimulations in glabrous and hairy skin are sensed differently when the temperature at receptor level is similar. One possibility is that the nociceptors could be more abundant in glabrous skin, causing more nociceptors to be activated, thus increasing the sensation reported by the subjects. Another explaination could be that the central sensory system reacts differently to the same receptor temperature depending on the skin type. This could help to ensure that when the skin touches a warm element it is sensed equally in both skin types. This central mechanism would cause a bias when the thermal energy no longer is absorped at the skin surface but is absorped inside in the tissue close to the receptors. However, this is contradicted by the fact that the CO_2 laser stimulations evoked less intense sensations in the glabrous skin than in the hairy skin. A third possibility is that the receptors in the skin depends on the skin type. A claim which previously has been postulated by others [Treede et al., 1995]. Treede et al. (1995) postulated that the reason why first pain could not be elicited in glabrous skin was due to different populations of afferent in different skin types, a claim which later has been modified by Ianneti et al. (2006) who were able to elicit first pain in glabrous skin.
Finally, the staircase stimulations provide evidence how the ability to discriminate between different temperatures increases with temperature (Table 5.3).

Following the staircase stimulations a offset analgesia test was conducted and the results of this test were analysed. The first repeated measures ANOVA showed a significant difference between the changes in sensation intensty following a 1 °C decrease and increase. The change in VAS following a 1 °C decrease was significantly larger than the change in sensation intensity following a temperature increase of 1 °C.
The ANOVA test of similar temperatures (48 or 49 °C) showed there were significant differences between the groups. The posthoc test showed that for the 48 °C temperature group *d* was significant different from all other groups, this serves as evidence that the developed system is able to evoked offset analgesia, since group *d* was a stimulation at 48 °C following a stimulation of 49 °C.
During the stimulations there was a possibility of habituation in the sensory system, causing the evoked sensation to decrease eventhough the intensity of stimulation remains constant. In order to control this, two stimulations of constant temperature were administrered (groups *a* and *b* for 48 °C & groups *c* and *d* for 49 °C) if habituation occurs this would be visible as a decrease in the VAS score in the latter of the groups (group *b* for the 48 °C and group *d* for 49 °C). However, the posthoc test showed that habituation alone could not be responsible for the offset analgesia seen. Since group *d* was different from group *b* which would both be habituated, this provides evidence that the change seen in group *d* (offset analgesia group) is not solely due to habituation, but the analgesic effect reported by Grill and Coghill (2002) could be reproduced.
Furthermore, the 49 °C test provides evidence how the sensory system shows sign of habituation during a 49-49 °C stimulation paradigm. However, group *d* for this temperature was only significantly different from groups *a* and *b*. The high significance found between groups *a* and *d* is possible due to a sharp reaction from the subjects, caused by the 1 °C step-up in temperature.

Eventhough the stimulation methods used in this thesis are somewhat different compared to those used by Grill and Coghill (2002 and others [Yelle et al., 2008] [Derbyshire and Osborn, 2008] [Derbyshire and Osborn, 2009], offset analgesia could still be evoked. These different stimulation methods could cause some variations in the results.
These differences are multiple, first comparing the controller in the developed system and the controller in previous offset analgesia studies (Medoc CHEPS system) [Grill and Coghill, 2002] [Yelle et al., 2008] [Derbyshire and Osborn, 2008], it can from figures 5.1 and 5.2 be seen how the magnitude of the overshoot in both the heating and cooling phase are larger (0.5 °C) than the one in the developed system (0.2-0.3 °C). Undoubtly this overshoot combined with higher rise times will increase the temporal contrast of the stimulations. Since offset analgesia most likely is a mechanism to

enhance the temporal contrast in stimuli [Grill and Coghill, 2002] [Yelle et al., 2008], the overshoot will increase the analgesics effect reported by the subjects tested. This is especially important during cooling where the difference is exacerbated. The developed system utilizes slow (< 1 °C per second) passive cooling with no overshoot; in contrast the Medoc system have fast (8 °C per second) active cooling with an overshoot of $\sim$ 0.5 °C. This will increase the temporal contrast during stimulus decrease, however, this is not the only difference between the two stimulation methods.
In the Medoc device the stimulation area is fixed at either 16x16 mm [Grill and Coghill, 2002] [Yelle et al., 2008] or a diameter of 27 mm [Derbyshire and Osborn, 2008] (depending on the probe), for the non-contact system the beam diameter of the incoming laser light is approximately 6-7 mm. Meaning that the developed system has a much smaller stimulation area. This opens the possibility that a difference could occur due to spatial summation [Lautenbacher et al., 2001]. A larger stimulation area will increase the pain sensation reported by the subjects [Lautenbacher et al., 2001]. The large stimulation area of the Medoc system will most likely, cause an increase of the pain sensation to similar stimulation temperatures, this increase could increase the sensation difference between the 49 °C stimulation and the following 48 °C, resulting in more pronounced offset analgesia sensations.
Another possible factor which could cause different results is the actual paradigm used. Grill and Coghill (2002) evoked the offset analgesia by using a three temperature paradigm, e.g. 48-49-48 °C the two first steps was held in 5 seconds and the final in 20 seconds. In this thesis two paradigms were used which divide the two steps into two trials, one testing 48-49 °C step. And one testing the 49-48 °C step, each step was held for 5 seconds. This was done to ensure easier seperation of the two steps. However, it is possible that the initial step up 'primes' the sensory system so that it is following more susceptable to any following decreases. The increase could also cause some sensitization in the sensory system [Raja et al., 1999], this could increase the sensations reported by the subjects, and thus possibly increase the sensation intensity during the decrease of the temperature.

To sum up it is concluded that proof of concept has been reached since it was possible to evoke offset analgesia using a non-contact thermal stimulator. We have shown that the passive cooling is sufficient to evoke offset analgesia. However, the magnitude of the offset analgesia would propably increase with increasing cooling rate, thus increasing the temporal contrast.
Putting in the developed system into a broader perspective, offset analgesia is only one of many types of studies which can be conducted with the system. Compared to contact stimulators, the non-contact stimulator developed provides a number of advantages; the heat is absorped directly at receptor level, and the controlled temperature is equal to the temperature at receptor level; the size of the stimulation area can be changed; and finally the stimulation location can rapidly be moved.

Appendix

IV

Monte Carlo simulation

A

This appendix is a selected chapter of the authors eight semester project. This appendix is an excact copy of the chapter from the authors 8th semester (2nd semester of the Master) project, no modications have been made to it. This chapter describes the theory behind the Monte Carlo simulation used in chapter 2, to model the photon absorption from the laser.

A.1 Monte Carlo method

The Monte Carlo method is a stochastic approach useful to simulate the photon propagation in a medium, this chapter will focus on the photon propagation in the skin, caused by the irradiation of a near infrared laser.
The Monte Carlo method simulates a number of photons being scattered within the tissue. The number of photons should be high enough to give a representative result of the real radiation from the laser. The exact number of simulations needed depends the problem being modelled [Welch and van Gemert, 1995b].
The Monte Carlo method is basicly a so-called random walk where a single photons path through out the tissue is followed. The key concepts of the random walk is two decisions, the path each photon travels before an absorption or scattering event occurs and the angle the photon is scattered into, if not absorped. As the reader can appreciate the Monte Carlo method simulates the photons as particles, not electromagnetic waves, so phase and polarisation are ignored.
Several approaches exists, the simplest and most straightforward method is to simulate a single photon at a time, this approach requires a large number of photons to be simulated before an accurate result can be achieved. Another approach is the so-called implicit photon capture where a photon package is being simulated. Each package is initiated with a certain weight and after each mean free path a certain percentage of the photon weight is absorped, the remaining photon package is scattered and moved to a new interaction position. After a number of interaction the photon weight has become very low and the photon package is terminated. When using the implicit photon capture method a fewer number of photons needs to be simulated which reduces the computational cost [Welch and van Gemert, 1995b]. For this project the implicit photon capture method was used.
This project will investigate the propagation of photons from a diode laser into the cutaneous layers (epidermis, dermis, blood vessel) and subcutaneous tissue. The basic problem can be seen in figure A.1.

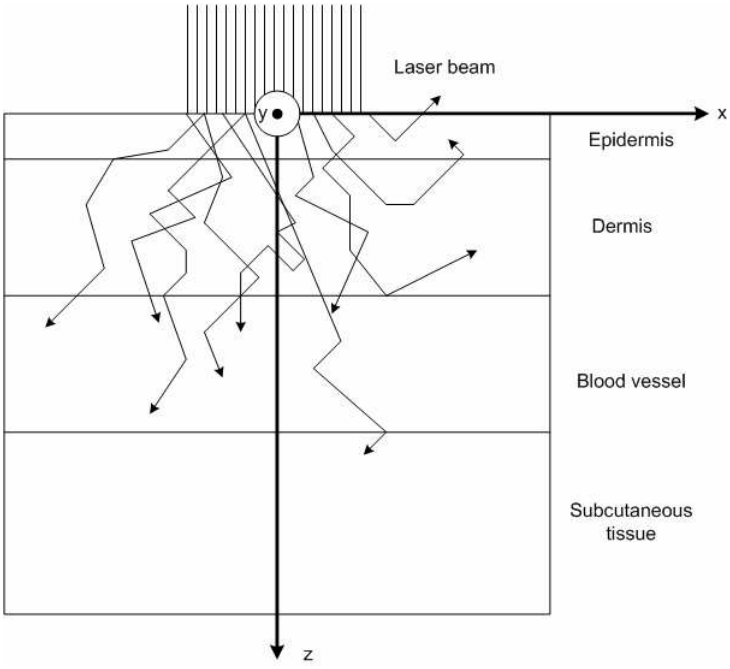

Figure A.1: The figure illustrates how the layers of the epidermis, dermis, blood vessel and subcutaneous tissue are located. In the figure it can also been seen how the centre of the laser beam is located in the origin of the cartesian coordinate system (0,0,0) and how the photons are scattered through out the tissue.

In the following the different components of the Monte Carlo method will be explained, first a brief overview.

A.2 Overview of the method

As mentioned above the implicit photon capture method was used. The method starts with a photon package being initiated, the photon weight is set to unity. A fraction of the photon weight will be reflected at the tissue surface, due to specular reflection, so this amount, R_{SP}, is subtracted from the photon weight. The remaining photon weight enters the tissue and the first mean free path or propagation distance, Δs, is generated and the photon package is moved. Each time the photon is moved, it is checked whether an internal boundary is crossed, if that is the case, the possibility for either internal reflection or refraction is checked. At each new position a fraction of the photon package is absorped, the position and the photon weight absorped is stored. After each interaction the scattering angle is calculated and a new Δs is generated and the steps described above is repeated until the last photon package has been reached.
After a number of interactions the photon weight becomes low and thus the propagation of the photon package will not provide much further information. In this situation it becomes relevant to consider terminating the photon package. Therefore a so-called roulette is played, here the photon package has a m to one chance of surviving (m is simply a chosen number e.g. 5 or 10, deciding the change of the photon being terminated in the roulette), if the photon survives the weight is increased m times. If the photon is terminated, the weight is set to zero and a new photon package will be initiated. If the photon leaves the tissue, i.e. if the photon is scattered out, the weight is also set to zero. For the backscatter problem in this project is it also of interest to know the photon weight which leaves the tissue therefore this amount is stored together with weight being reflected, R_{SP}.
The entire process can be seen on the flow chart below (Fig. A.2).

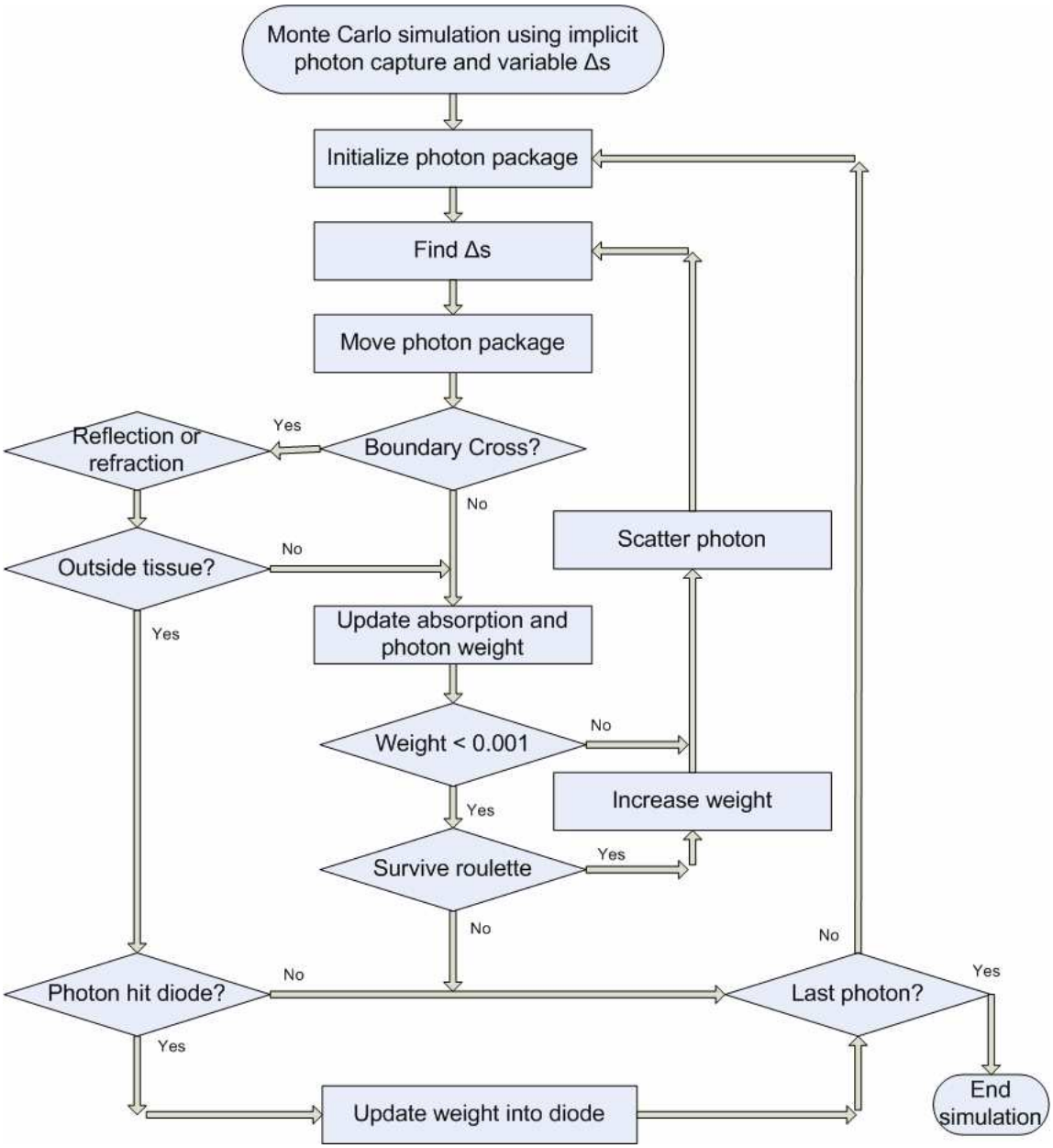

Figure A.2: This flowchart illustrates the basic idea in the developed Monte Carlo algorithm. Adapted from [Prahl et al., 1989] and [Welch and van Gemert, 1995b].

For the model used in this project the following conventions have been used:

- All units are in SI-units.
- Each incoming photon package has a weight of unity
- A 3D setup using cartesian coordiantes, the x and y axis are parallel to the tissue surface and the z axis is perpendicular to the tissue surface.
- Every internal boundary is normal to the z axis
- z is positive within the medium (the tissue) - zero at the air-tissue boundary
- A total incoming energy of 1 joule (meaning 1 W in 1 second) was simulated
- Coefficient and constants used in the model can be seen in table A.1

Coefficients	**Epidermis**	**Dermis**	**Blood**	**Subcutaneous tissue**
μ_a [m^{-1}]	100	100	168	120
μ_s [m^{-1}]	15067.5	15067.5	66800	16000
n	1.34	1.41	1.4	1.46
g	0.9	0.9	0.9	0.9

Table A.1: Optical coeffcients used in the Monte Carlo simulations.

A.2.1 Reflection at the tissue surface

When the photons enters the tissue some of them will be reflected at the surface, due to specular reflectance. The amount of the photons reflected depends on the mismatch of the refractive indices between the tissue surface (epidermis), n_1 and the air, n_2. The fraction reflected, R_{SP} can be expressed as

$$R_{SP} = \frac{(n_1 - n_2)^2}{(n_1 + n_2)^2} \tag{A.1}$$

Using implicit photon capture means that the weight of each photon package entering the tissue will be less than unity. The weight of each package entering the tissue can be expressed as

$$W = 1 - R_{SP} \tag{A.2}$$

A.2.2 Creating the propagation distance, Δs

The propagation distance before the photon interacts with the tissue, Δs, depends on the absorption (μ_a) and scattering coefficient (μ_s) of the tissue. The propagation distance should be small compared to the mean free path of the photon in the tissue [Prahl et al., 1989]. The mean free path is equal to the reciprocal of the total attenuation coefficient, μ_t, which equals

$$\mu_t = \mu_a + \mu_s \tag{A.3}$$

The propagation distance should then satisfy

$$\Delta s << \frac{1}{\mu_t} = \frac{1}{\mu_a + \mu_s} \tag{A.4}$$

[Prahl et al., 1989]
The simplest approach is to choose a constant propagation distance, however it can be difficult to choose the best value. Since if the propagation distance is too small the photon will rarely interact with the tissue and if it is too large

the simulation is a poor approximation of the path a photon really follows [Prahl et al., 1989].
For the reasons mentioned above another approach is used when choosing the propagation distance. Instead of using a constant value, the step size varies. The probability density function (pdf) of the propagation distance can be described using Beers law - i.e. the photon is more likely to travel a short distance than a long, and the probality is equal to $e^{-\mu_t \Delta s}$ [Prahl et al., 1989]. By using a random number ζ, uniform distributed between 0 and 1, which is the same interval as the pdf is in, this can be written as

$$\zeta = e^{-\mu t \Delta s} \tag{A.5}$$

Isolating with respect to Δs results in the following expression for the propagation distance

$$\Delta s = \frac{-ln(\zeta)}{\mu_t} \tag{A.6}$$

[Prahl et al., 1989]

A.2.3 Moving the photon

After having found the propagation distance the photon will now be moved. The new x,y and z are calculated based on the previous coordinates (x',y', z'), the direction cosines μ_x, μ_y and μ_z and the propagation distance, Δs

$$x = x' + \mu_x \cdot \Delta s \tag{A.7}$$
$$y = y' + \mu_y \cdot \Delta s \tag{A.8}$$
$$z = z' + \mu_z \cdot \Delta s \tag{A.9}$$

The calculation of μ_x, μ_y and μ_z will be derived below.

A.2.4 Internal reflection or refraction at smooth boundaries

Internal reflection

The mismatch of refractive indices can cause photon to be internally reflected. Since the Monte Carlo model being developed is multilayered there exist several boundaries inside the tissue which can cause internal reflection or refraction. The model contains the following layers

- Epidermis
- Dermis
- The blood vessel
- Subcutaneous tissue

Inbetween all of these layers the possibility of internal reflection exits, therefore this has to be checked everytime a photon crosses a boundary. If so, the chance of internal reflection depends on the refractive indices of the two layers. Again random number, uniform distributed between 0 and 1, is created, if this number is greater than a value R, then internal reflection occurs. R is calculated as

$$R = 0.5 \cdot \left(\frac{sin^2(\theta_i - \theta_t)}{sin^2(\theta_i + \theta_t)} + \frac{tan^2(\theta_i - \theta_t)}{tan^2(\theta_i + \theta_t)}\right) \tag{A.10}$$

θ_i is the incident angle and θ_t is the transmission angle, see figure A.3 on the following page. The incidence angle can be found as

$$\theta_i = cos^{-1}(|\mu_z|) \tag{A.11}$$

The transmission angle is found using Snell's law, stating

$$n_i sin(\theta_i) = n_t sin(\theta_t) \tag{A.12}$$

Isolating θ_t gives

$$\theta_t = sin^{-1}(\frac{n_i}{n_t} \cdot sin(\theta_i)) \tag{A.13}$$

However, if $n_i > n_t$ then the critical angle needs to found. The critical angle is defined as

$$\theta_c = sin^{-1}(\frac{n_i}{n_t}) \tag{A.14}$$

The above is simply Snells formula, with θ_t being 90 degrees or $\frac{\pi}{2}$. If the incident angle is higher than the critical angle, then internal reflection will always occur, and then the formulas for internal reflection are used to find the new coordinates and directional vectors.
If internal reflection occurs then a new z coordinate needs to be calculated, the x and y coordinates do not change in the case of internal reflection. The calculation of the z coordinate can be seen from the following illustration.

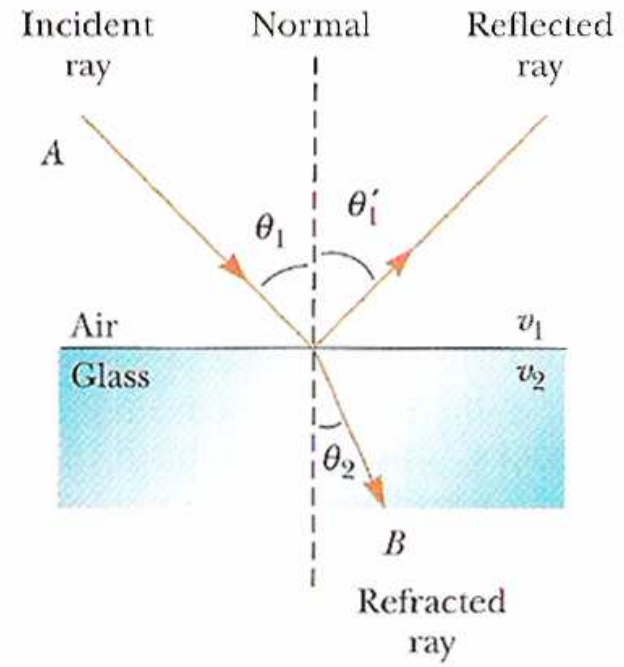

Figure A.3: The figure illustrates the how the light is either reflected or refracted at a boundary [Serway and Jewett, 1995].

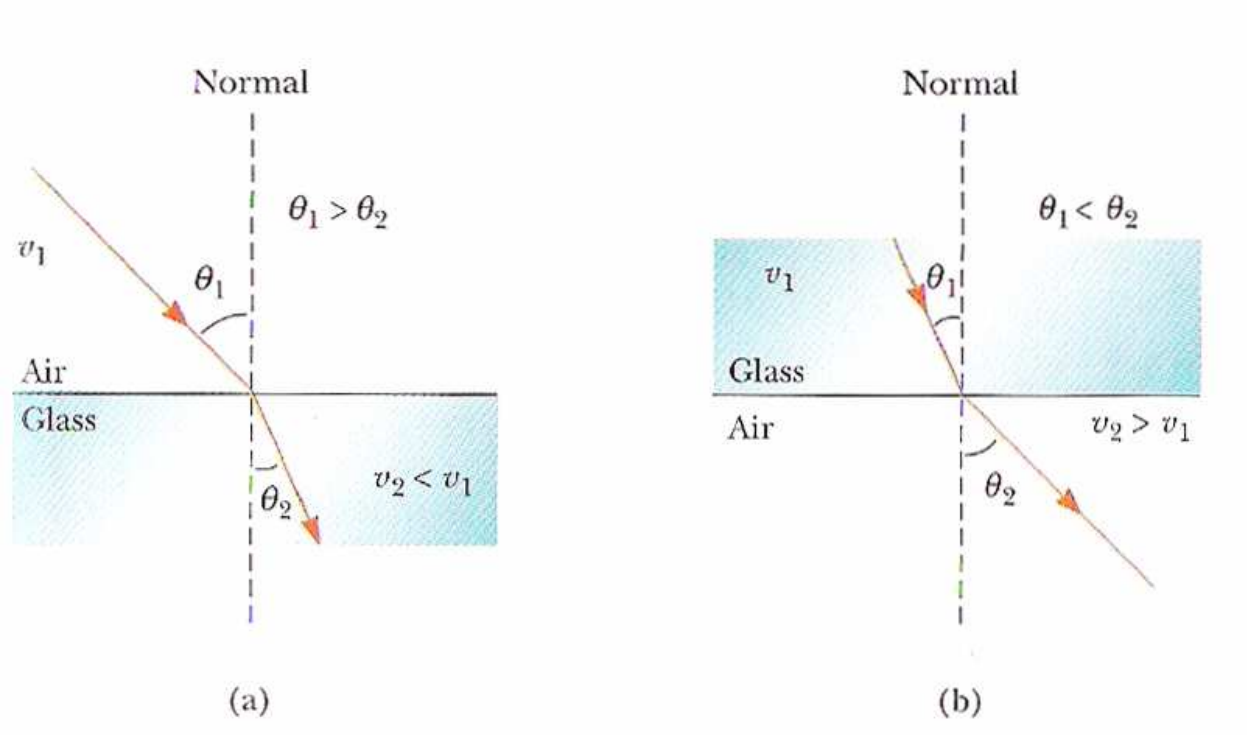

Figure A.4: The figure illustrates the how the light is transmitted via refraktion at a boundary. When the refractive index is lower in the transmitting tissue than in the receiving tissue, the transmission angle θ_t (θ_2 in the figure) is smaller than the angle of incidence θ_i (θ_1 in the figure), this situation can be seen on (a) and vice versa can be seen on (b) [Serway and Jewett, 1995].

When the photon is reflected the directional cosines of x and y, μ_x and μ_y remain unchanged and the directional cosine of z μ_z is negated. This means that the directional vectors after an internal reflection equals

$$\mu_x = \mu_x \quad \text{(A.15)}$$
$$\mu_y = \mu_y \quad \text{(A.16)}$$
$$\mu_z = -\mu_z \quad \text{(A.17)}$$

[Welch and van Gemert, 1995b]

Refraction

If no internal reflection occurs then the photon will be refracted at the tissue surface or internal boundary. In this case both new x,y,z coordinates have to be found and so will the directional vectors μ_x, μ_y and μ_z. First the three new directional vectors are found. These can be derived by taking a look at the 3D unit circle the relationship between two vector i and t can be described as

$$\mu_{x_t} \cdot sin(\theta_t) = \mu_{x_i} \cdot sin(\theta_i) \quad \text{(A.18)}$$
$$\mu_{y_t} \cdot sin(\theta_t) = \mu_{y_i} \cdot sin(\theta_i) \quad \text{(A.19)}$$
$$\mu_{z_t} \cdot cos(\theta_t) = \mu_{z_i} \cdot cos(\theta_i) \quad \text{(A.20)}$$

θ_i and θ_t are the angles between the two vectors, i and t, and the z axis. Isolating the new cosines (μ_{x_t}, μ_{y_t} and μ_{z_t}) gives

$$\mu_{x_t} = \mu_{x_i} \cdot \frac{sin(\theta_t)}{sin(\theta_i)} \quad \text{(A.21)}$$

$$\mu_{y_t} = \mu_{y_i} \cdot \frac{sin(\theta_t)}{sin(\theta_i)} \quad \text{(A.22)}$$

$$\mu_{z_t} = sign(\mu_{z_i}) \cdot cos(\theta_t) \quad \text{(A.23)}$$

[Wang et al., 1995]
Using Snells law this can be reduced to

$$\mu_{x_t} = \mu_{x_i} \cdot \frac{n_i}{n_t} \quad \text{(A.24)}$$

$$\mu_{y_t} = \mu_{y_i} \cdot \frac{n_i}{n_t} \quad \text{(A.25)}$$

$$\mu_{z_t} = sign(\mu_{z_i}) \cdot cos(\theta_t) \quad \text{(A.26)}$$

[Wang et al., 1995]
The calculations of the new coordinates require a few more calculations, for this figure A.5 will be used. In this figure only the (x,z) plane is shown but the deriviations are very similar in the (y,z) plane . Again the unit circle can be thought of when deriving the equations for the new coordinates, the only problem is that the refraction of the photon does not always occur in the origin (0,0,0). Therefore before using the unit circle, and using a similar approach to the one above, the coordinates of the refraction site needs to be known, these coordinates are named $x_{boundary}$, $y_{boundary}$, and $z_{boundary}$. $z_{boundary}$ is known (we know the depth of the boundary) therefore only $x_{boundary}$ and $y_{boundary}$ need to be calculated. This is done by linear interpolation between the previous coordinates in the first medium (x_{old}, y_{old} and z_{old}) and the new, unrefracted (and therefore incorrect) coordinates in the new medium (x_0, y_0 and z_0). Therefore $x_{boundary}$ and $y_{boundary}$ becomes

$$x_{boundary} = \frac{z_{boundary} - z_{old}}{z_0 - z_{old}}(x_0 - x_{old}) + x_{old} \quad \text{(A.27)}$$

$$y_{boundary} = \frac{z_{boundary} - z_{old}}{z_0 - z_{old}}(y_0 - y_{old}) + y_{old} \quad \text{(A.28)}$$

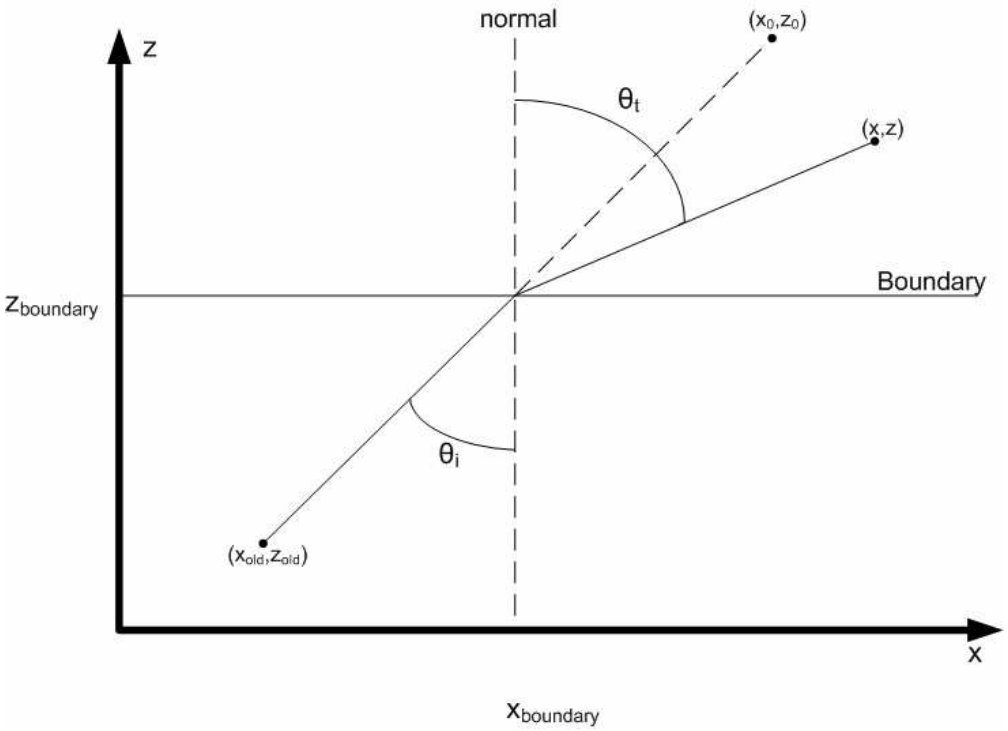

Figure A.5: The figure illustrates the how the light is transmitted via refraktion at a boundary. The coordinates used in the formulas above and below can be seen. The figure is only made in the (x,z) plane but obviously the (y,z) plane is very similar, and should be easy to understand.

On figure A.5 the basis for calculating the new, refracted coordinates after a boundary has been crossed, can be seen. The calculations are simply based on trigonometry.

$$x = x_{boundary} + sign(\mu_x) \cdot |(x_{old} - x_{boundary})| \cdot \frac{sin(\theta_t)}{sin(\theta_i)} \quad (A.29)$$

$$y = y_{boundary} + sign(\mu_y) \cdot |(y_{old} - y_{boundary})| \cdot \frac{sin(\theta_t)}{sin(\theta_i)} \quad (A.30)$$

$$z = z_{boundary} + sign(\mu_z) \cdot |(z_{old} - z_{boundary})| \cdot \frac{cos(\theta_t)}{cos(\theta_i)} \quad (A.31)$$

A.2.5 Absorption

Using the implicit photon capture method implies that a certain part of the photon package should be absorped at each interaction site, the part absorped is named a. And this fraction is determined by the absorption and scattering coefficient in the following way

$$a = \frac{\mu_a}{\mu_s + \mu_a} \quad (A.32)$$

[Prahl et al., 1989]
This means that the weight after an interaction will be reduced to

$$W = W_{old}(1 - a) \quad (A.33)$$

W_{old} is the photons weight before the interaction.

A.2.6 Termination of the photon package

The simulation of each photon package will, not continue indefinitely. Therefore the way of terminating the photons have to be defined. First, if the photon should ever leave the tissue, the propagation of that photon stops and a new photon package is launched.
Second if the photon remains within the tissue its weight will, after a certain number of interactions, be very low. In this case it does not make sense to continue propagation the photon since it gives very little information [Prahl et al., 1989] [Welch and van Gemert, 1995b]. One possibility is to terminate every photon package when the weight becomes small enough, however, doing so will bias the results since the remaining weight is discharted [Prahl et al., 1989] [Welch and van Gemert, 1995b]. Instead a technique called roulette is used, every time the photon weight becomes less than a certain amount, the roulette is played (in this project the roulette will be played when the weight becomes less than 0.01). The roulette gives the photon one change in *m* of surviving (in this project *m* is set to 10), should the photon survive the roulette, its weight is increased *m* times [Prahl et al., 1989] [Welch and van Gemert, 1995b].

A.2.7 Changing photon direction - scatter

The implicit photon capture method dictates that the absorption occurs at every interaction site, and so does scattering. To find the direction into which the photon is scattered into two angles have to be known, first the azimuthal angle have to found. Secondly the deflection angle, which is the angle between the normal to the surface (in this project the angle to the z -axis). The azimuthal angle, ϕ ([0,2π]), is very easy to find, since it does not depend on the optical properties of the tissue, this angle can be found as

$$\phi = cos^{-1}(2\pi\zeta) \tag{A.34}$$

ζ is here, as above, a random number uniform distributed between 0 and 1.
The deflection angle, θ ([0,π]), however, depends on the optical properties of the tissue, especially the anisotropi, determined by the anisotropy factor, *g* ([-1,1]). For tissue this factor is usually approx. 0.9, for light in near infrared range. This means that scattering approaches Mie-scattering which is mainly forward directed. If *g* = 0 the tissue has isotropic properties and the probability of the scattering angle is uniform distributed between 0 and π. If *g* is negative then mostly backwards scattering occurs. The probability density function of the deflection angle can be described used the Henyey-Greenstein phase equation, originally intended for galatic light scattering. The Henyey-Greenstein equation gives the following pdf

$$p(cos(\theta)) = \frac{1-g^2}{2(1+g^2-2g\cdot cos(\theta))^{3/2}} \tag{A.35}$$

[Welch and van Gemert, 1995b] [Henyey and Greenstein, 1941]
By replacing the left expression in equation A.35 with ζ, a random varibel uniform distributed between 0 and 1, and isolate the deflection angle, θ, then the following expression for the deflection angle is derived

$$\theta = cos^{-1}\{\frac{1}{2g}(1+g^2-[\frac{1-g^2}{1-g+2g\zeta}]^2)\} \tag{A.36}$$

The distribution of the deflection angle in 1,000,000 scatterings with an anisotropy factor of 0.9 can be seen in the following histogram, (figure A.6). It is seen that the angles are concentrated around the low angles, indicating that the scattering is very forward-directed.

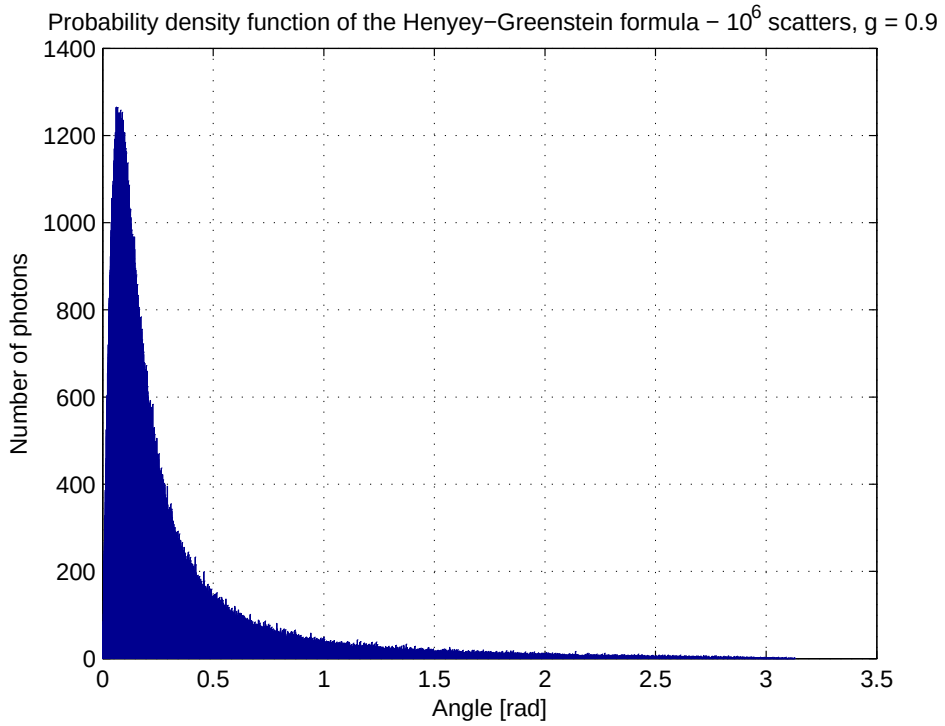

Figure A.6: The figure illustrates a histogram to display the probability density function of the Henyey-Greenstein formula for one million scattering events and an anisotropic factor of g = 0.9. Mean angle is 0.3072 rad.

When both the azimuthal and deflection angles for the scatter event have been found three new directional cosines can be calculated. To derive the formulas a few steps has to be made. The calculation of the new directional cosines is basically two rotations of a point on the unit sphere. Each rotation of a point about an axis can be expressed as a real and an imaginary part. A rotation of the point $(x + i \cdot y)$ in an angle θ can be expressed as $(x + i \cdot y)(cos(\theta) + i \cdot sin(\theta))$ [Cashwell and Everett, 1958].
Each of the rotation from both the azimuthal and deflection angles can be expressed as above. First the basic idea behind the rotation will be explained. A point (x,y,z) will be rotated twice on the unit sphere first in an angle γ around the y axis then an angle ψ around the z axis the first rotation can be expressed as

$$z' + i \cdot x' = (z + i \cdot x)(cos(\gamma) + i \cdot sin(\gamma)) \quad \text{(A.37)}$$

$$y' = y \quad \text{(A.38)}$$

[Cashwell and Everett, 1958]
Where (x',y',z') are the new coordinates after the first rotation.
And the second rotation around the z axis is

$$x'' + i \cdot y'' = (x' + i \cdot y')(cos(\psi) + i \cdot sin(\psi)) \quad \text{(A.39)}$$

$$z'' = z' \quad \text{(A.40)}$$

[Cashwell and Everett, 1958]
Where (x'',y'',z'') are the new coordinates after the second rotation.

Now (x',y',z') will be isolated and inserted into (x'',y'',z'').

$$z' + i \cdot x' = (z + i \cdot x)(cos(\gamma) + i \cdot sin(\gamma)) \quad (A.41)$$
$$= z \cdot cos(\gamma) + i \cdot z \cdot sin(\gamma) + i \cdot x \cdot cos(\gamma) - x \cdot sin(\gamma) \quad (A.42)$$

[Cashwell and Everett, 1958]
First the real and imaginary parts are isolated and then (x',y',z') are isolated

$$x' = x \cdot cos(\gamma) + z \cdot sin(\gamma) \quad (A.43)$$
$$y' = y \quad (A.44)$$
$$z' = -x \cdot sin(\gamma) + z \cdot cos(\gamma) \quad (A.45)$$

[Cashwell and Everett, 1958]
For the second rotation around the z axis similar steps are taken

$$x'' + i \cdot y'' = (x' + i \cdot y')(cos(\psi) + i \cdot sin(\psi)) \quad (A.46)$$
$$= x' \cdot cos(\psi) + i \cdot x' \cdot sin(\psi) + i \cdot y' \cdot cos(\psi) - y' \cdot sin(\psi) \quad (A.47)$$

Now the (x'',y'',z'') becomes

$$x'' = x' \cdot cos(\psi) - y' \cdot sin(\psi) \quad (A.48)$$
$$y'' = x' \cdot sin(\psi) + y' \cdot cos(\psi) \quad (A.49)$$
$$z'' = z' \quad (A.50)$$

Then Eqs. A.44, A.45, A.45 are inserted into Eqs. A.49, A.50, A.50, and this gives the following result

$$x'' = x \cdot cos(\gamma)cos(\psi) - y \cdot sin(\psi) + z \cdot sin(\gamma)cos(\psi) \quad (A.51)$$
$$y'' = x \cdot cos(\gamma)sin(\psi) + y \cdot cos(\psi) + z \cdot sin(\gamma)sin(\psi) \quad (A.52)$$
$$z'' = -x \cdot sin(\gamma) + z \cdot cos(\gamma) \quad (A.53)$$

In the three equations just above a few rewritings are made from the following expressions

$$sin(\gamma) = p \quad (A.54)$$
$$cos(\psi) = \bar{x}/p \quad (A.55)$$
$$sin(\psi) = \bar{y}/p \quad (A.56)$$
$$cos(\gamma) = \bar{z} \quad (A.57)$$

[Cashwell and Everett, 1958]
where p is the distance from the origin in the unit sphere to the projection of the new point (x'',y'',z'') onto the xy plane - which can be derived using pythagoras formula. And ($\bar{x}$,$\bar{y}$,$\bar{z}$) is the components of the vector from the origin of the unit sphere to the previous point (x,y,z). Since these deriviation are made on the unit sphere this vector is the same as the original directional vector (μ_x, μ_y , μ_z).
Now the (x'',y'',z'') can be expressed as

$$x'' = x\mu_z\mu_x/p - y\mu_y/p + zp\mu_x/p \quad (A.58)$$
$$x'' = x\mu_z\mu_y/p + y\bar{x}/p + zp\mu_y/p \quad (A.59)$$
$$x'' = -\mu_x/p - z\mu_z \quad (A.60)$$

[Cashwell and Everett, 1958]
To calculate the scattering direction from a scattering event occuring in the origin of the unit sphere. The (x',y',z') are the coordinates of the point into which the photon is scattered. Again since the deriviation take place on the unit

sphere the (x'',y'',z'') are the same as the new directional vectors of the photon, (μ'_x, μ'_y , μ'_z).
Using the azimuthal and deflection angle found above, ϕ and θ, instead of ψ and δ, after the two rotations, the point (x,y,z) on the unit sphere can be described as ($cos(\phi)sin(\theta)$,$sin(\theta)sin(\phi)$,$cos(\theta)$) [Cashwell and Everett, 1958]. The polar argument can be described as $\sqrt{1-\mu_z^2}$ - which can be derived using pythagoras formula [Cashwell and Everett, 1958].
Hence the new directional cosines can be described as

$$\mu_x = \frac{sin(\theta)}{\sqrt{1-\mu_z^2}}(\mu_x\mu_z cos(\phi) - \mu_y sin(\phi)) + \mu_x cos(\theta) \quad (A.61)$$

$$\mu_y = \frac{sin(\theta)}{\sqrt{1-\mu_z^2}}(\mu_y\mu_z cos(\phi) + \mu_x sin(\phi)) + \mu_y cos(\theta) \quad (A.62)$$

$$\mu_z = -sin(\theta)cos(\phi)\sqrt{1-\mu_z^2} + \mu_z cos(\theta) \quad (A.63)$$

[Prahl et al., 1989] [Welch and van Gemert, 1995b]
However, it can be seen that a angle very close to normal, will give problems with the fractions in the equations above (divide by zero if $\mu_z \approx 1$). Therefore the following equations should be used, if $\mu_z > 0.9999$

$$\mu_x = sin(\theta)cos(\phi) \quad (A.64)$$

$$\mu_y = sin(\theta)sin(\phi) \quad (A.65)$$

$$\mu_z = \frac{\mu_z}{|\mu_z|}cos(\phi) \quad (A.66)$$

[Cashwell and Everett, 1958] [Welch and van Gemert, 1995b] The three directional cosines will be used when propagating the photon to the next interaction site, as described above under section A.2.3 on page 77.

A.2.8 Simulating the spatial profile of the laser beam

Since the laser beam has a certain width it can not be seen as a point source, instead the photons will enter the tissue distributed through out the beam. This means that varying initial x and y surface coordinates have to be used instead of (0,0) [Prahl et al., 1989] [Welch and van Gemert, 1995b]. Typically two models for the beam profile are used, the beam can either be modelled as a flat or gaussian beam. In a flat beam the intensity of the beam is the same everywhere within the beam, where the gaussian has higher intensity at the beam centre and the intensity decrease with the distance to the centre. The radius of the beam is abbriviated, w. The radiant exposure within a flat beam can be expressed as

$$S(r) = \frac{1}{\pi}w^2 \quad (A.67)$$

Outside the beam the exposure is zero. Since the Monte Carlo is a stochastic method, the probability density function of the exposure is used to express the distribution within the beam, and again a random number uniform distributed between 0 and 1 is used instead of the pdf. The pdf of the exposure can be expressed as

$$p(r) = \frac{2r}{w^2} \quad (A.68)$$

[Welch and van Gemert, 1995b]
Changing $p(r)$ into a random number, ζ, uniform distributed between 0 and 1, yields

$$\zeta = \frac{2r}{w^2} \quad (A.69)$$

Since the Monte Carlo simulation being made is in cartesian coordinates and a short expansion is made. The x and y coordinate can be expressed using the r coordinates and a cosine and sinus calculation of a random angle between 0 and 2π, defined as $2\pi\zeta_2$. Then the x and y coordinate for a flat beam then becomes

$$x = w\sqrt{\zeta}cos(2\pi\zeta_2) \quad (A.70)$$

$$y = w\sqrt{\zeta}sin(2\pi\zeta_2) \quad (A.71)$$

[Welch and van Gemert, 1995b] Note that for each new set of start coordinates the same values of ζ and ζ_2 must be used.
For a Gaussian beam the x and y start coordinates are

$$x = w\sqrt{-ln(1-\zeta)/2}cos(2\pi\zeta_2) \quad (A.72)$$

$$y = w\sqrt{-ln(1-\zeta)/2}sin(2\pi\zeta_2) \quad (A.73)$$

[Welch and van Gemert, 1995b]
For the simulation either a 2 mm or 3.5 mm beam radius was used, corresponding to the lenses of the used laser. Since the light from a diode laser neither is stricly flat or Gaussian a compromise must be made. For the laser used in this project the beam profile was closest to a flat beam, so a flat beam model was used.

A.2.9 The Monte Carlo simulation as a heat source in heat distribution modelling

To use the results from the Monte Carlo to simulate the heat generation and transfer after irridiation from a diode laser, the results needs to altered a bit. If the heat transfer models are in 2D axial coordinates (often used to limit the computional burden) then x and y must combined into a radial coordinate, r, in following way

$$r = \sqrt{x^2 + y^2} \quad (A.74)$$

First, the heat source Q expression, was developed as a large empty matrix (100 x 100), with r being the first coordinate (or index in the matrix) and z being the second. For each interaction in the Monte Carlo, the coordinates of the interaction site was used to index the matrix and then add the absorped weight into the appropriate entry of the matrix, representing the area of the tissue where the interaction and therefore absorption occured. The entries of the matrix, $r_{coordinate}$ and $z_{coordinate}$, was calculated as

$$r_{coordinate} = ceil(r/dr) \quad (A.75)$$

$$z_{coordinate} = ceil(z/dz) \quad (A.76)$$

Where ceil rounds to next integer towards infinity, and dr and dz is the width and height of the tissue area, represented by a single entry in the heat source matrix Q, each entry has the size 5e-5 m x 5e-5 m (50 μm x 50 μm). And r and z are the coordinates of the interaction.
To minimize the computational burden only weight absorped within a 5 mm x 5 mm square, centered at (0,0) was retrieves from the Monte Carlo simulation and used to describe the heat source in the heat transfer models. After the Monte Carlo simulation the weight added in the entries in Q must by diveded by a scalar in order to change the values from weight to power pr. cubic meter [W/m^3]. The size of the scalar depends on the distance from the axis of symmetry to the entry (the r coordinate). The scalar is expressed as

$$(2i+1)\pi \cdot dr^2 \cdot dz \quad (A.77)$$

[Welch and van Gemert, 1995b]
where i is the radial index ($r_{coordinate}$) in the heat source matrix, Q. Furthermore each entry should be divided with the total amount of incoming photons, $photonsimulations$, to normalize the power to watts [W]. (Recall that it was chosen that Monte Carlo model simulated a incident power of 1 W in 1 s, a total energy of 1 joule). The means that the entries in Q, all should be divided by

$$(2i+1)\pi \cdot dr^2 \cdot dz \cdot photonsimulations \quad (A.78)$$

After this the Q matrice can multiplied by a scalar to take the power setting and duration of the stimulus into account. This means that it is very easy to test different power settings and duration based on the same Monte Carlo simulation.

Control theory

B

In this chapter the control basics used in this project is elaborated. This is used in chapters 3 and 4.
In order to continously control the skin temperature the infrared camera and diode laser must be combined. As one might except the concept of controlling such a proces is an area of intense theory and research. Previously a somewhat similar system to this have been developed [Meyer et al., 1976], using a CO_2 laser with all the disadvantages of that type laser, see chapter 3. If one wishes to control a certain process there are a number of approaches. But first the control theory basics will be discussed.

B.0.10 Control theory basics - closed and open loop control

First a bit of control nomenclature. Four basic elements are found in most control systems.

Process, which as the name implies is the proces or action which we wish to control. In this case it is the laser heating of the skin, causing the skin temperature to rise to a certain level.

Measuring element or *sensor* which measures the output of the process, in our case the skin temperature measured by the infrared camera.

Regulator, which is the control unit which regulates the process, here the regulator will control the power setting of the laser.

Actuator - the element which is controlled to affect the process, in this case the laser

[Haugen, 1994]
The different signals in between the elements are referred to as

Process output - the skin temperature

Reference - desired skin temperature

Output measurement - temperature measured by the infrared camera

Error - difference between reference and the output

Control input - control signal from the regulator to the actuator (laser)

Disturbance - cooling of the skin

[Haugen, 1994]
Many others describtions and nomenclature exist [Haugen, 1994] [Franklin et al., 1994], however, the nomenclature listed above is what have been chosen by the author and will be used in the rest of this rapport.
When describing the reaction characteristics of a controller some terms should be known, see figure B.1. When changing the reference the time it takes the controller to reach the new reference is known as the rise time, mostly used when discussing reference increases. The exceeding of the reference after a reference change is known as the

overshoot, and the decaying oscillations after an overshoot are known as riples. The time it takes for the controller to settle at the reference is called the settling time, this is not displayed in figure B.1.

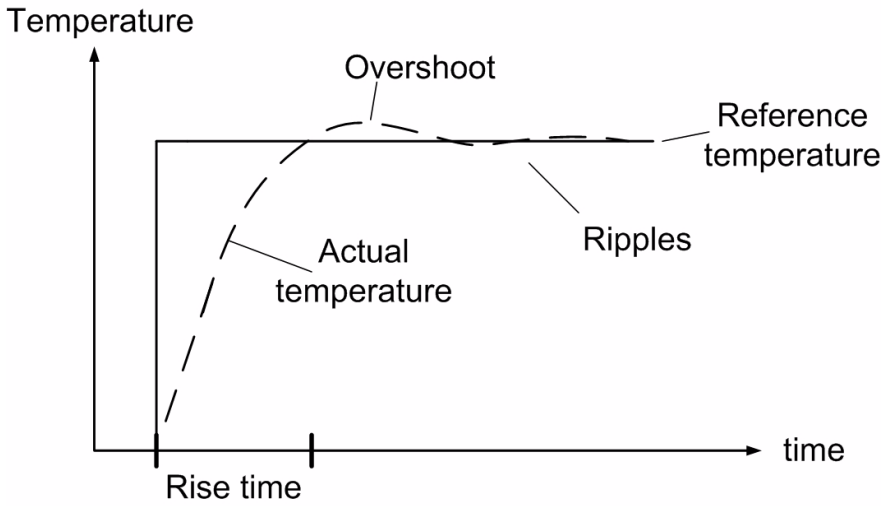

Figure B.1: The figure illustrates some characteristics of a controller. The rise time is the time it takes a controller to reach a new reference when the reference is changed. Overshoot is when the controller exceeds the reference after a change of the reference. The decayin oscillations following the overshoot is called riples. In the figure the actual temperature is the process output, and the reference temperature is the reference.

Two basic principals of control exist, closed and open loop. Both principals can be seen in figure B.2. In closed loop control, the current output of the process is measured and used to adjust the process (Figure B.2 - a). In open loop control the output is not measured, but the process is controlled based on the reference and a measurement of any disturcances effecting the process (Figure B.2 b)). Open loop control requires very precise knowledge of how the process changes whenever the reference or the disturbances changes. The two principals can be combined into a control system which utilises both closed and open loop techniques, such can be seen in figure B.2 c). Inside the regulater the open loops from the reference and disturbance is combined with the closed loop based on the output

measurement. The combination of both techniques exploit the advantages of each; the open loop provides fast initial adjustment and thereafter, the closed loop keeps the process at the desired point [Haugen, 1994].

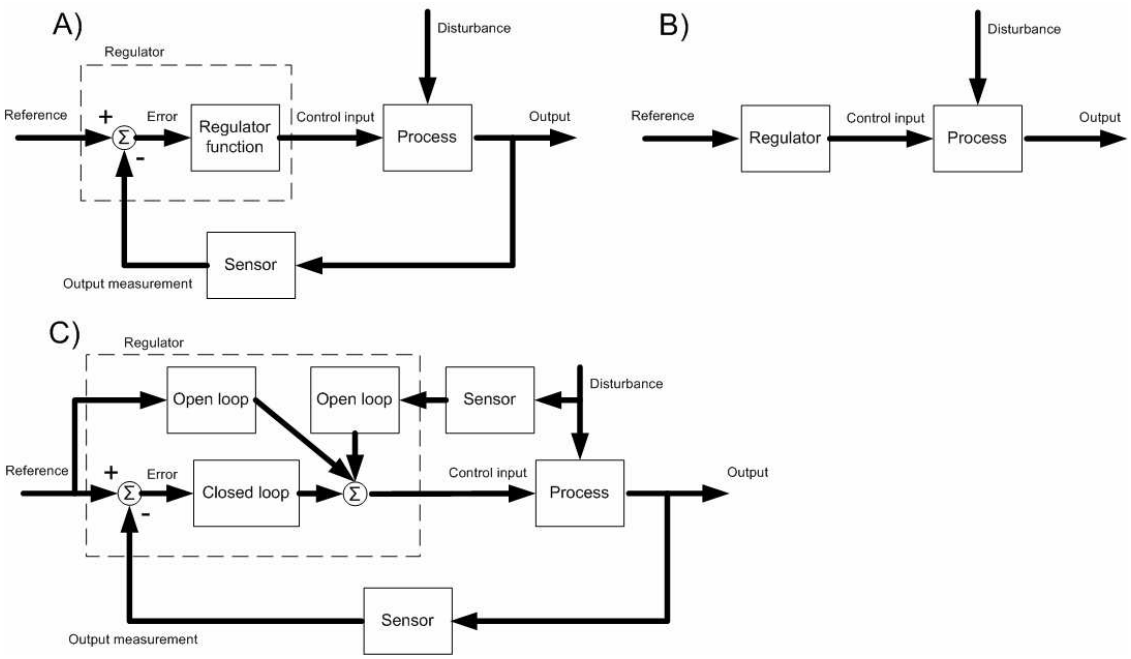

Figure B.2: The figure illustrates the principals of a) closed loop control, b) open loop control and c) the combination of closed and open loop control. Developed from [Haugen, 1994] and [Franklin et al., 1994].

Since an open loop technique is very subtle to noise, and small indifference in the model describing the process will result in errors. Instead closed loop control continously monitores the output of the system and alters the process input when the process output is different to the reference. In this project closed loop control was used, see chapter 3 for justification.
One problem of all closed loop controllers is the possibility for instability. Instability occurs when the socalled loop gain becomes too large or if the time delay in the system is too large.
In the case of too large gain the closed loop system will react too violently to any error. E.g. if the loop gain is high, errors will cause the regulator to pull the process in the opposite direction, to try and reduce the error. If the loop gain is too high the controllers reaction will be too large, causing the controller to either overshoot or undershoot the reference.
Similar is the problem when the time delay is too large, e.g. large time delay means that the system will not react fast enough whenever the reference is reached, then the regulator will cause a too extreme change of the control input, making the output shoot past the reference, and so on. This will continue until the physical limitation of the actuator is reached, in this case the maximum and minimum power setting of the laser. Therefore, the temporal resolution of the system should be as high as possible.
In our current problem the risk of instability is moderate since we cannot control how fast the skin cools. Compared to how fast we can heat the skin (severeal $^{\circ}$C per second), the cooling is relatively slow.

B.1 The PID controller

The Proportional-Integral-Derivative controller, is also called the three term controller, and it consist of the parts which each react differently to any errors. Depending on the type of process being controlled, sometimes, not all three term are used, creating controller such as the Proportional (P) or Proportional-Integral (PI), or Proportional-Derivative (PD),

especially PI is often used since the derivative term can be very sensitive to measurement noice [Haugen, 1994].
In the PID controller the control input (CI) is calculated as the the sum of the output from each of three terms as

$$CI = P_{out} + I_{out} + D_{out} \tag{B.1}$$

[Haugen, 1994]
Below the effect for each term is explained, including the reasoning for each term.

B.1.1 The proportional term

The proportional term or sometimes simply called the gain, causes a change in the control input proprotional to the error. The output from this element is calculated as

$$P_{out} = K_P * e(t) \tag{B.2}$$

K_P is the proportional gain, and e(t) is the error at the present time, t [Haugen, 1994].
The proportional term ensure that if the error is large a large change to the control input will be made, but if the error is small the correction is small.
The effect of altering K_P can be seen in figure B.3, as the figure illustrates, increasing K_P will reduce rise time [Haugen, 1994]. Reducing K_P will cause the system to react slower to changes in the reference. Increasing K_P will move the system towards being more unstable [Haugen, 1994].

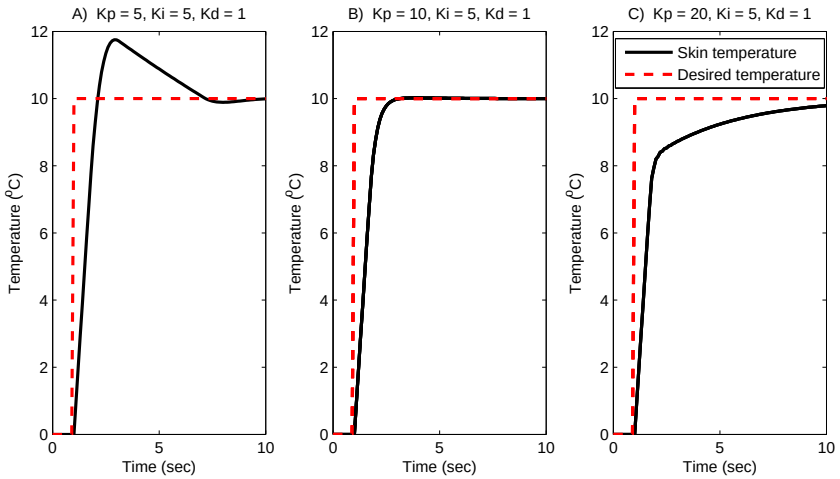

Figure B.3: The figure illustrates how changing the proportional gain K_P in a PID controller effects the output, if K_P is increased the reaction time of the controller is reduced, but the controller will become more unstable. In A) the proportional gain is reduced meaning the controller will give overshoot, because the controller does not react to the process output have reached the desired value. In B) a good setting of the proportional term is seen. In C) the proportional gain is too high, actually causing the controller to react very slow. Based on [Haugen, 1994].

In a purely P controller, the change of the control input is dependend on the error. If the gain is too small then the controller is unable to correct the error and, the output of the process never reaches the reference value. Increasing K_P will cause the output process to approach the reference.

B.1.2 The integral term

The integral term or reset term, corrects the control input based on the previous and present error meaning it integrates the error over time, hence the name [Haugen, 1994]. The summed error is multiplied by the integral gain K_I such that the output from the integral term, I_{Out}, becomes

$$I_{Out} = K_I \cdot \int_0^t e(\tau)d\tau \tag{B.3}$$

where K_I is the integral gain. The integral term is responsible for accelerating the output of the process towards the reference, eliminating any steady-state errors which can occur when only using a P controller [Haugen, 1994]. Increasing K_I will decrease the time it takes the system to reach the reference value. Increasing K_I will however, increase the overshoot of the system and cause the system to become more unstable [Haugen, 1994].
One problem of the integral term is that it accumulates the previous errors, it can cause the system to overshoot the value, due to accumuluated integral errors, a situation called "Integral windup", see more about this phenomenon below.

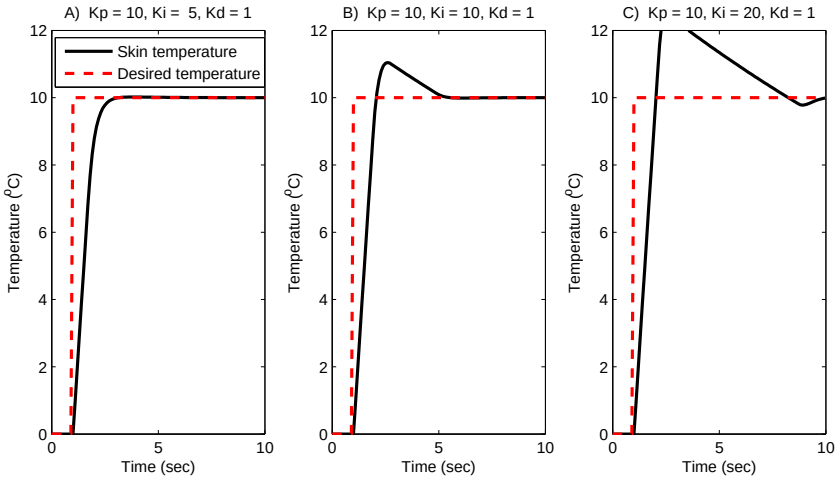

Figure B.4: The figure illustrates how changing the integral gain K_I in a PID controller effects the output, if K_I is increased the reaction time of the controller is reduced, but the controller will have more overshoot and longer settling time. The process in this example react quite fast, meaning the rise, however, as K_I is increased the overshoot and settling time increases, (see B) and C)). If the integral gain is reduced to very low level, all overshoot can be eliminated but the settling time will then also increase, due to slow response of the controller. Based on [Haugen, 1994].

B.1.3 The derivative term

The derivative term, effects the control input by differentiation the error and effecting the control input, by a factor proportional to the derivative of the error [Haugen, 1994] [Franklin et al., 1994]. A derivative gain is multiplied to the derivitative of the error, so the output of the derivative term becomes

$$D_{Out} = K_D \cdot \frac{de}{dt}(t) \tag{B.4}$$

where K_D is derivative gain. de/dt is calculated as

$$\frac{de}{dt}(t) = \frac{present\_error - previous\_error}{dt} \tag{B.5}$$

Increasing K_D will decrease overshoot but will also decrease the settling time of the system, ensuring that large changes are reduced [Haugen, 1994]. But the disadvantages of the derivative term is that increasing K_D will increase the system susceptability to high frequency measurement noise [Haugen, 1994], any high frequency noise can cause large changes in the control input making the system unstable [Haugen, 1994]. Therefore in systems with high measurement noise, the derivative term is left out and instead a PI controller is applied. Another approach is the low-pass filter the measurement, however, this can cancel out the effect of the derivative term.

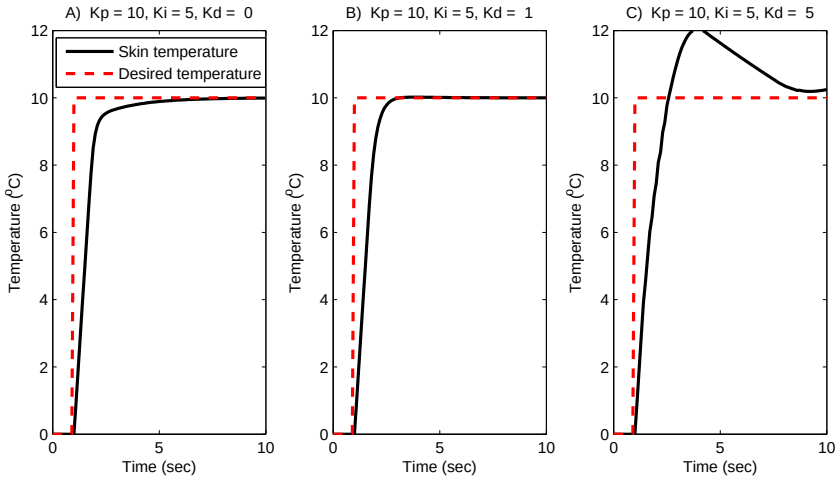

Figure B.5: The figure illustrates how changing the derivative gain K_D in a PID controller effects the output, if K_D is increased the reaction time of the controller is increased, but the controller will have less overshoot A). However, if K_D is increased too much any small changes in the error will cause overshoot C). In B) a good value of K_D have been found, giving good response, and no overshoot.

B.2 Controller modelling

B.2.1 PID controller model

The modelling of the PID controller is fairly simple and resembles the flow diagram seen in figure B.2. The Simulink implementation of such a controller is seen in figure B.6. As described above the controller consist of three gains and a derivator and a integrator.

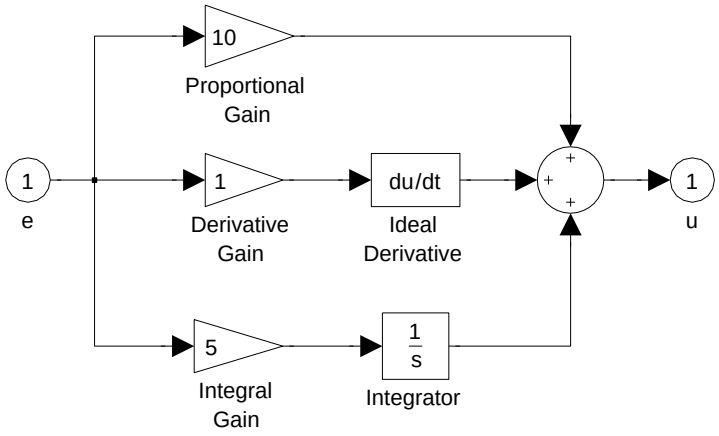

Figure B.6: The figure illustrates a Simulink model of a basic PID controller. The controller has one input, the error, e, and one output, u.

Integral windup

One thing the simulation can help to preventntegral windup. This occur when the output from the actuator (laser) saturates letting the integral become unproportionally large and then accumulates the error unintentionally. The laser will saturate if the control input grows outside the range 0 to 20 W (theoretical - in practice 0 to 16W), which is the power range of the laser. When the laser saturates the loop is no longer closed because the process is no longer affected by the output of the controller because the saturated laser can no longer provide the output intended by the controller, the controller does not 'know' this and continue integrating the error, which is increasing.

When the system desaturates the accumulated error may take a long time to remove the error, and thus causing the controller to either extensively over- or undershoot the set point, see figure B.7.

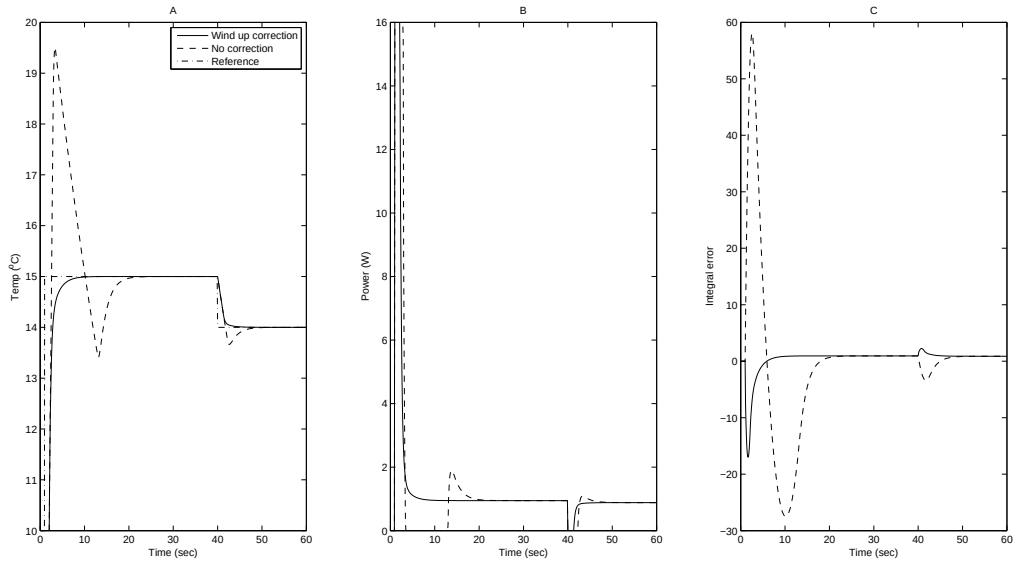

Figure B.7: The figure illustrates how integral windup decreases the performance of the controller. At time, t = 1 sec, the reference is increased from 0 °C to 15 °C at time, t = 40 sec, it is again decreased a single degree to 14 °C. A) is the temperature °C, B) is the power setting of the laser (W), and C) is the integral error. A) The controller without integral windup correction overshoot the reference temperature by almost 5 °C, again when the reference is decreased it undershoot by almost 0.5 °C. Applying integral windup correction eliminates both the overshoot and undershoot. B) The power without windup correction both overshoots and overshoots the power necessary necessary to obtain the desired temperature. C), it is clear to see that the integral term is the reason of the overshoot and undershoot seen in A). The same K_P, K_I, and K_D gains were used in both simulations, were the same, 10, 5, and 1 respectively, the integral correction gain was 1.

Integral windup correction is very simply applied to the controller whenever the actuator reaches its limit [Franklin et al., 1994]. In practice this is done by comparing the desired output from the controller and the actual output from the actuator. Whenever this is different from zero the actuator has been saturated, then the difference between the controller output and actuator output is multiplied by the integral correction gain and fed back into the integral term,

see figure B.8. This ensures that the error integration stops whenever the actuator is saturated. The implementation of integral windup in the simulink model can be seen in figure B.8

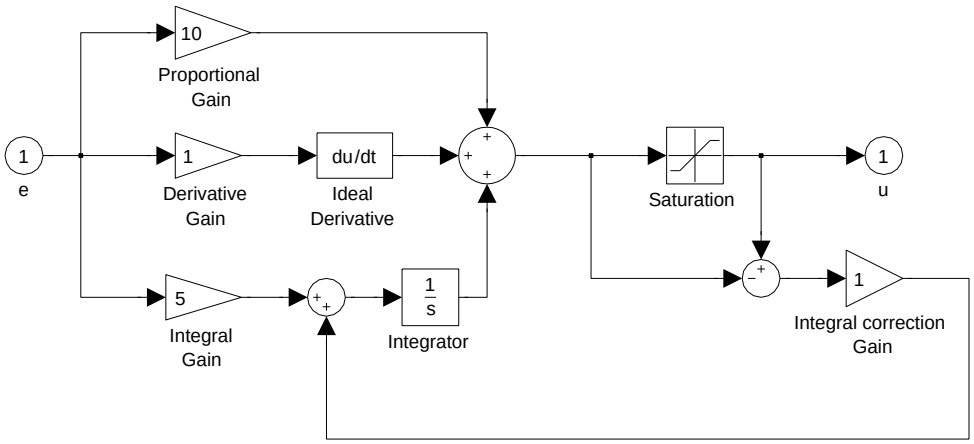

Figure B.8: The figure illustrates a Simulink model of a PID controller fitted with integral windup correction. Adapted from [Franklin et al., 1994].

B.3 Tuning the controller

Designing and implementing a controller based on the PID principle is fairly easy. However, in order to obtain good controller performance, the controller must be tuned, i.e. adjusting the gains to give desirable results. As described above, setting the three gains K_P, K_I, and K_D are typically a trade off between the behavior wanted from the system [Haugen, 1994], in chapter 4 this tradeoff is further discussed. Meaning must the controller react very fast to any changes in the reference and will the user in return accept some overshoot, or is overshoot completely unacceptable and should be avoided at all costs, meaning more sluggish reponse from the controller [Haugen, 1994] [Franklin et al., 1994].

There exists several tuning techniques which can be applied, first is simple trial and error, which has the advantages of being very simple and requires no theory or model of the system, however, this approach can easily prove to be very time consuming [Haugen, 1994] [Franklin et al., 1994]. Another is the Ziegler Nichols method where the tuning take its starting point in the P controller, meaning the gain of the integral and derivative terms are both set to zero. Then proportional gain, K_P, is increased until the point at which the output from the controller contionously oscilates around the reference (without the actuator saturating), this gain is called the critical gain K_C. The period of the oscillations is then determined and is refererred to as the critical period, P_C. The formulas for P, PI, and PID controllers are found in table B.1 [Haugen, 1994] [Franklin et al., 1994].

	$\mathbf{K}_P$	$\mathbf{K}_D$	$\mathbf{K}_D$
P	$K_C/2$		
PI	$0.45 \cdot K_C$	$1.2 \cdot K_C / P_C$	
PID	$0.60 \cdot K_C$	$2 \cdot K_C / P_C$	$P_C \cdot K_C / 8$

Table B.1: The table displays the parameters applied in the process model. [Haugen, 1994] [Franklin et al., 1994]

Selecting the gain of the integral windup correction is usually done by trial and error, or should be chosen large enough to keep the output of the integral term from saturating [Franklin et al., 1994].

B.4 Stability of closed loop control

As mentioned above the PID controller as any closed loop controller can become unstable, causing increasing oscillations, until eventually the actuator reaches its limits [Haugen, 1994]. The actuator used in this project can only heat the skin, meaning drag the process in one direction, the cooling of the skin is 'passive' and outside control. Since it is decided to develop a complete non-contact system, any cooling should be of similar type but no non-contact cooling devices are readily available for the use in this project. Therefore, we rely only on the passive skin cooling. Passive might not be the entirely correct term, but the convection of the heat due to blood flow is outside our control, and thus for the controllers point of view, the cooling is passive. However, since the cooling is slow compared to the rate, it aids the system to become more stable, if the laser is shut off the temperature drop per loop cycle will be much slower that the heating when the laser is on.
In order to test the system for instability there are a number of approaches to take. One theoretical method of preventing this is to develop a mathematical model of the process and control, as seen above. These models can then be tested in a simulation software such as Simulink. During the simulation different gain settings can be tested to see whether such give rise to any steady state oscillations [Haugen, 1994]. Steady state refers to situation when the process has reached the reference value, and the actuator theoretically should settle at a constant level, in figure B.7 - A it is seen as when temperature profile is horisontal.
Another approach is using LaPlace theory and transformations to analyse the system. The model which describes the system impulse response can be transformed into the LaPlace (or s) domain, the transformed function, is called the systems transfer function (TF). The location of the zeros and especially the poles in the TF in the complex plane will then give an idea of whether the system has a tendency to be stable (none or decreasing oscillations in steady state), unstable (increasing oscillations), or marginal stable (oscillations with constant amplitude) [Haugen, 1994].

Controlling the infrared camera

C

To control and use the infrared camera the connection to the camera must be etablished and the camera must be initialised, this is done using the `Thermovision Open` block. The camera is then focused using the Auto focus setting in the `Thermovision Focus` block. Then the camera is calibrated using the build calibration mechanism in the camera, this is done using the `Thermovision CameraAction` block, with the input set to `'Internal Image Calibration'`, the camera will automatically perform an internal calibration everytime the internal temperature of the camera changes 1 °C or at least every 15 minutes. During the internal calibration, which takes approximately 5 seconds, the camera does not record any frames, meaning no temperature measurement will be performed. Therefore, the automatic internal calibration is disabled so that during the skin heating, the temperature readings will be continously. To minimize the possibility of the camera output drifting, the manufactorer recommends that the camera is turned on for 5 minutes, to let the internal temperature settle, before disabling the automatic calibration.
Next the system is initialised for starting to sample frames from the cameras. Using the IMAQ module in Labview a empty image array is preallocated using the `IMAQ Create` block. In fact two such images are preallocated using this block. One image is for the raw infrared image, the second is for the ROI image, more about this below.
After have initialised the camera, focused the image, and disabled the internal calibration, the system starts acquiring frames. This is done using the while loop as explained above, each iteration acquires a new from the camera. Inside the while loop is a event structure with five events, a timeout - the default action, and four events representing buttons on the GUI. The first case is simply a timeout which is run whenever neither of the four other cases are active.

C.0.1 Image acquisition

In the timeout the actual image is acquired, this is done using the `Thermovision GetImage` block, the `IMAQ ArrayToImage` block, a ROI property node, and a home made sub_vi `Extract ROI & Max`. The handle to camera connection is led into the `Thermovision GetImage` block. That block outputs a 2D array which is transposed and the input is led into the IMAQ array to image block and the `Extract ROI & Max` block, the image from the `IMAQ ArrayToImage` block the raw infrared image is the displayed on the GUI using an indicator - named Raw IR image.

Labview implementation

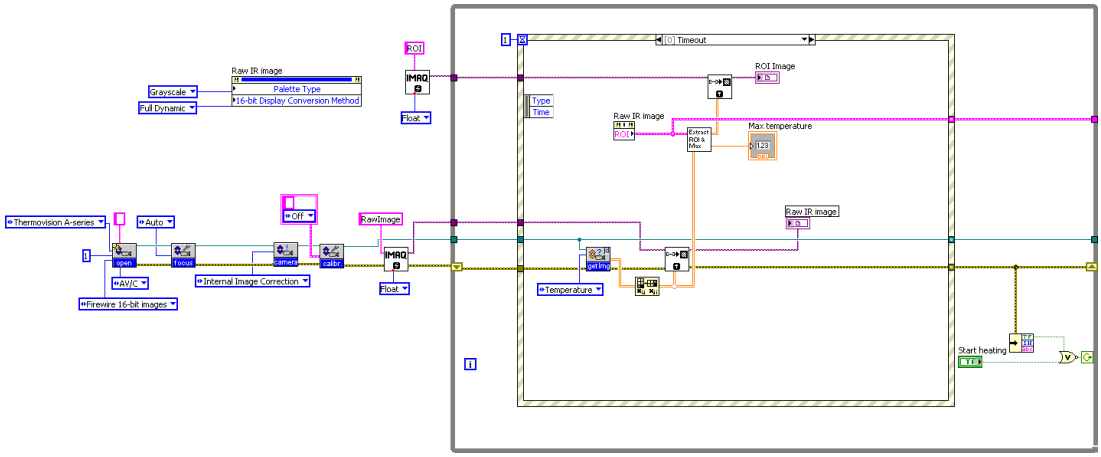

Figure C.1: The figure illustrates how the interface to the infrared camera is set up and how a new frame is acquired in each iteration of a while loop. The blocks `Thermovision Open, Focus, CameraAction,Calibrate, and GetImage` are all part of the FLiR Thermovision toolkit. Thus, this must be installed in order to use the software. The `IMAQ` blocks are part of the Labview IMAQ toolkit which also must be installed in oder to use the software.

C.0.2 ROI extraction

The `Extract ROI & Max` block is a sub_vi created to extract the ROI and max temperature. The ROI is selected on the GUI by drawing a rectangle on the raw infrared image. The coordinates of the ROI is extracted using a Property node of the ROI. The maximum temperature is extracted from the ROI and raw image using the `Array Max & Min` block . The temperature measurement is in Kelvin, therefore 273.15 is subtracted to get the reading in °C. If the ROI max value is lower than -273, no ROI have been selected (the developer expect that all measured temperature will be higher than 0.15 K - a valid assumption), instead will the maximum temperature of the raw image be the output - hence the case structure.
Inside the `Extract ROI & Max` sub_vi there is another sub_vi which extracts the ROI, named `ROI extraction` based see the labview implementation below. This sub_vi takes two inputs, the ROI cluster from the Property node, and the raw image array. Based on the information in the ROI cluster the ROI area is substracted as a subarray. Back in the main VI this array is converted to an image and displayed on the GUI.

Labview implementation

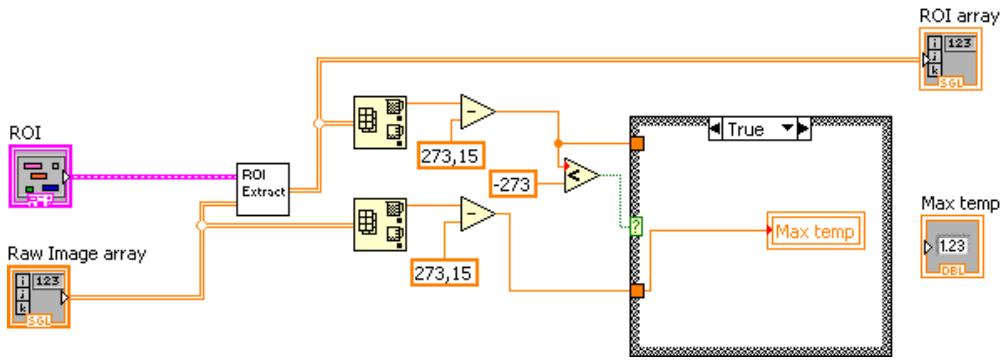

Figure C.2: The figure illustrates the sub_vi, `Extract ROI & Max`, it has two input `ROI`, and `Raw Image array` and two outputs `ROI array` and `Max temp`. This sub_vi extracts the ROI array from the raw image array, this is done using the sub_vi ROI extract, see image C.3. In the figure it is also seen how the sub_vi converts the temperature reading from Kelvin to Celcius by subtracting 273.15. This sub_vi controls that if no ROI is selected, the maximum temperature of the entire frame will be used as the output `Max temp`.

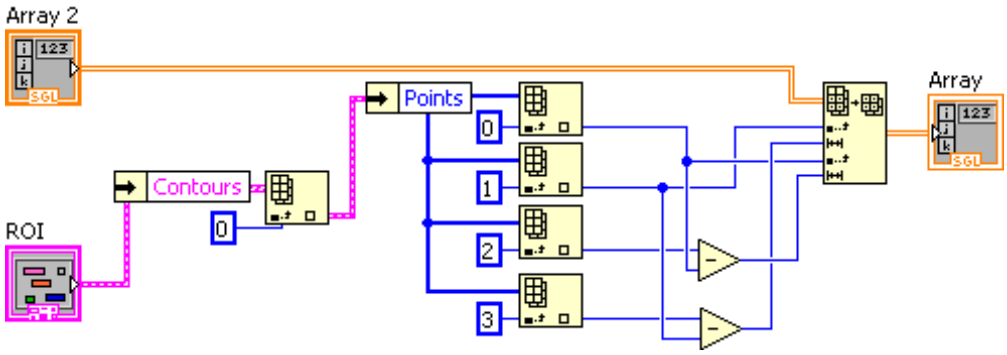

Figure C.3: The figure illustrates the sub_vi, `ROI Extract`, it has two inputs `Array 2`, and `ROI` and one output `Array`. Based on property node data in `ROI` the sub_vi extracts a subarray from `Array 2` and outputs it into the variable `Array`.

C.0.3 Focusing and internal calibration - during initial system setup

The four other cases in the event structure correspond to buttons, which tells the camera to change focus (near/far), auto focus and activate the internal calibration. The four buttons will only be visible before the system starts stimulating the skin. When the stimulation begins it is no longer possible to focus or internally calibrate the camera.
In the manual focus mode, the focus point can either be moved nearer or farer from its present state, by pressing the either *Focus near* or *Focus far* button. 14 bits are used to define the focus range (0-16384 steps). When pressing either of the two manual focuses the current focus setting is found using `Thermovison GetFocus` block. Then current focus is changed in steps of 500 in either direction using the `Thermovison SetFocus` block, and setting the attribute to `'Absolute position'`. The direction depends on which button is pressed. However, the camera will take no action if the current focus is under 500, and the *Focus near* button is pressed - or over 15800 and the *Focus far* button is pressed.
Pressing the *Auto focus* button will activate `Thermovison SetFocus` block with the input attribute set to `'Auto'`, then the camera will auto focus the image.
Pressing the *Auto adjust* button will activate the `Thermovison CameraAction` block, with the input attribute set to `'Internal Image Correction'`.
When the *Start heating* button is pressed, the two frames displaying the raw infrared and ROI images are inactivated and the *Focus near*, *Focus far*, *Auto focus*, and *Auto adjust* buttons are made invisible.

Labview implementation

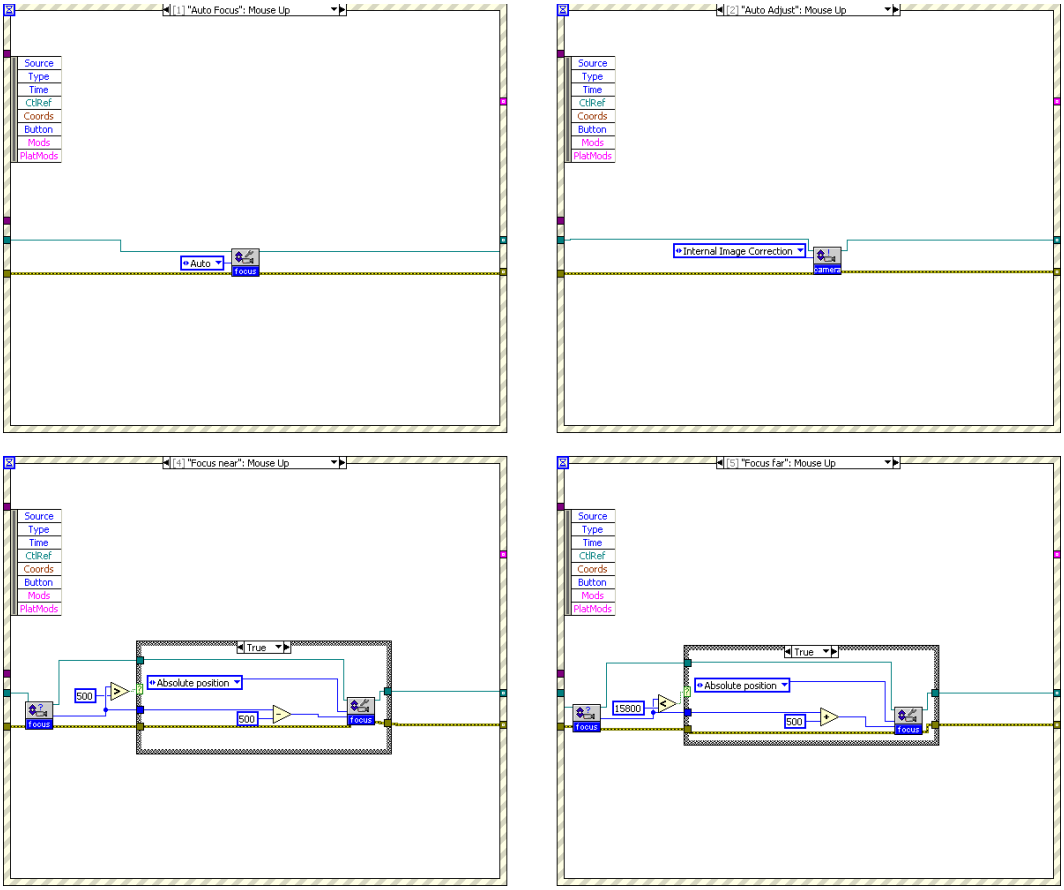

Figure C.4: The figure illustrates the four other event cases in the event structure seen in figure C.1. Each of then four cases represent a button click on the GUI. The upper left image illustrates the event of the user pressing the *Auto focus* button. The upper right the *Internal image caibration* button. The lower left the *Focus near* button. The lower right the *Focus far*.

C.0.4 Image acquisition during stimulation

When the *Start heating* button is pressed, the initial while loop stops, the camera is internally calibrated,, then the heat stimulation starts. From the initial while loop three signals are led into the stimulation while loop; the handle to the infrared camera, the error state and the ROI cluster. During the heat stimulation one frame will be sampled in each iteration in the while loop, based on the information in these three signals. The frame acquisition is done as described above using the *Thermovision GetImage* and *Extract ROI & Max* blocks.

Controlling the laser

D

The DL-20 diode laser is controlled via a RS-232 interface. The laser can both receive and send signals via the RS-232 interface. This is done by sending a number of bytes to or from the laser. To control the lasers output five bytes must be sent to the laser. To control the emitted power and shoot duration, the first byte must have the value, 192, in this project only this command will be used.
The next two bytes correspond to the desired amount of current sent through the diodes. The values can range from 0 to 3000 mA, in practice the maximum input is 2950 mA, which in theory correspond to a range of 0 to 20 W, more about this below. The transfer function from desired power, P, into current, I, is then $I = P \cdot 150$. In table D.1 the five bytes sent to the laser to control it, the bits C0...C11 is the current through the laser diodes, only 12 bits are used since the maximum value is 3000. The bits D0...D13 determine the shoot time of the laser. Each bit of those two bytes correspond to a step of 100 μs. With two bytes available the maximum shoot time per sent command is 1635 ms.
Note that the bit corresponding to 128 is zero in all of the four final bytes, since the bit is preserved control commands.

Byte #	**Bit**	2^7	2^6	2^5	2^4	2^3	2^2	2^1	2^0
1		1	1	0	0	0	0	0	0
2		0	0	0	C11	C10	C9	C8	C7
3		0	C6	C5	C4	C3	C2	C1	C0
4		0	D13	D12	D11	D10	D9	D8	D7
5		0	D6	D5	D4	D3	D2	D1	D0

Table D.1: The table displays the five bytes being sent to laser to control current and duration (Little endian).

For the rest of this chapter the command sent to the laser will be referred to as the power, not current, for easier understanding.
The emitted light from the laser is outputted into and conducted via an optic fiber, the light leaving the fiber is completely uncollimated. The two hand pieces which is equipped to the laser, collimates the laser beam into two different beam diameters, one hand piece gives the lase beam a diameter of approx. 4 mm and the other a diameter of approx. 7 mm. To ensure stimulation of an area as large as possible, the hand piece with the larger beam diameter is used. This should ensure that the laser does not shoot inbetween the receptive fields of the skin nociceptors.

D.0.5 Laser power correction

As indicated above the actual power of the emitted laser light does not entirely correspond to the power setting. In fact the actual power is always lower than the theoretical. To correct for this, a small experiment was made. Using steps of 1 W the power of the emitted light was compared with the desired power setting. The actual emitted power was

measured using a power meter (Coherent Field Max II power meter and Coherent PM 150 transducer). The results of this can be seen in figure D.1.

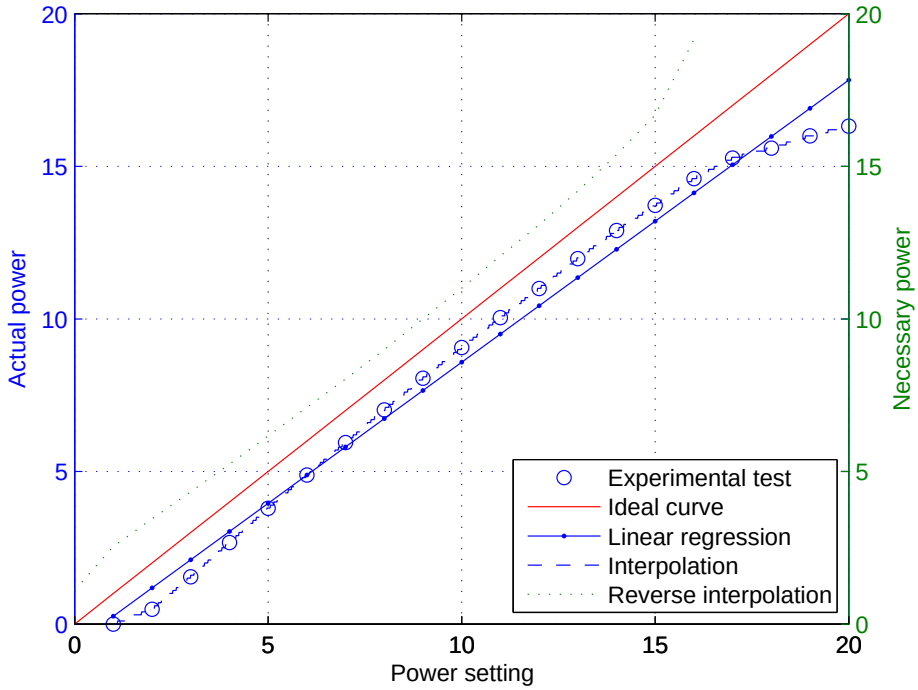

Figure D.1: The figure illustrates the relationsship between the power setting and actual power emitted from the laser. On the figure four plots are seen, first the experimental data (blue 'o'), the ideal curve (red '-'), a linear regression of the theoretical and experimental data (blue '-.-') the interpolated date of the experimental data (blue '- -') and finally the reverse interpolation, how high power setting is necessary to obtain certain powers (green '...'). The first four plots are related to Y-axis on the left, whereas, the reverse interpolation is related to the Y-axis on the right. The two Y-axis are identical but the on the right is the necessary power setting to reach a certain level, not the actual output to certain power setting.

In figure D.1 it is seen that the maximum emitted power is approximately 16 W. The relationship between the actual and desired power level is almost linear, however, near the minimum and maximum power settings the relationship is far from linear, and therefore a simple linear regression approximation is undesirable (Figure D.1 Linear regression (blue '-.-')). Instead linear interpolation will be used to find the needed power setting to obtain a certain output power. This was done in the range 0 to 16 W, using a step of 1 W. The simple formula for linear interpolation is

$$y = y_0 + (x - x_0)\frac{y_1 - y_0}{x_1 - x_0} \tag{D.1}$$

where x is the power setting inbetween to two theoretical power settings x_0 and x_1, corresponding to two levels of output power, y_0 and y_1. The reverse interpolation is then done using the formula below, where x is isolated instead of y

$$x = x_0 + (x_1 - x_0)\frac{y - y_0}{y_1 - y_0} \tag{D.2}$$

Where y_0 and y_1 are the lower and higher step of the 0 to 16 W output range. And x_0 and x_1 are the needed power settings to achive these output powers. Since the interpolation data is no as neat the values needed for the reverse

interpolation must be read off the interpolation plot.
A final remark on the advantages of using a laser based on a semiconductor technology, (such as the diode laser) is that the effect of such laser does not vary much over time, compared to gas lasers such as the CO_2 laser. Therefore, after one calibration of the laser, this should be valid for future uses.

Labview implementation

The control of the laser is implemented in Labview in two VI's the first the VI communicates with the RS232 interface and takes three inputs and sends the appropriate command to the laser. The VI receives an input about the comport to use for the communication, the power setting (W) and shoot duration (ms). The VI has no outputs. The Labview implementation is seen in figure D.2.

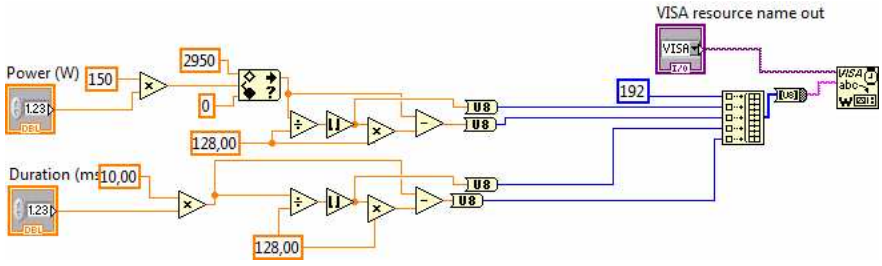

Figure D.2: The figure illustrates the Labview implementation of the laser control. This VI receives three inputs, the comport for communication, the power setting (W) and the shoot duration (ms).

The next VI corrects the power setting so the output from the laser corresponds to that intended by the controller. This VI is placed just before the laser control VI, so that receive the correct power setting. If the case sentence is true then

y0 is simply led through the case into the output. The VI receives one input, the Wanted power, and has one output the Needed power. The labview implementation of this is seen in figure D.3

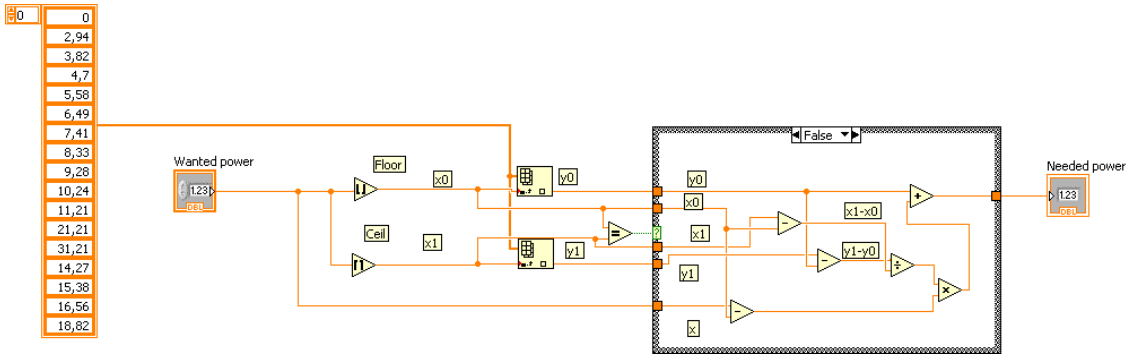

Figure D.3: The figure illustrates the Labview implementation of the power correction. The VI has one input, the Wanted power, and one output, the Needed power, to reach the wanted power. The VI converts the laser setting based on simple linear interpolation between the experimental data point seen in array constant to the left.

Cutaneous pain reception, processing, and perception

E

This appendix is a selected chapter of the authors 8th semester project. This appendix is an excact copy of the chapter from the authors 8th semester (2nd semester of the Master) project, no modications have been made to it. This appendix describes the physiology and anatomy behind the cutaneous (skin) sensory system. This appendix is ment as a service to the reader if he or she is unfamilar with such receptor physiology.

E.1 Introduction

This appendix gives an overview of mechanisms involved in the reception, processing, and perception of skin pain. Of the different types of pain especially thermal pain will be in focus.
This appendix is divided into two main sections, first the anatomy and physiology of the receptors in the skin including pain receptors, socalled nociceptors, will be described. Secondly the processing of the pain stimuli in the CNS and brain will be described.
The generel senses in the human body is a term covering pain-sensation, thermal sensation, mechanical injury and chemical disorders. Besides these senses the human body has the special senses; smell, taste, hearing, vision and balance which will not be described in this paper.
When the nervous system registrers stimuli it is called sensation, when these sensations become present in our consciousness it is called perception [Martini, 2004a].

E.2 Anatomy and physiology of receptors in the skin

The receptors in the skin can be divided into four groups 1) nociceptors (painreceptors) 2) thermoreceptors 3) mechanoreceptors and 4) chemoreceptors. The nociceptors will be described more detailed later in this section. Basically the neurons which provide the sensation of any of these four groups are dorsal root ganglion neurons, the cell body of these neurons are placed in the dorsal root of a spinal nerve. The neurons two branches reach the periphery and the CNS, respectively. The type of stimuli which the neurons transduce to a nervous signal depends on the peripheral terminal of the neuron. Neurons for transducing for example touch have speciel non-neural structures at their terminal for transducing the signal, where neurons for transducing thermal and pain sensation are free nerve endings. Neurons with specialised terminals are called epicritic and neurons with free nerve endings are called protopathic, generally epicritic sensations are spatial specific, where as protopathic sensations are more crude [Martini, 2004a]. Crude in this case means that the receptive fields are larger, so two stimuli at two different points has to be placed further apart to be distingusable from each other, than in areas which smaller receptive fields.

E.2.1 Anatomy - placement of the receptors in the skin

First it should be noted that these receptors, as mentioned above, can be found at several locations in the body not just in the skin. For example the receptors can be found in internal organs, called visceral receptors. The receptors in the skin are called somatic receptors [Martini, 2004a]. In this paper only the receptors in the skin will be described. The receptors in the skin are usual placed in the dermis, a few in the epidermis. C type nociceptors are according to Bromm and Treede [Bromm and Treede, 1983] terminating in the superficial skin layer (< 300 μm). Bromm and Treede show that more than 90 % of the power from a CO_2 (wavelength 10.6 μm) is absorbed in the superficial 50 μm of the skin. However, this is sufficient for activating the *C* fibre nociceptors. One might conclude from this that some of the C fibres are placed in the superficial part of the skin (< 50 μm) [Bromm and Treede, 1983]. Tillman et al. 1995 found that the receptors of C fibres nociceptors, of macaca monkeys, were placed within depths ranging from 20 μm to 570 μm, with a mean of 201 μm. Comparing their results with the anatomy of the skin, the receptors is placed in

the epidermis and the superficial layers of the dermis [Tillman et al., 1995]. It is unknown how directly their results from the monkeys can be converting into the human anatomy.

E.2.2 Physiology - function of the receptors

As mentioned there exits different types of receptors in the skin. Three types of these receptors sense stimuli within the normal range whereas the nociceptors sense extreme (and painfull) conditions. These three types are thermal, mechano and chemo receptors.
Receptors can be classified as tonic or phasic, a phasic receptor only fires if there is any change of the stimuli where a tonic receptor always fires in the presence of a stimulus.
Some receptors can adapt to continues unpainful stimulaton. For example you do not notice the slight rumbling when driving in a car. Besides adaption in the receptors, the CNS can also adapt to stimulations. Phasic receptors adapts to a stimuli where tonic do not.
The signal being produced by these receptors are, like all nervous signals, frequency modulated. The nerve signal are being produced in different types of specialized receptors. The six different types of receptors can be seen on figure E.1. The letters in the following refer to the letters on figure E.1

a. Free nerve endings - usual found as nociceptors or thermoreceptors. These receptors are placed between the epidermal cells. There is no structural difference between the cells which registrer pain or temperature.

b. Root hair plexus - sense touch and displacement of hair. These receptors adapts very quickly which is the reason why you do not notice the close touching your skin.

c. Merkel cells and tactile discs - sense fine touch and pressure. These receptors are tonic and have very small receptive field. The merkel cells are pressure sensitive and secrete chemicals which are noticed by the adjacent tactile disks. The merkel cells are found in the superficial layers of the skin, at the papillary ridge between the epidermis and dermis.

d. Tactile corpuscle or Meissner's corpuscle - like the merkel cells these sense touch and pressure and also low-frequency vibration. They are most abundant in fingertips, eyelibs, lips and external genitalia. The corpuscles are also placed superficially connected to papillary ridge. They rapidly adapt to stimuli making them phasic receptors.

e. Lamellated corpuscle or Pacinian corpuscle - sense deep pressure. The corpuscles are placed in the deep dermis. The receptors are very fast adapting, these receptors adapt within a second to the new stimuli. This means that they can sense minute vibration and high-frequency stimuli. Physiologically this corpuscle is very similar to the Meissner's corpuscle, however, not anatomically. The lamellated is constructed as a single dendrite is placed in the center of severel collagen layers. This construction ensures that the dendrite only will be stimulated by direct pressure, when the collagen layers are compressed.

f. Ruffini corpuscle - are placed in the deep dermis. These receptors also registrer pressure and other distortion of the skin. The receptors are tonic and do not adapt very much. The corpuscle surrounds collagen fibres which are part of the dermis, so any distortion of these fibres will be registrered by the corpuscle.

[Kandel et al., 1991a] [Martini, 2004a]
The receptors described above most often produce nerve signals which reaches our consciousness and therefore cause perception of stimuli.
The superficial receptors; the Meissner's corpuscle and the Merkel cells provide rather specific spatial sensing. Each neuron is innervated from about 10-25 Meissner's corpuscle or Merkel disks [Kandel et al., 1991a] [Martini, 2004a]. These receptors have a reception area of 2 - 10 mm. The receptive fields for the Pacinian corpuscle and Ruffini corpuscle are much larger since the receptors are placed deeper in the skin. The spatial sensitivity also depends on the density of receptors in the skin, the density is highest at the fingertips < 5 mm and lowest on the back, thigh and calf

40 - 50 mm [Kandel et al., 1991a].
The recognition of pressure and shape of object are computed from the input from several receptors [Martini, 2004a].

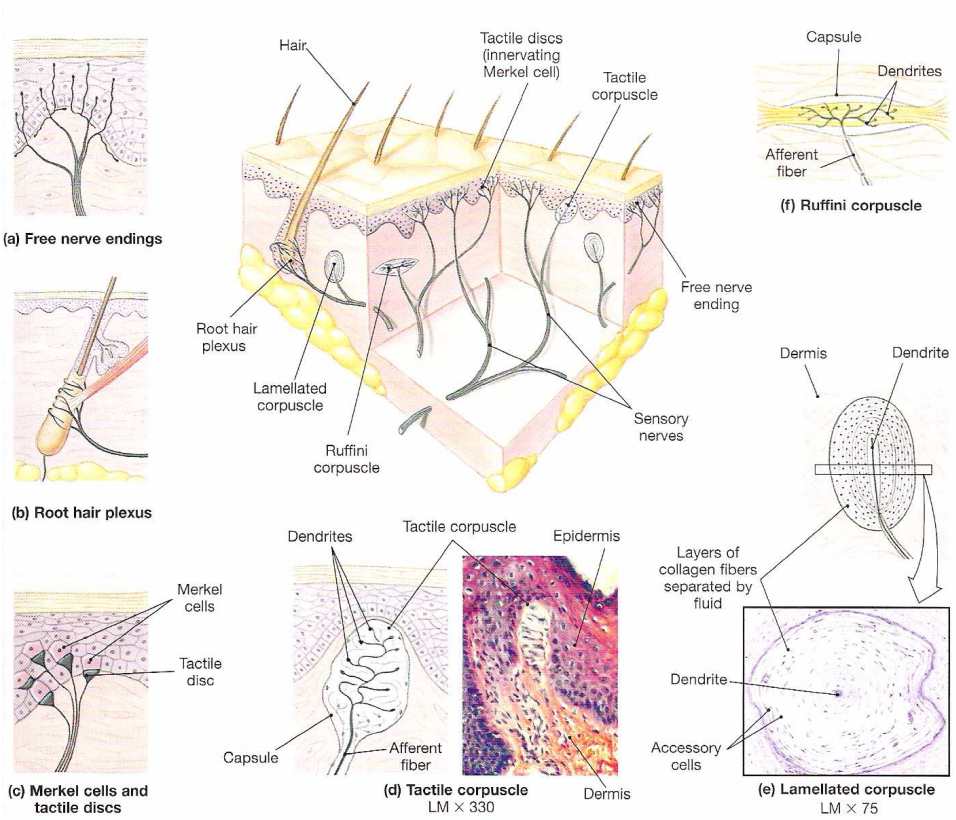

Figure E.1: The figure illustrates the six difference types of terminal structures on somatic sensory neurons [Martini, 2004a].

As mentioned above three types of receptors registrer stimuli within the normal and unpainful range.
Thermoreceptors are free nerve endings which are in steady state tonic receptors, they continously fire discharges when the temperature changes. Their activity increases but settles to steady state after some time giving them some of the characteristics of phasic receptors. You usually do not notice the current room temperature, but if it suddenly changes you will notice this. There exits receptors for registering both warm and cold, and there are no structural difference between them. The cold receptors are three to four times as abundant as the heat receptors [Kandel et al., 1991a] [Martini, 2004a]. The thermal sensation is created from inputs from both the cold and warmth receptors. The receptors respond to temperatures between 5 °C and 45 °C [Kandel et al., 1991a] [Martini, 2004a]. Besides those found in the skin, thermoreceptors can be found in skeletal muscles, the liver and the hypothalamus.
The mechanoreceptors can be subdivided into another three groups; tactile receptors, baroreceptors and proprioceptors. Tactile receptors which sense fine touch and pressure can be found as any of the six types of receptors seen on figure E.1. The density of the tactile receptors are greatest in the glabrous (hairless) skin, e.g. in the palm and fingertips, which provides these areas with high sensitivity. Most of the tactile sensors have specialised structures surrounding the periphiral terminal of the neurons, figure E.1 c) - f) only a few are free nerve endings, figure E.1 a) [Kandel et al., 1991a]. Baroreceptors are free nerve endings placed in the epithel walls of an internal organ, e.g. a blood vessel. The sensation from baroceceptors are usually not perceived. Proprioceptors sense the position of joint, the tension in ligaments and muscular contraction. These receptors can for example be bare nerve endings placed in joint capsules. Proprioceptors do not adapt to stimuli but continously send signals to the CNS [Martini, 2004a].

Chemoreceptors respond to water soluble and lipid soluble substances in the surrounding fluid. These sensors are typically placed in the larger blood vessel e.g. in the carotid bodies and the aortic arch. The signal from these receptors do not reach our consciousness [Martini, 2004a].
The sensation of pain does not occur by overstimulation of any of these receptors, for an example if the skin temperature exceeds 45 °C the stimuli will not be sensed by the thermoreceptors but instead by high threshold receptors socalled nociceptors [Schmidt, 1986], these will be described in the following.

E.2.3 Nociceptors and nociception

Pain sensation (and perception) or nociception in the normal healthy subject occurs whenever nociceptors are actived. However, it can occur both with and without the activation of nociceptors [Schmidt, 1986]. This can have several causes, certain psychogenic states can cause perception of pain eventhough no physical reason for the pain exits [Schmidt, 1986]. Furthermore patophysiological states in the CNS can cause sensititation (e.g. after a prolonged period of painful stimuli) such that even un-painful stimuli will cause a perception of pain [Schmidt, 1986]. Another cause of pain perception without the activation of nociceptors can be secondary algesia, where pain is percived as originating from the uninjuried surrounding tissue of an injuried region.
Also the CNS is also capable of filtering nociceptive such that no perception of pain occurs, in spite nociceptors actually are activated [Schmidt, 1986].
This section will focus on acute, somatic pain, no visceral or chronic pain will be discussed. The somatic pain can be divided into both superficial and deep, the superficial pain originating from the skin or similar, and the deep pain originating from the muscles, joint and head (headaches) [Schmidt, 1986]. This section will furthermore focus on the superficial part of the somatic pain.
Some previous theories suggested that nociceptors were normal receptors which simply were oversimulated but research have proven that nociceptors actually are different receptors, with high excitation threshold, which only will be excited by stimuli causing or capable of causing tissue damage (noxious stimulus) [Schmidt, 1986].
Nociceptors are like thermal receptors free nerve endings, which have a large receptive fields which is the reason why it can be difficult to pinpoint the exact source of a painful stimuli. Nociceptors are divided into the same three groups, as the non-pain receptors are, being sensitive of 1) extreme temperatures, 2) mechanical destruction of tissue and 3) nociceptors that recept the chemicals released by stressed cells or the presence of any alien chemicals. Intense stimuli will often trigger all three types of receptors.
The nociceptors in the skin are like other receptors placed in the superficial layers of the dermis (some few in the epidermis). *Very simplifyed*, nociceptors can be classified strictly as tonic receptors - meaning they continue producing the nervous signals until the painful stimuli ceases. However, the CNS can adapt to a painful stimuli causing the perception of pain to decline [Martini, 2004a].
The information about the painful stimuli is sent to the CNS via two types of nervefibres, *A* and *C* fibres. *A* (group-III [Schmidt, 1986]) fibres which are slightly myelinated carry so-called first pain to the CNS. *C* (group-IV [Schmidt, 1986]) fibres which are unmyelinated carry the slow pain, often described as burning pain or second pain [Schmidt, 1986]. The signal from the *A* fibres reach the CNS quickly and trigger somatic reflexes [Kandel et al., 1991a]. The perception of the second pain are typically more spatially diffuse and remains for a prolonged period [Schmidt, 1986].
Thermal nociceptors are *A* fibres with small diameter which conducts at a speed of 5-30 m/s. The fibres for mechano nociceptors are also *A* similar to the fibres of the thermal nociceptors. Polymodal nociceptors which reacts to both thermal, mechanical and chemical stimuli use *C* fibres which conducts at much lower speed, < 1 m/s. Very intense stimuli triggers the polymodal receptors. [Kandel et al., 1991b] Nociceptive *A* fibres are categorised into δ and β fibres depending on their conduction velocities, δ fibres have a lower conduction velocity (15 m/s) than β fibres (45 m/s). The *A* fibres conducting the signal from the nociceptors are mostly *A*δ fibres [Kandel et al., 1991a] [Treede et al., 1998].
However, Treede et al. [Treede et al., 1998] [Treede et al., 1995] suggest that two very different types of *A* fibres exist, which exhibit quite different characteristics. Treede et al. have done their research using macaques (Macaca fascicularis) monkeys. The first type, type I has a higher heat threshold than type II. (>53 ° C vs. 46 ° C). The type I nociceptors are found both in glabrous and hairy skin whereas type II is absent in glabrous skin. Type I fibres have very high conduction velocity (25 m/s) in comparation type II conducts with a velocity of 14 m/s. But inspite of the

high conduction velocity of type I fibres, these fibres do not conduct first pain according to Treede et al. The reason for this is the long response latency for type I fibres ($\sim$5 sec.) in comparation it is only 0.22 sec. for type II [Treede et al., 1998] [Treede et al., 1995]. Treede et al. also suggest that nociceptors are *not* stricly tonic receptors, some fibres adapt. Type II *A* fibres and *C* fibres are very similar in many ways, according to Treede et al., they both adapt to a long duration stimuli and they both have relatively short response latency. The greatest difference between the two types of fibre is the conduction velocity, as mentioned *C* fibres have very low conduction velocity which means that only type II fibres are able to carry first pain [Treede et al., 1998] [Treede et al., 1995]. Treede also found that no first pain could be registrered in glabrous skin, which is consistent with the absense of type II fibres in these areas [Treede et al., 1995].
Treede also suggest that polymodal receptors are not only *C* fibres but also Type II *A* fibers might be polymodal receptors since these also are sensitive to capsaicin. [Treede et al., 1995] *C* fibres are found in both skin types and exhibit adaption to stimuli [Treede et al., 1995].
Type I fibres are to higher extend than type II fibres, capable of sensing mechanical pain. Type II fibres have a very high mechanical threshold, some research indicate that type II fibres are mechanically insensitive [Treede et al., 1995] [Treede et al., 1998]. Research have also shown that type I fibres eventhough they do not carry thermal first pain, they are capable of carrying mechanical first pain [Treede et al., 1998].
The sensation of pain, as other sensory sensations, contains four components

- Cognitive
- Affective
- Autonom
- Motor

The cognitive component is the recognizing of the stimuli as being painful. This depends on the intensity being high enough to activating , which the CNS then will have to interpret as painful [Schmidt, 1986].
The affective component causes changes in the emotional state. A painful sensation will always effect us emotionally, typically it will create anxiety long-term, chronic pain can cause depressions [Schmidt, 1986].
The autonomic component can be seen as certain autonomic responses to the pain causing e.g. blood pressure and heart rate to change [Schmidt, 1986].
The motor component is typically seen as a form of protection e.g. the removal of the hand, if placed upon a hot plate. Such reflexes will be further discussed below.
In superficial pain the sensory or cognitive component will typically be the most dominant [Schmidt, 1986].

E.3 Transport and processing of sensation

The general senses of which pain sensation is one, is processed in the several different sites in the brain.
The signal from the peripheral receptors reach the primary sensory cortex through a number of pathways through the peripheral nervous system (PNS), the CNS and in the brain. The sense of a peripheral stimuli is conducted through three neurons before reaching the sensory cortex. The peripheral neuron which conducts the signal to CNS through the dorsal root ganglion is called the first-order neuron. The second neuron which brings the signal from the CNS to the thalamus in the brain, is called the second-order neuron. And finally the neuron which brings the signal from the thalamus to the primary sensory cortex is called the third-order neuron. Somewhere along the pathway the signal crosses from one side of the body to the other, e.g. a stimuli sensed a the right arm in conducted through these neurons and ends up on the left cortex, and vice versa [Martini, 2004a].
The exact pathway which the signal follows depends on the kind of signal. There exist three pathways for bringning the signal from the periphery to the cortex. These are the posterior column pathway, the spinothalamic tracts, which are subdivided into the anterior and lateral spinothalamic tracts and the spinocerebellar pathway [Martini, 2004a].
Most mechano sensation such as fine touch, vibration and some proprioception are conducing through the posterier column pathway. Sensation coming from the inferior half of the body is conducted in the most lateral part of the pathway called the fasciculus gracilis where as the sensation from the superior half is conducted in the more lateral part,

called the fasciculus cuneatus. The axons of the second-order neurons cross over to the other side of the brain stem just before reaching the thalamus (at the medulla obglongata), the pathway can be seen of figure E.2 as a) [Martini, 2004a] [Kandel et al., 1991a].
The spinothalamic tracts conduct the sensations of crude touch and pressure along with sensation of pain and temperature. The sensations of pain and temperature are conducted in the anterior tracts, where as the other sensations are caried in the lateral tracts. The cross-over in these pathways happens immediately after the first-order neuron has synapsed onto the second-order neurons which cross over before ascending in the spinal cord. This pathway can be seen on figure E.2 as b) and on figure E.3 as c) [Martini, 2004a] [Kandel et al., 1991a]
The spinocerebellar pathway conducts sensation of proprioception from receptors placed inside muscle and order organs. The pathway can also be subdivided into posterior and anterior spinocerebellar tracts, however, the sensation carried in both are the same. This pathway seperate it self from the two other because the third-order neurons do not reach the primary sensory cortex or any part of the cortex for that matter. Neither do any cross-over occur (actually some second-order axons cross but recross in the cerebellum). The signal from the left side of the body is conducted to the cerebellum where second-order neurons synapse to the left cerebellar cortex. No third-order neurons are present in this pathway. The sensations conducted through this pathway never reach our consciousness. This pathway can be seen on the right of figure E.3. [Martini, 2004a]

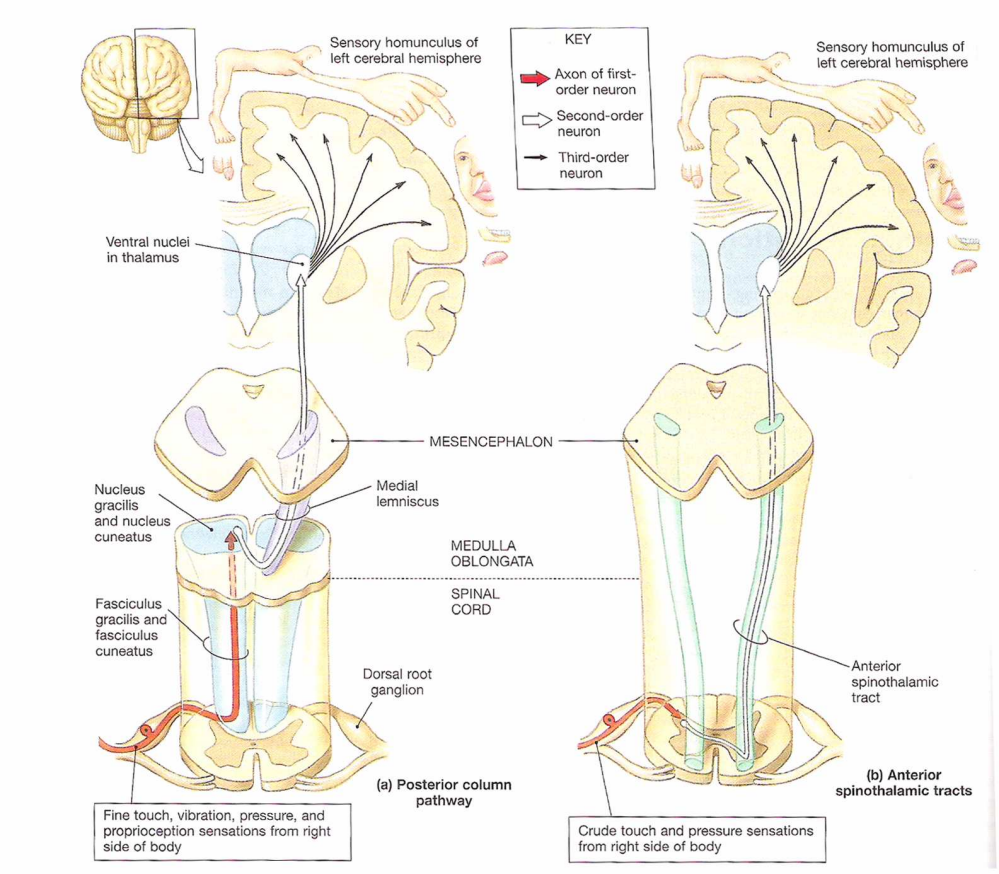

Figure E.2: The figure illustrates the posterior column pathway a) and the anterior spinothalamic tracts b). The first-order neurons are illustrated as red, the second-order as white and third-order as black, see the legends [Martini, 2004a].

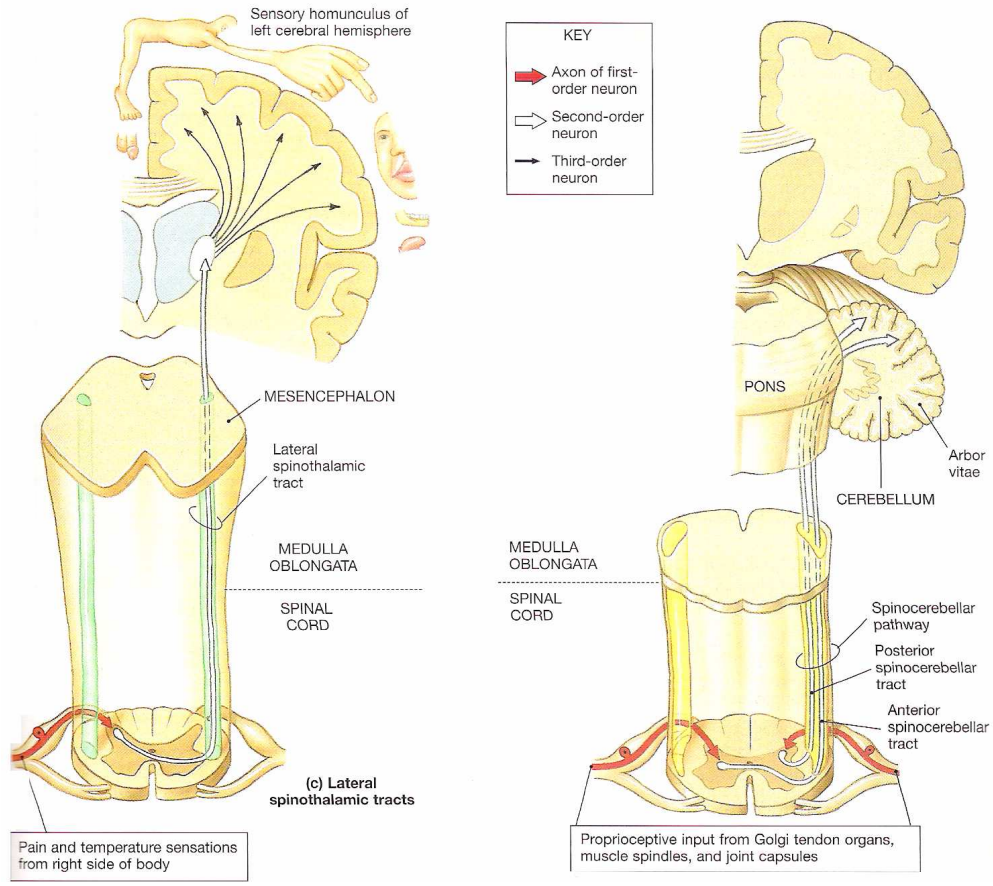

Figure E.3: The figure illustrates the lateral spinothalamic tracts c) and the spinocerebellar pathway, left. The first-order neurons are illustrated as red, the second-order as white and third-order as black, see the legends [Martini, 2004a].

E.3.1 Processing

The signals transported to the brain are first processed in the thalamus and from there some of the information is sent to different cortical areas and subcortical areas. However, processing of sensations can not take place with the involvement of the sensory cortex [Schmidt, 1986]. The thalamus filters some of the information and determines some of the characteristics of the signal e.g. the origin of the signal, the thalamus is responsible for sending the information to the correct part of the cortex. A great part of the signal reach the primary The primary sensory cortex is divided into regions each representing certain parts of the body. The regions of the cortex vary in size accordingly to the importance of body part from which it receives stimuli, e.g. the regions covering the fingertips, and the lips and tongue are very large compare to for example the back, see figure E.4. The size of the regions correspond to density of receptors found

in the bodypart, eg. the fingertips have large density of receptors and therefore a large region on the cortex [Martini, 2004a].

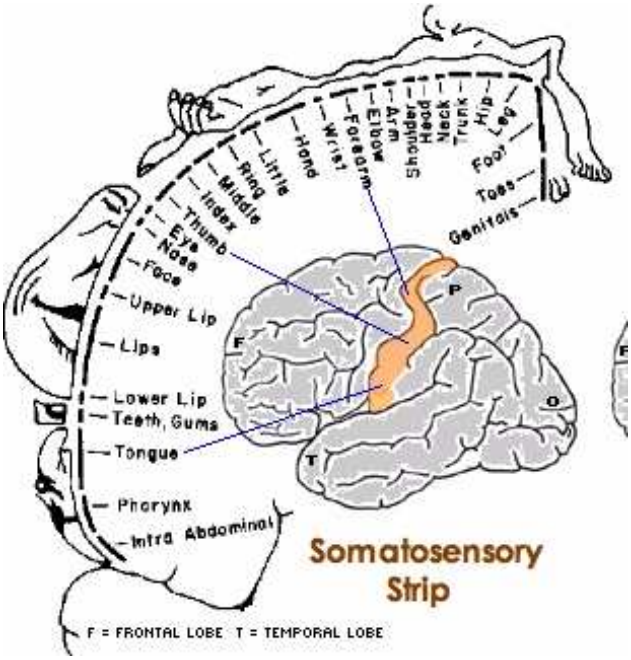

Figure E.4: The figure illustrates how the diffent regions of the primary sensory cortex is connected to certain parts of the body [M. Schmolesky, 2000].

Figure E.4 illustrates how the socalled homonculus at the primary sensory cortex. It clearly shows that some parts of the body fill more in our consciousness than other, and moreover the sensitivity in these regions are much higher than other parts of the body.
The perception of stimuli which pain are much more present in our awareness than other types of stimuli. However, sometimes the brain can filter the perception of pain from our consciousness. As mentioned above processing take place in other locations than the primary sensory cortex. Since this project have been partly focussing on pain research the processing of pain sensation will be the focus in the paragraph. Studies have shown that brief heat noxious stimuli will activate both cortical and subcortical areas [Bushnell and Apkarian, 2006]. Pain will most often activate the following cortical and subcortical areas

- S1 and S2 (the first and second somatosensory cortical areas.)
- ACC - anterior cingulate cortex
- IC - insular cortex
- PFC - pre frontal cortex
- Th - thalamus
- CB - Cerebellum

[Bushnell and Apkarian, 2006]
Most of these areas can be seen on figure E.5

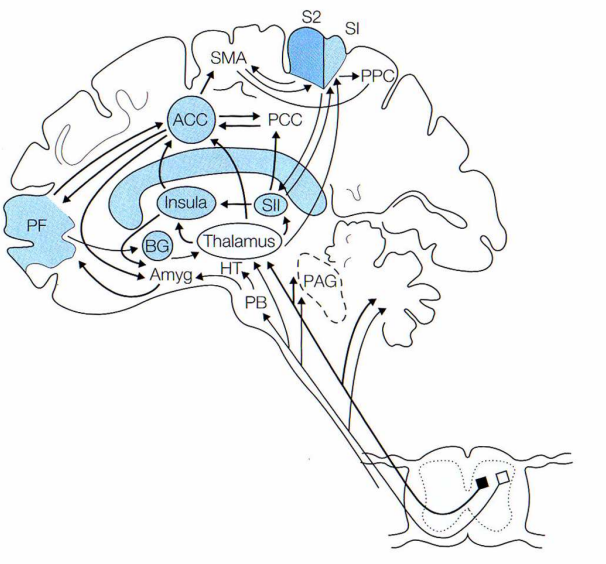

Figure E.5: The figure illustrates the diffent cortical and subcortical regions which activates during perception of pain [Bushnell and Apkarian, 2006].

Research have indicated that S1 and S2 is involved with decoding of signals with respect to location, duration, and intensity [Bushnell and Apkarian, 2006]. Injuries within S1 or S2 will lead to reduced perception of pain, and furthermore a more diffuse perception [Bushnell and Apkarian, 2006]. While the limbic system is important for the pains affective component [Bushnell and Apkarian, 2006]. The activation of the PFC is highest when the stimulus intensity is just above the nociceptor activation threshold [Bushnell and Apkarian, 2006]. The earliest activity, caused by a noxious stimulus, is seen in S2 [Bushnell and Apkarian, 2006]. Some research have suggested that first and second pain activates both the same and also different areas [Bushnell and Apkarian, 2006]. Both will activate S2, where as first pain will mainly cause activation of S1, giving a precise spatially perception of the stimulus. Second pain will mainly activate ACC, causing more diffuse spatial perception and furthermore the second will activate the affective (emotionel) component of pain, this motivates behavioural responses to limit injury and optimize recovery [Bushnell and Apkarian, 2006]. Still there are some uncertainties concerning the temporal perception of pain [Bushnell and Apkarian, 2006].
Visceral receptors can cause stimuli to misinterpreted as originating from external stimuli. An example for this case could be a myocardial infarction where you do not only feel pain from your chest, but the pain will also radiate into the left arm, because the neurons carrying pain sensation from the left arm and myocardium converges on the same neuron in the CNS.

E.3.2 Reflexes

Besides the processing which takes place in the brain and upper CNS a lot of processing happens in the inferior parts of the CNS, i.e. the spinal cord. This processing also involves creation of a response, typically in the form of activiting a motor unit. This form of processing is know as reflexes.
Monosynaptic reflexes typically is the stretSch of a muscle which is registrered by a muscle spindle (a form of mechano receptor) which in the CNS synapses onto a motor neuron which causes the muscle to contract. The name monosynaptic comes from the fact that these reflexes only involve two neurons, the first-order neuron which brings the signal

from the muscle spindle to the CNS and the second-order motor neuron which causes the muscle to contract. The first-order neurons are large, highly myelinated type *A* fibres with high conduction velocity. [Martini, 2004b]

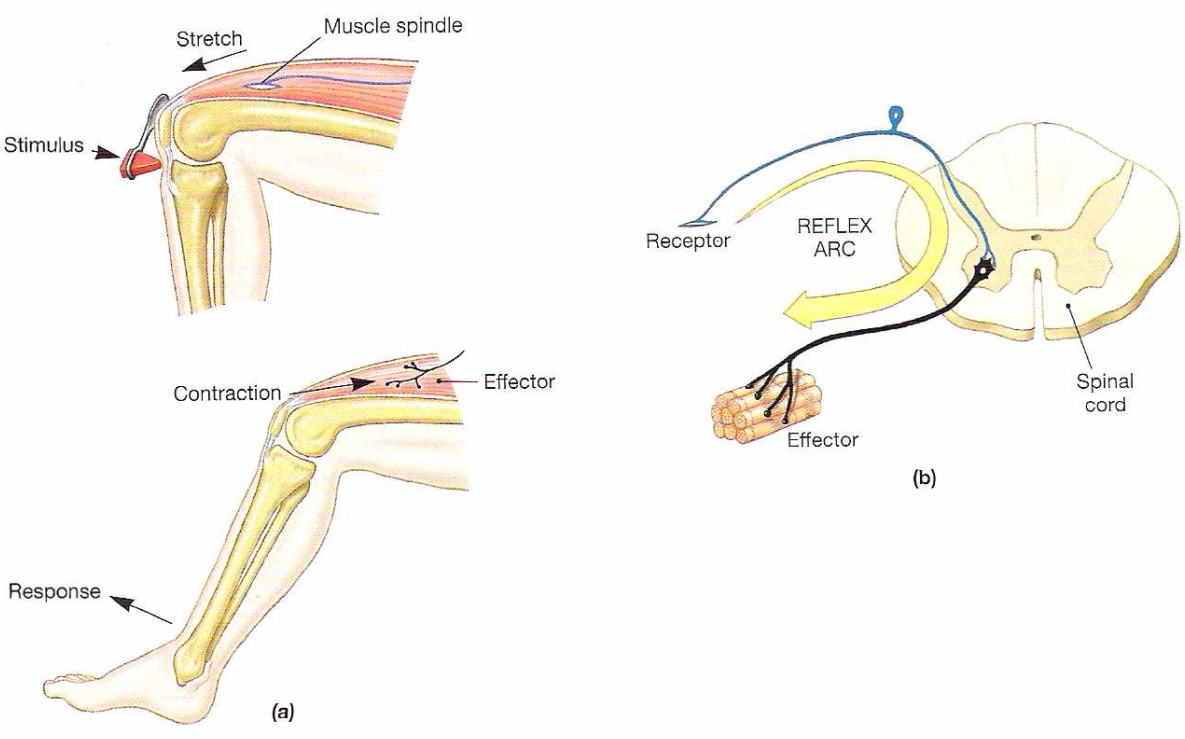

Figure E.6: The figure illustrates how monosynaptic reflexes will make you contract a muscle if it is stretched [Martini, 2004b].

Polysynaptic reflexes involves more neurons. An example could be the prick of a needle on your finger which will make you remove the finger. Nociceptors sense the prick of the needle and send the signal through a first-order neuron to the spinal cord, here a second-order neuron diverge the signal both sending the painful sensation to the brain and also activating a motor neuron which cause muscles to contract which removes the hand from the needle. Some polysynaptic reflexes will not only trigger the activation of a motor neuron. As seen on figure E.7 the reflex will also inhibit the motor neurons with the opposite function. As seen on figure E.7 the reflex caused by stepping on a needle will not only flex the leg but also inhibit the extensors in the thigh. On b) it can be seen how the reflex makes you remove your foot from the needle but also makes you shift your weight to the other leg. Besides the activation of

the motor neurons, signal are sent to the brain for processing in the thalamus and sensory cortex. [Martini, 2004b] Therefore we typically have already moved our foot from the needle before we become aware of the pain.

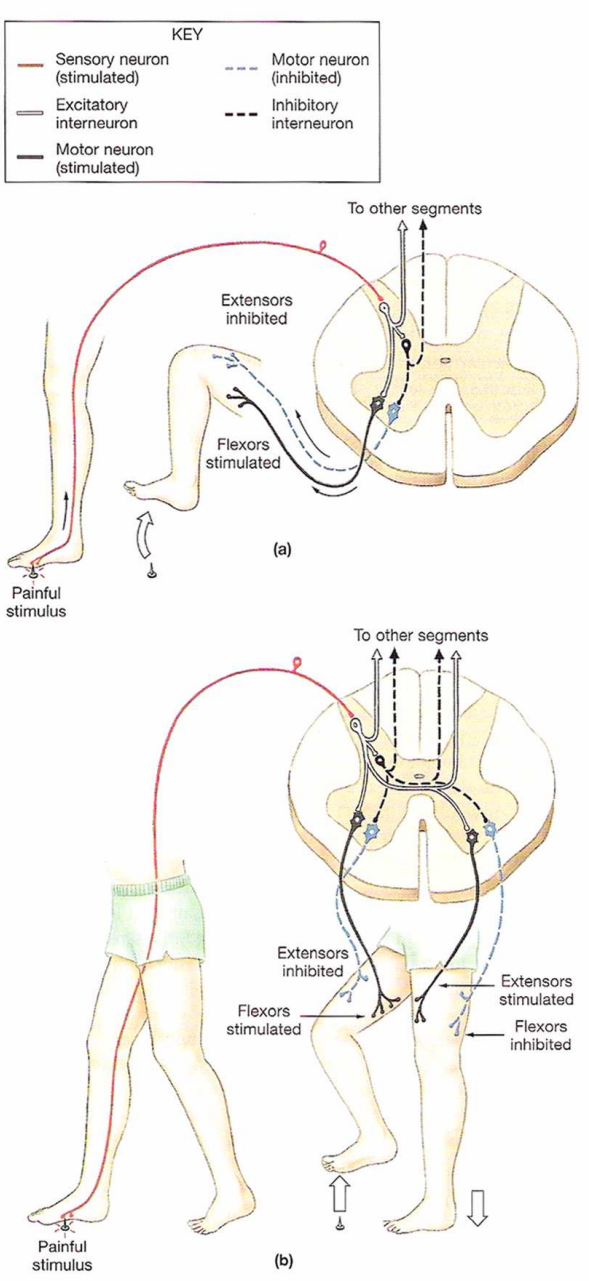

Figure E.7: The figure illustrates how polysynaptic reflexes makes you remove your leg if you step on a needle [Martini, 2004b].

Bibliography

[Al-Saadi et al., 2006] Al-Saadi, M., Nadeau, V., and Dickinson, M. R. (2006). A novel modelling and experimental technique to predict and measure tissue temperature during co_2 laser stimuli for human pain studies. *Lasers in science and medicine*, 21:95–100.

[Anderson and Parrish, 1981] Anderson, R. and Parrish, J. A. (1981). The optics of human skin. *The journal of investigative dermatology*, 77:13–19.

[Arendt-Nielsen and Chen, 2003] Arendt-Nielsen, L. and Chen, A. (2003). Lasers and other thermal stimulators for activation of skin nociceptors in humans. *Neurophysiologie Clinique*, 33:259–268.

[Bromm and Treede, 1983] Bromm, B. and Treede, R.-D. (1983). Co_2 laser radiant heat pulses activate c nociceptors in man. *Pflügers archiv European journal of Physiology*, 399:155–156.

[Brugmans et al., 1991] Brugmans, M., Kemper, J., Gijsbert, G., van der Meulen, F. W., and van Gemert, M. (1991). Temperature response of biological materials to pulsed non-ablative co_2 laser irridiation. *Lasers in Surgery and Medicine*, 11:587–594.

[Bushnell and Apkarian, 2006] Bushnell, M. C. and Apkarian, A. V. (2006). *Textbook of pain*, pages 107–124. Elsevier, 5th edition.

[Cashwell and Everett, 1958] Cashwell, E. and Everett, C. (1958). *A practical manual on the Monte Carlo Method for random walk problems*, pages 103–107. Pergamon press, first edition.

[Cervero and Laird, 1996] Cervero, F. and Laird, M. (1996). Review article - mechanisms of touch-evoked pain (allodynia): a new model. *Pain*, 68:13–23.

[Cortex technology, 2007] Cortex technology (2007). Derma scan c v. 3. `http://www.cortex.dk/images/50/20MHz_flyer_WEB.pdf`. Visited May 15th 2009.

[Derbyshire and Osborn, 2008] Derbyshire, S. and Osborn, J. (2008). Enhancement of offset analgesia during sequential testing. *European Journal of Pain*, 12:980–989.

[Derbyshire and Osborn, 2009] Derbyshire, S. and Osborn, J. (2009). Offset analgesia is mediated by activation in the region of tehperiaqueductal grey and rostral ventromedical medulla. doi:10.1016/j.neuroimage.2009.04.032. Found 27th of May 2009.

[Dimitrijevic et al., 1972] Dimitrijevic, M., Faganel, J., Gregoric, M., Nathan, P., and Trontelj, J. (1972). Habituation: effects of regullar and stochastic stimulation. *Journal of Neurology, Neurosurgery and Psychiatry*, 35:234–242.

[Franklin et al., 1994] Franklin, G. F., Powell, J. D., and Emami-Naeini, A. (1994). *Feedback control of dynamic systems*. Addison Wesley, third edition.

[Gowrishankar et al., 2004] Gowrishankar, T., Stewart, D., Martin, G., and Weaver, J. (2004). Transport lattice models of heat transport in skin with spatially heterogeneous, temperature-dependent perfusion. *Biomedical engineering online*, 3:42.

[Gracely, 1999] Gracely, R. (1999). *Studies of pain in human subjects - In Textbook of Pain*, pages 385–407. ISAP Press, Seattle, fourth edition.

[Granovsky et al., 2008] Granovsky, Y., Granot, M., Nir, R., and Yarnitsky, D. (2008). Objective correlate of subjective pain perception by contact heat-evoked potentials. *Pain*, 9(1):53–63.

[Grill and Coghill, 2002] Grill, J. and Coghill, R. (2002). Transient analgesia evoked by noxious stimulus offset. *Journal of Neurophysiology*, 10:2205–2208.

[Haugen, 1994] Haugen, F. (1994). *Regulering av dynamiske systemer (Norwegian)*. Tapir forlag, first edition.

[Henyey and Greenstein, 1941] Henyey, L. and Greenstein, J. (1941). Diffuse radiation in the galaxy. *The Astrophysical Journal*, 93:70–83.

[Iannetti et al., 2006] Iannetti, G. D., Zambreanu, L., and Tracey, I. (2006). Similar nociceptive afferents mediate psychophysical and electrophysical responses to heat stimulation of glabrous and hairy skin in humans. *Journal of Physiology*, 577.1:235–248.

[IASP, 2009] IASP (2009). Iasp pain terminology. `http://www.iasp-pain.org/AM/Template.cfm?Section=Home&Template=/CM/HTMLDisplay.cfm&ContentID=6632`. Visited May 27th 2009.

[Infrared Systems, 2009] Infrared Systems (2009). Flir thermovision a40 series infrared camera. `http://www.infraredsys.com/FlirA40Series.htm`. Visited April 28th 2009.

[Jiang et al., 2002] Jiang, S., Ma, N., Li, H., and Zhang, X. (2002). Effects of thermal properties and geometrical dimensions on skin burn injuries. *Burns*, 28:713–717.

[Kandel et al., 1991a] Kandel, E. R., Schwartz, J. H., and Jessell, T. M. (1991a). *Principles of neural science, 4/e*, pages 430–449. McGraw-Hill, fourth edition.

[Kandel et al., 1991b] Kandel, E. R., Schwartz, J. H., and Jessell, T. M. (1991b). *Principles of neural science, 4/e*, pages 472–491. McGraw-Hill, fourth edition.

[Lautenbacher et al., 2001] Lautenbacher, S., Nielsen, J., Andersen, T., and Arendt-Nielsen, L. (2001). Spatial summation of heat pain in males and females. *Somatosensory and motor research*, 18(2):101–5.

[M. Schmolesky, 2000] M. Schmolesky (2000). Homonculus. `http://web.lemoyne.edu/~hevern/psy340/graphics/homunculus.jpg`. Visited April 20th 2009.

[Martini, 2004a] Martini, F. H. (2004a). *Fundamentals of anatomy and physiology*, page 509 Ű 529. Benjamin Cummings, sixth edition.

[Martini, 2004b] Martini, F. H. (2004b). *Fundamentals of anatomy and physiology*, pages 446–459. Benjamin Cummings, sixth edition.

[Merskey et al., 1994] Merskey, H., Lindblom, U., Mumford, J., Nathan, P., and Sunderland, S. S. (1994). *Part III: Pain Terms, A current list with definitions and notes on usage - In Classification of Chronic pain*, pages 209–214. ISAP Press, Seattle, second edition.

[Meyer et al., 1976] Meyer, R. A., Walker, R. E., and V. B. Mountcastel, J. (1976). A laser stimulator for the study of cutaneous thermal and pain sensations. *IEEE transactions on Biomedical Engineering*, 23(1):54–60.

[Mørch et al., 2008] Mørch, C. D., Andersen, O. K., and Coghill, R. (2008). Graphesthesia and two-point discrimination of painful heat stimulation. *Abstracts of the 12th World Congress on Pain, International Association for the Study of Pain (IASP), 17-22 August 2008, Glasgow, Scotland*, 12.

[Pennes, 1948] Pennes, H. (1948). Analysis of tissue and arterial blood temperatures in the resting human forearm. *Journal of applied Physiology*, 1:93–122.

[Prahl et al., 1989] Prahl, S., Keijzer, M., Jacques, S., and Welch, A. (1989). A monte carlo model of light propagation in tissue. *Dosimetry of Laser Radiation in Medicine and Biology*, IS 5:102–111.

[Quevedo and Coghill, 2007] Quevedo, A. and Coghill, R. (2007). An illusion of proximal radiation of pain due to distally directed inhibition. *The Journal of Pain*, 8(3):280–286.

[Raja et al., 1999] Raja, S., Meyer, R., Ringkamp, M., and Campbell, J. (1999). *Peripheral neural mechanisms of nociception - In Textbook of Pain*, pages 11–58. ISAP Press, Seattle, fourth edition.

[Schmidt, 1986] Schmidt, R. (1986). *Sensory physiology*, pages 117–143. Springer-Verlag, 5th edition.

[Serway and Jewett, 1995] Serway, R. A. and Jewett, J. W. (1995). *Physics for scientists and engineers with modern physics*, pages 1094–1125. Thomson - Brooks/Cole, sixth edition.

[Seteikin and Krasnikov, 2006] Seteikin, A. and Krasnikov, I. (2006). An analysis of thermal effects resulting from laser radiation interaction with a multilayered biotissue. *Russian Physics Journal*, 49 No 10.

[Shy et al., 2003] Shy, M., Frohman, E., So, Y., Arezzo, J., Cornblath, D., Giuliani, M., Kincaid, J., Ochoa, J., Parry, G., and L.H. Weimer, M. (2003). Quantitative sensory testing. *NEUROLOGY*, 60:898 Ű 904.

[Thermotec, 2009] Thermotec (2009). Infrared camera agema thermovision 900sw. `http://www.thermotec-es.de/Dienstleistung_Messen_Agema_e.html`. Visited 28. april 2009.

[Tillman et al., 1995] Tillman, D.-B., Treede, R.-D., Meyer, R. A., and Campbell, J. N. (1995). Response of c fibre nociceptors in the anaesthetized monkey to heat stimuli: estimates of receptor depth and threshold. *Journal of Physiology (1995)*, 485.3:753–765.

[Treede et al., 1998] Treede, R.-D., Meyer, R. A., and Campbell, J. N. (1998). Myelinated mecheniccaly insensitive afferents from monkey hairy skin: Heat-response properties. *The American Physiological Society*, pages 1082–1093.

[Treede et al., 1995] Treede, R.-D., Meyer, R. A., Raja, S. N., and Campbell, J. N. (1995). Evidence for two different heat transduction mechanisms in nociceptors primary afferent innervating monkey skin. *Journal of Physiology (1995)*, 483.3:747–758.

[Verhey et al., 2003] Verhey, J., Mohammed, Y., Ludwig, A., and Giese, K. (2003). Implementation of a practical model for light and heat distribution using laser-induced thermotherapy near to a large vessel. *Physics in Medicine and Biology*, 48:3595–3610.

[Wang et al., 1995] Wang, L., Jacques, S. L., and Zheng, L. (1995). Mcml - monte carlo modeling of light transport in multi-layered tissues. *Computer methods and programs in biomedicine*, 47:131–146.

[Welch and van Gemert, 1995a] Welch, A. J. and van Gemert, M. J. (1995a). *Optical-thermal response of laser-irridiated tissue*, page 367 Ű 384. Plenum Press, first edition.

[Welch and van Gemert, 1995b] Welch, A. J. and van Gemert, M. J. (1995b). *Optical-thermal response of laser-irridiated tissue*, pages 73–100. Plenum Press, first edition.

[Wilson and Spence, 1988] Wilson, S. and Spence, V. (1988). A tissue heat transfer model for relating dynamic skin temperature changes to physiological parameters. *Physics in Medicine and Biology*, 8:895–912.

[Yelle et al., 2008] Yelle, M., Rogers, J., and Coghill, R. (2008). Offset analgesia: A temporal contrast mechanism for nociceptive information. *Pain*, 134:174–186.